

Timber and Steel Railway Bridge Design

H.L.B. van Looveren



Cover Image: An architectural visualisation of the Tangenvika Railway Bridge design in this thesis.
3D model drawing created by by Zwarts and Jansma Architects.

Timber and Steel Railway Bridge Design

by

H.L.B. van Looveren

in partial fulfilment of the requirements of the degree of

Master of Science
in Structural Engineering

at the Delft University of Technology
to be defended publicly on Thursday April 28, 2022 at 1:00 PM

Student number: 4392795

Thesis committee

Prof. dr. ir. M. Veljkovic	TU Delft, chair
Ir. P.A. de Vries	TU Delft
Ir. M. Mirra	TU Delft
Ir. J. Koeken	Iv-consult, daily supervisor

An electronic version of this thesis is available at <http://repository.tudelft.nl/>.

Preface

My student era has finally come to an end by finishing this last work at the Delft University of Technology. It marks the end of my time as ‘Delftste student’, and it has been quite a journey with many experiences. Some were more positive than others, but overall I enjoyed my life to the fullest. I met many wonderful people with whom I shared both serious study and less serious party time—creating friendships that hopefully will last at least a lifetime.

Handing in the work that lies before is a big relief. I started diligently on this project; it was my wish to design and engineer something while simultaneously trying to make the world a more sustainable big ball in space. Using timber in construction is definitely one of the solutions to our many challenges. However, individually working on a design project was emotionally exhaustive. There are so many details to think about or different solutions and new possibilities that could be integrated into my design. But there was limited time and knowledge, which was sometimes frustrating. Sadly, I also needed time to process some discomforts within my family. Nevertheless, I am proud of what I produced in the end.

I could not have done it alone, though. First, I need to thank my supervisor at Iv, Jeroen. He helped me with my struggles and sometimes pushed me just to start and produce some numbers. I’d also like to thank Wouter and Teodora from Iv for helping me during my thesis. And all my colleagues with whom I enjoyed walking outside during lunch.

Secondly, I would like to thank my committee members at the TU Delft. My chair, Milan, was always very critical and on point during our meetings but never left without assuring me that I had done a good job. Peter helped me with the connection design and understanding of timber connections in general; thank you. Last but not least I must thank Michele. He reviewed most of my report and gave plenty of very useful feedback. Also, figuring out specific timber issues together was very supportive.

Of course, I cannot forget about all my friends who either joined me during my coffee breaks, helped me explain thesis issues to them (but mainly myself), supported me with kind words, or enjoyed dinner together—studying at Studoc or the library and motivating each other to stay just a little longer. All these small moments were very important to keep going and continue my thesis work. Special thanks go out to my roommates, who had to hear me complain (probably too much), and my close friends, who reviewed my work and gave advice. Thank you all.

I want to end by expressing my appreciation for my family. Throughout my whole student life, you have supported me in many ways, and I am most grateful to have had the privilege to have studied without any major worries. With the closure of my thesis, I am ready to start and enjoy the next step; the dreaded ‘burgerleven’.

*H.L.B. van Looveren
Delft, April 2022*

Abstract

Timber usage in construction works has increased over the past years due to its better environmental performance. Applying timber elements instead of steel or concrete decreases the emissions impact of the built environment. Architect firm ZJA and Iv-consult are interested in investigating a timber railway bridge as part of the Norwegian infrastructure plan. A kilometre-long double-track railway bridge with 50 m spans is used as a case study to investigate the possibilities of timber application. The objective is to design and assess a timber beam bridge with steel sections at the support.

The aim of this research is to design the sections and their connection. The design requirements and calculation methods used are based upon the Eurocodes. The design is considered to be part of the preliminary design phase of a project. Unity checks of the cross-section and deflection are calculated by use of linear mechanics. An FE model with beam elements is created to determine the force distribution of the bridge and calculate deflection. The strength and stiffness of the connection are calculated using empirical and plastic mechanic methods given in the standards. The resulting stiffness is used in the model to determine the final deflection when accounting for the semi-rigid joint.

The design consists of timber and steel box girders that only carry a single track. On top of the support, a slender stiffened steel box girder of 10 m length is situated, 5 m to both sides. Between the steel sections, there are timber box girder sections of 40 m that have very thick flanges and webs. On top of the structure lies a slab track that is only considered as weight. A dowel-type connection is used with double slotted-in steel plates in all flanges and webs of the timber section. The slotted-in plates have a slightly smaller width than the timber elements and have a depth of around 2.7 m. The steel fasteners are simple dowels.

This thesis has found that a timber and steel beam bridge with box girder cross-sections is governed by the creep deflection, shear strength of the timber, fatigue strength of the steel, and the dimensional stability of the connection. Except for the last issue, each of these limits can be satisfied by increasing the dimensions of each cross-section. Dimensional stability is the timber size change due to moisture content variation. The perpendicular-to-grain stresses become too large due to the configuration of the steel in the connection. The use of modified timber, which decreases the dimensional stability effect drastically, is only suggested as a solution.

An architecturally pleasing structure is designed by adding very limited visual elements but mainly practical and structural elements that have two functions, shown in the figure below. The desired continuity and bridge rhythm is accomplished via a line concept. The abrupt material cross-section changes are partly covered by continuous timber elements. From the practical and architectural adjustments, new cross-section dimensions were determined. The governing unity checks of the new design were calculated and showed the possibility of the design under the assumption the connection shrinkage issue is resolved.

Thus a timber and steel railway bridge has potential. It should be stressed that methods and factors from the Eurocodes are assumed to be applicable to the large timber box girder sections. This assumption is recommended to be checked by means of experimental research on large timber specimens. Additional research on the semi-rigid is advised, as introducing slotted-in steel plates in the web and flange plane can significantly improve the moment capacity.

Finally, two alternative suggestions are given to avoid solving the dimensional stability issue. The first is to design a bridge with lower loading demands, like a road bridge. Secondly, the bridge can be made of only timber sections. Alternating spans would have two hinged connections to form a continuous cantilevered bridge. While the first alternative creates easier circumstances to solve for dimensional stability, the second alternative completely removes the issue by having a connection with lower demands. It is recommended to incorporate connections early on in timber design.



Impression of railway bridge design

Contents

Preface	iii
Abstract	v
Nomenclature	ix
List of Figures	xiii
List of Tables	xv
1 Introduction	1
1.1 Motivation and objective	2
1.2 Research questions	4
1.3 Methodology	4
1.4 Report structure	6
I Concept phase	7
2 Design considerations	9
2.1 Structural model	9
2.2 Span length	9
2.3 Cross-section	11
2.4 Steel	12
2.5 Wood	13
2.6 Timber	15
2.7 Tracks and speed	17
2.8 Loading	19
3 Single material design	21
3.1 Loading and limit states	21
3.2 Timber design	24
3.3 Class 2 steel design	26
3.4 Class 4 steel design	27
3.5 Concluding remarks	29
4 Model and loading	31
4.1 Model	31
4.2 Load factors and combinations	32
II Global design	37
5 Combined timber-steel design	39
5.1 Implementation	39
5.2 ULS	40
5.3 SLS	42
5.4 Fatigue	44
5.5 Global design conclusions	50
6 Dynamic analysis	51
6.1 Induced vibrations	51
6.2 Continuous bridge	53
6.3 Eigen frequency bridge	53

6.4 Eurocode dynamics	55
6.5 Remarks	55
III Connection Design	57
7 Dowel-type calculation models	59
7.1 Principle	59
7.2 Local criteria	60
7.3 Global criteria	63
8 Connection	67
8.1 Connection options	67
8.2 Resistance	68
8.3 Connection stiffness	72
IV Design assessment	75
9 Current Design	77
9.1 Design	77
9.2 Discussion of design	79
10 Practical and architectural assessment	83
10.1 ZJA inspiration	83
10.2 Practical assessment	84
10.3 Architectural assessment	86
10.4 Manufacturing and handling	88
10.5 Environmental impact	89
11 Definitive design	91
11.1 New cross-section	91
11.2 Alternatives	93
12 Final remarks	95
12.1 Conclusions	95
12.2 Recommendations	96
Standards	99
Bibliography	105
V Appendices	107
A Span length	109
A.1 Temperature length effect	109
A.2 Outer spans	109
B Loads	113
B.1 Permanent loads	113
B.2 Train loads	113
B.3 Temperature	114
B.4 Wind	115
C Steel cross-sections	119
C.1 Steel class 2 design	119
C.2 Steel class 4 design	121
D Connection calculations	131
D.1 Local criteria - fastener	131
D.2 Global criteria	136

Nomenclature

Abbreviations

Abbreviation	
CLT	Cross Laminated Timber
CMC	Coefficient of Moisture Contraction
CME	Coefficient of Moisture Expansion
EC	Eurocode
FE	Finite element
FEA	Finite element analysis
FEM	Finite element method
FRP	Fibre Reinforced Polymer
glulam	GLued Laminated Timber
hss	High Strength Steel
INDC	Intended Nationally Determined Contributions
LVL	Laminated Veneer Lumber
MC	Moisture Content
SLS	Serviceability Limit State
UC	Unity Check
ULS	Ultimate Limit State
vhss	Very High Strength Steel
1D, 2D, 3D	One-, two-, three-dimensional

Symbols

Symbol	Definition	Unit
Latin letters		
A	Area of section	m^2
$A_{i,eff}$	Effective area in direction i	m^2
A_m	Area enclosed by the centre line of the section	m^2
$A_{net,j,l}$	Net area in condition j for element l	m^2
D_d	Cumulative damage during a structures service life	-
d	Diameter	mm
EI_i	Bending stiffness as double letter symbol in direction i	MNm^2
$EI_{i,eff,j}$	Effective bending stiffness in direction i and condition j	MNm^2
$E_{mean,fin}$	Mean final elastic modulus due to creep	MPa
$E_{0,g,mean}$	Mean elastic modulus parallel-to-grain	MPa
$E_{0,g,0.05}$	Fifth percentile elastic modulus parallel-to-grain	MPa
$E_{90,g,mean}$	Mean elastic modulus perpendicular-to-grain	MPa
$E_{90,g,0.05}$	Fifth percentile elastic modulus perpendicular-to-grain	MPa
$F_{b,Rd,l}$	Bearing strength for element l	MN
F_i	Force in direction i	MN
F_{res}	Resultant force	MN
$F_v(\alpha)$	Characteristic resistance of fastener with angle to the grain	MN
F_y	Force in y-direction on a slotted-in steel plate	kN
$F_{v,Rk}$	Characteristic steel fastener strength	kN
$f_{c,0,g,d}$	Design timber compression strength parallel-to-grain	MPa
$f_{c,0,g,k}$	Characteristic timber compression strength parallel-to-grain	MPa

Symbol	Definition	Unit
$f_{c,90,g,d}$	Design timber compression strength perpendicular-to-grain	MPa
$f_{c,90,g,k}$	Characteristic timber compression strength perpendicular-to-grain	MPa
$f_{m,g,d}$	Design timber bending strength	MPa
$f_{m,g,k}$	Characteristic timber bending strength	MPa
$f_{t,0,g,d}$	Design timber tensile strength parallel-to-grain	MPa
$f_{t,0,g,k}$	Characteristic timber tensile strength parallel-to-grain	MPa
$f_{t,90,g,d}$	Design timber tensile strength perpendicular-to-grain	MPa
$f_{t,90,g,k}$	Characteristic timber tensile strength perpendicular-to-grain	MPa
$f_{r,g,d}$	Design timber rolling shear strength	MPa
$f_{r,g,k}$	Characteristic timber rolling shear strength	MPa
f_u	Steel ultimate strength	MPa
$f_{v,g,d}$	Design timber shear strength	MPa
$f_{v,g,k}$	Characteristic timber shear strength	MPa
f_y	Steel yield strength	MPa
GA_i	Shear stiffness as double letter symbol in direction i	MN
$GA_{i,eff,j}$	Effective shear stiffness in direction i and condition j	MN
G_j	Permanent loading during condition j	kN/m
$G_{g,mean}$	Mean shear modulus parallel-to-grain	MPa
$G_{g,0.05}$	5 th percentile shear modulus parallel-to-grain	MPa
$G_{mean,fin}$	Mean final shear modulus due to creep	MPa
$G_{r,g,mean}$	Mean rolling shear modulus perpendicular-to-grain	MPa
$G_{r,g,0.05}$	5 th percentile rolling shear modulus perpendicular-to-grain	MPa
I_i	Second moment of area in direction i	m ⁴
K_r	Rotational stiffness of connection	MNm/rad
K_{ser}	Stiffness per shear plane per fastener in dowel-type connection	N/mm
k_{cr}	Crack factor for combining shear and bending	-
k_{def}	Creep factor	-
k_m	Bi-axial bending reduction factor	-
k_{mod}	Timber modification factor	-
L	Length of span	m
$M_{i,Ed}$	Design bending moment in direction i	MNm
$M_{i,Rd}$	Design bending moment resistance in direction i	MNm
M_{i-}	Negative bending moment in direction i	MNm
M_{i+}	Positive bending moment in direction i	MNm
$M_{T,Ed}$	Design torsional moment	MNm
$M_{T,Rd}$	Design torsional moment resistance	MNm
m_j	Mass per length for element j	kg/m
m_j^*	Fictitious mass per length for element j	kg/m
$N_{i,Ed}$	Design normal force in direction i	MN
$N_{i,Rd}$	Design normal resistance in direction i	MN
N_{Ri}	Endurance value for specific design stress range σ	-
n_{Ei}	Number of cycles with specific design stress range σ	-
n_{ef}	Number of effective fasteners in a row	-
n_{req}	Required number of fasteners	-
P	Point load	kN
Q_j	Variable load during condition j	kN/m or kN/m ²
$q_{i,j}$	Distributed load in direction i and condition j	kN/m or kN/m ²
T_{Rd}	Design torsional moment resistance	MNm
t_j	Thickness of element j	mm
	Twist of element, only without j	mm/3m
$V_{i,Ed}$	Design shear force in direction i	MN
$V_{i,Rd}$	Design shear resistance in direction i	MN
V and v	Train speed	km/h

Symbol	Definition	Unit
v_{cr}	Critical train speed	km/h
W_i	First moment of area in direction i	m ³
w_c	Precamber	mm
$w_{EI,perm}$	Bending deflection under permanent loading	mm
$w_{EI,live}$	Bending deflection under live loading	mm
w_{GA}	Shear deflection	mm
$w_{lim,j}$	Deflection limit for condition j	mm
w_j	Deflection for condition j	mm
	sls, uls, frequent, quasi, the latter two are also passenger comfort and creep	
Greek letters		
α	Factor to relate outer span to middle span length	-
	Classification factor for train loads	-
α_F	Angle between force and timber grain	°
γ_j	Partial safety factor for loading condition j	-
γ_M	Timber safety factor	-
	Steel safety factor	-
	Timber connection safety factor	-
γ_{M2}	Partial safety factor for steel connections	-
γ_{Ff}	Partial safety factor for constant amplitude stress ranges	-
$\Delta\sigma$	Characteristic stress range	MPa
$\Delta\sigma_C$	Detail category	MPa
$\Delta\sigma_D$	Constant amplitude fatigue limit	MPa
$\Delta\sigma_{E,2}$	Design stress range	MPa
$\Delta\sigma_L$	Cut-off limit	MPa
ϵ	Strain	-
ϵ_{MC}	Strain due to moisture content change	-
θ	Angular rotation	mrad
λ	Damage equivalent factor	-
ξ	Reduction factor permanent loading for governing live load	-
$\rho_{g,k}$	Characteristic timber density	kg/m ³
$\rho_{g,mean}$	Mean timber density	kg/m ³
ρ_m	Mean timber density, equal to $\rho_{g,mean}$	kg/m ³
ρ_s	Structural steel density	kg/m ³
σ_{MC}	Stress due to moisture content change	MPa
σ_j	Stress due to condition j	MPa
$\sigma_{m,i}$	Bending stress from bending moment i	MPa
$\sigma_{t,0}$	Tensile stress parallel-to-grain	MPa
τ_i	Shear stress from shear force in direction i	MPa
τ_j	Shear stress due to condition j	MPa
$\tau_{t,i}$	Shear stress from torsion in direction i	MPa
ϕ	Dynamic amplification factor	-
ϕ_i	Rotation of element around axis i	rad
ψ_i	Load combination factor	-
Subscript use		
$\cdot x, \cdot y, \cdot z$	Coordinate direction	
$\cdot eff$	Effective	
$\cdot uls$	Ultimate limit state	
$\cdot sls$	Serviceability limit state	
$\cdot d$	Design value	
$\cdot k$	Characteristic value	

List of Figures

1.1	Examples of timber bridges.	1
1.2	Map of train tracks in Norway and Sweden.	2
1.3	close-up map with the 30 km new double track (Bane Nor, 2019).	2
1.4	Impression of the gradual transition of timber (brown) to steel (dark grey).	3
1.5	Design process of this thesis.	5
2.1	Different schemes of a bridge structure.	9
2.2	Moment distribution for constant stiffness and distributed load in terms of $qL^2/8$	10
2.3	Continuous beam with introduced hinges and unknown moments.	10
2.4	Bending moment ratio with different outer span ratios.	11
2.5	Concrete railway bridge examples with varying construction height.	12
2.6	Anisotropy of wood explained via multiple figures.	13
2.7	Graphs to determine expected moisture content equilibrium of timber.	14
2.8	Fatigue diagrams.	15
2.9	An example of a trestle bridge, the Kinsol trestle in Victoria, Canada.	16
2.10	Block glulam cross-sections and rolling shear in a CLT cross-section.	17
2.11	RHEDA2000 system cross-section drawing (Rail One, 2011).	19
3.1	Mechanic schemes	22
3.2	Deflection limit for passenger comfort, figure A2.3 in EN1990.	23
3.3	Individual contributions to total deflection, figure 7.1 in EN1995-1-1.	23
3.4	Timber cross-section.	24
3.5	Steel cross-section with thick plates such that it is class 2.	26
3.6	Steel cross-section for class 4 design with only stiffeners at the bottom flange.	28
4.1	SCIA model screenshot	31
5.1	Renders of the beam models	40
5.2	Snapshot of an SW/0 load with its bending moment diagram.	40
5.3	An example bending moment diagram from the SCIA model	41
5.4	An example shear force diagram from the SCIA model	41
5.5	Deflection unity checks of the combined girder	43
5.6	Definition of deck rotation t with track width S of 1435 mm, figure A2.1 in EN1990.	43
5.7	Definition of angular rotations, figure A2.2 in EN1990.	44
5.8	Combined welded profiles class one to four from table 8.2 EN1993-1-9.	45
5.9	Welded stiffeners class six to eight from table 8.4 EN1993-1-9.	46
5.10	Orthotropic deck open stiffeners from table 8.9 EN1993-1-9.	46
5.11	Bending moment at three positions for several LM71 positions	47
5.12	Bending moment at sn3 for several SW/0 positions	47
5.13	Fatigue strength curves for normal stress	49
6.1	Critical train speeds of HSLM-A train models	52
6.2	Vibrational modes of timber and steel beam SCIA model with purple=0 and red=1	54
6.3	Dynamic flow chart of EN1991-2	56
7.1	A schematic view of a dowel connection with a single fastener	59
7.2	Three main plastic failure modes for a double shear connection	61
7.3	Seven failure modes for double slotted-in steel plates	61
7.4	Edge distance definition of timber elements using dowel-type fasteners	62
7.5	Failure modes for a connection with multiple dowel-type fasteners	64

7.6	Schematic representation of stresses around fastener	64
7.7	Dowel failure modes for steel-to-timber connections from EN1995-1-1.	65
7.8	Example of one-sided shear plug with multiple fasteners, figure A.2 in EN1995-1-1.	65
8.1	Connection examples sketches	68
8.2	Dowel-type connection drawing made in Rhino	68
8.3	Force distribution to determine force slotted-in steel plates require to resist.	69
8.4	A structural model representation of timber shrinkage	72
8.5	Mechanics scheme with rotational springs.	72
8.6	Schematising slotted-in steel plates by springs and the rotational capacity.	73
8.7	Unity check creep deflection for different rotational spring stiffness values	74
9.1	Render of the current design	77
9.2	Timber and steel boxgirder of current design	78
9.3	Dowel-type connection in Rhino with dimensions.	78
10.1	Visual designs by ZJA of an arch-beam girder and a continuous curved-truss bridge.	83
10.2	Cross-section drawing of improved box girder including additional components.	84
10.3	Sketches of a conceptual diaphragm structure between the box girders.	85
10.4	Detail of double slotted-in steel plates connection to steel section.	86
10.5	Sketch to visualise line play near the support of the timber on steel section.	87
10.6	Sketches from architecture meeting with ZJA.	87
10.7	An impression of many small lamellae that leads to a cluttered effect.	87
10.8	Architecture drawing of the line concept design by ZJA.	88
11.1	Schematised continuous cantilevered bridge.	93
A.1	Moment distribution for constant stiffness and distributed load in terms of $qL^2/8$	110
A.2	Continuous beam with introduced hinges and unknown moments.	110
A.3	Mechanic schematics for simply supported structures.	111
A.4	Optimisation of α with respect to a minimal hogging moment difference	112
A.5	Bending moment ratio with different outer span ratios.	112
B.1	Vertical train load models from EN1991-2.	113
B.2	Eccentricity of vertical train loads, figure 6.3 in EN1991-2.	114
B.3	Monthly average wind speeds in Lillehamer (Windfinder, n.d.).	116
B.4	Monthly average wind speed distribution in Lillehamer (Windfinder, n.d.).	117
C.1	Steel cross-section with thick plates such that it is class 2.	119
C.2	Shear lag reduction to b_{eff} according to EN1993-1-5.	121
C.3	Steel cross-section for slender design with only stiffeners at the bottom flange.	122
C.4	Orthotropic stiffened plate	125
C.5	Stress distribution inner element in bending	128
D.1	Sketch of rotational stiffness principle based on Figure 8.5	135

List of Tables

2.1	Glulam strength class properties copied from table 5 in EN14080.	18
3.1	Cross-sectional forces of single distributed load for ULS.	22
3.2	Deflection limits in SLS.	23
3.3	Timber cross-section properties.	24
3.4	Material properties of GL30h.	24
3.5	Unity check timber cross-section for each stress at the support and midspan	25
3.6	Deflection check timber cross-section.	25
3.7	Effective cross-sectional properties due to shear lag.	26
3.8	Material properties S355.	26
3.9	Unity check steel class 2 cross-section per individual force.	26
3.10	Effective cross-section properties due to shear lag for SLS.	27
3.11	Deflection check steel thick cross-section.	27
3.12	Reduced steel cross-section properties.	28
3.13	Unity check steel slender cross-section for major bending moment.	28
3.14	Deflection steel slender cross-section for two combinations in mm without precamber.	28
4.1	Partial safety factors for loads, based on table A2.4 in EN1990	32
4.2	Load combinations factors, table A2.3 in EN1990.	33
4.3	Load group factors for rail traffic taken from table 6.11 in EN1991-2.	34
4.4	Load multiplier for several loading combinations specified in EN1990.	35
4.5	Wind distribution for fatigue loading.	36
5.1	Maximal hogging and sagging moment values	40
5.2	Cross-sectional forces at the connection for four different positions.	41
5.3	Timber cross-section properties for a construction height of 3.5 m.	42
5.4	Unity checks of timber section starting at different positions.	42
5.5	Deflection unity checks of the combined girder	42
5.6	Deck rotation limits for different train speeds, table A2.7 in EN1990.	43
5.7	Horizontal rotation limits dependent on trains speeds, table A2.8 in EN1990.	44
5.8	Characteristic stress ranges from SCIA model.	48
5.9	Service life damage	49
6.1	High-speed load models from EN1991-2 for HSLM-A.	52
6.2	Vertical natural frequencies of IPE300	53
6.3	Eigen frequencies of non-prismatic cross-section with a construction height of 3.5 m	53
7.1	Minimal distances for bolts/dowels based on the definition in Figure 7.4 from EN1995-1-1.	62
8.1	Cross-sectional forces.	70
8.2	Resultant forces.	70
8.3	Required number of dowels for single and double slotted-in steel plates	70
8.4	Netto cross-section in tension and shear.	71
8.5	UC for shear strength, plate bearing, and net tension for the slotted-in steel plate.	72
8.6	Connection stiffness values for flange and web.	73
9.1	Several key unity checks of the current combined girder design.	79
11.1	Several key unity checks of the combined girder design.	92

B.1	Temperature values to use for design.	115
B.2	Speed transfer table knots to meter per second.	116
C.1	Classification plates in (partial) compression.	120
C.2	Classification for S355 grade for full compression and symmetric bending	120
C.3	Shear lag reduction factors for the flanges.	120
C.4	Effective cross-section properties due to shear lag.	121
C.5	Stiffener dimensions and properties.	122
C.6	Classification plates in (partial) compression.	122
C.7	Classification local plates in full compression.	123
C.8	Shear lag reduction factors for the flanges of slender steel section.	123
C.9	Effective width reduced for shear lag for SLS checks.	123
C.10	Orthotropic plate buckling reduction	125
C.11	Column buckling of a single stiffener with its parent plate.	126
C.12	Effective width reduced for shear lag and plate buckling.	127
C.13	Class 2 area ratios with respect to bottom flange area	129
C.14	Class 4 area ratios with respect to stiffened bottom flange area	129
D.1	Failure mode values for three angles to the grain for flange and web	132
D.2	Cross-sectional forces at the connection at five meter.	133
D.3	Calculation of resultant force at 5m connection for flange and web	133
D.4	Multiple effective number of dowels in a row.	135
D.5	Steel geometry edge and internal distances of steel plate	137

Introduction

Climate change is an undeniable challenge of the present. Society has to act to prevent irreversible negative changes. In 1987 the Brundtland committee released a book called 'Our Common Future' (Brundtland, 1987), to put global warming on the political agenda. Thirty years later, countries signed the Paris agreement (UNFCCC, 2015) stating their intention to tackle climate change. Nations determined national goals to mitigate emissions. The plan to limit global warming to 1.5 degrees Celsius could not have been achieved with these national goals (Rogelj et al., 2016). During a recent conference in Glasgow, countries have put forward new targets for mitigation, adaptation, finance, and collaboration and finished the Paris Rulebook (UNFCCC, 2021). Although the 1.5 degrees only remain insight when all pledges come true.

Global warming can be partly solved by reducing emissions, to which the built environment is one of the most significant contributors. This thesis presents an example to lower the amount of material-based emissions for a railway bridge. For infrastructure projects, around 90% of emissions can be accounted for by the materials (Huang et al., 2018). Timber is proven to have a smaller environmental footprint (Lefebvre & Richard, 2014; Mallo & Espinoza, 2014). Mainly due to the capture of CO₂ during growth. Its lightweight nature may lead to secondary reductions, like less transportation and lifting emissions. Timber has proven itself as a viable construction material for bridges, as examples in Figure 1.1 prove.



Figure 1.1: Examples of timber bridges. Wennerbrücke has a 45 metre span (top left), Tynnset bridge has a 70 metre span (top right), Flisa bridge also reaches 70 metre (bottom left), and Nyberg Sundbridge spans 40 metre (bottom right) (top left picture is of Pierer (2014), the other three of Aasheim (2019)).



Figure 1.2: Map of train tracks in Norway and Sweden. With a small red square around the railway track of which the bridge in this thesis is part (Bane Nor, 2019).

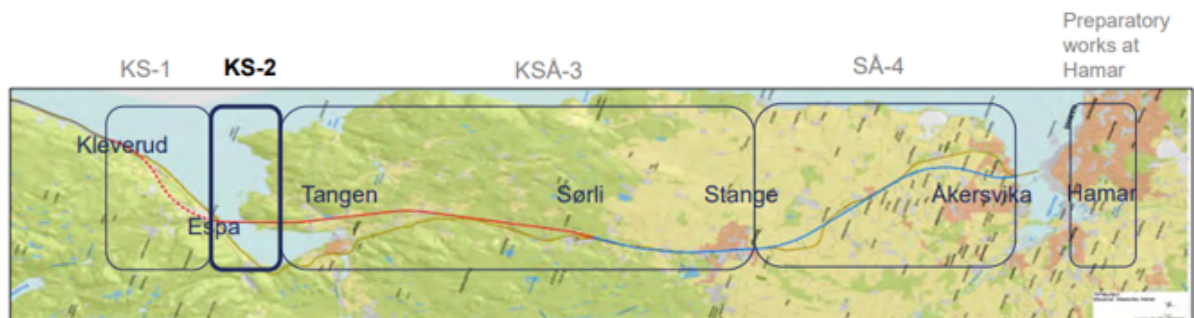


Figure 1.3: close-up map with the 30 km new double track (Bane Nor, 2019).

1.1. Motivation and objective

The Norwegian Ministry of transport has made a national transport plan concerning all infrastructure in Norway (Global Railway Review, 2018; Norwegian ministry of transport, 2021). Part of this plan is to extend the double-track railway to the north of Oslo. In Figure 1.2 the location is highlighted, with 30 km new double-track is planned to be built. Part of this new track is the longest railway bridge in Norway. The bridge crosses lake Mjøsa between Tange and Espa.

The Norwegian government invested in this new railway bridge, but Bane Nor, the Norwegian railway administrator, issued the tender for companies to design this bridge. Zwarts and Jansma Architects (ZJA) was interested in investigating a timber design for this specific project. Their number one reason was the expected lower environmental impact of using timber. The freedom of shape and form, and their strong affinity for natural environments and timber benefits, were two other reasons (ZJA, 2019). In collaboration with Iv-consult, the limitations of a stringer bridge with 50 m spans were investigated.

A short and global feasibility study was performed (Zweistra, 2020). The study compared different timber cross-sections, hollow and solid. The design height of 7 m was undesired, and high local stresses at the supports were suggested to be a difficult challenge to overcome. Connections, creep, fatigue, and dynamics were shortly or not addressed at all. It did spark the idea to investigate a design with a steel cross-section at the support and timber between the supports, to avoid large local stresses in timber elements. This design idea was the initiation of the thesis that lies before you.

It is common practice to combine steel and timber, e.g. steel-timber connections to connect beams and columns, steel shear studs to connect a timber deck to a steel beam, or timber beams with a concrete deck. However, the novel idea for this project has not been used in any current bridges to the author's knowledge. Aside from avoiding high local stresses in timber, steel can resist higher shear forces that occur at the supports than timber. The transition could be abrupt or gradual. An example of the latter is shown in Figure 1.4.



Figure 1.4: Impression of the gradual transition of timber (brown) to steel (dark grey).

Scope

The design idea of Iv-consult is based on a specific case, the double-track railway bridge in Norway. The requirements of this project are listed below, including the architectural choices of ZJA. Considering the number of challenges and the fact this idea is in a preliminary design phase, the scope is limited to only the superstructure. The design follows the requirements of the European standards. The environmental impact is only based on the amount of material.

- The bridge type is a stringer bridge, also called beam or girder bridge;
- Its total length is a little over a kilometre with a desired recurring span length of 50 m;
- Normal track with a width of 1435 mm are used;
- Train speeds up to 250 km/h.

Objective

This thesis aims to design a railway bridge in timber with a steel cross-section above the supports and investigate such a design. The design should be architecturally pleasing from the perspective of ZJA whilst considering the structural limits timber and steel impose on the design. Iv-consult is interested in understanding the possibilities to connect timber and steel at such a large scale and knowledge of the behaviour of such design. Therefore, the research objective of this thesis is to design a stringer railway bridge in timber and steel and assess it from an architectural and engineering perspective.

Challenges

There are multiple aspects that make this hybrid timber and steel design innovative. A design of a continuous beam that consists of a timber beam connected to a steel beam by means of a special connection, has not been made in the past, to the author's knowledge. Additionally, the span length is unusually long for a timber bridge and a timber high-speed railway bridge is new. The scale and difference in material behaviour of the hybrid bridge is challenging.

1.2. Research questions

The objective of this thesis can be transformed into the main research question.

Is a timber stringer railway bridge design with steel sections at the support feasible?

This question can be divided into several sub-questions.

1. What are the design considerations and requirements?
2. What is the global design of the bridge?
 - What cross-sections does the design have?
 - Where to connect the timber to steel?
3. How will the timber and steel section be connected?
 - What type of connection is suitable?
 - How does the connection influence global behaviour?
4. What results come from an architectural and practical assessment of the design?

1.3. Methodology

This thesis designs a timber railway bridge to address its feasibility. It is a design in a preliminary phase. The main research question is divided into four sub-questions representing different design process steps. Multiple iterations of these steps are necessary to reach a final construction design. However, this thesis only considers one iteration by elaborately discussing it. This process is visualised in Figure 1.5.

The first step is the concept phase. Design choices must be made to limit the number of possibilities of a bridge design. These choices follow from qualitative analyses of literature and quantitative analyses based on engineering knowledge. Following these choices, hand calculations are used to determine initial cross-section dimensions with simplified loading and strength and stiffness formulae. These dimensions are calculated as if a railway bridge was designed in only timber or only steel. The actual actions and their combination factors follow the standards and will be used as loading for the combined design. The combination of steel and timber is complex to calculate by hand, so a finite element model will be used to analyse the behaviour of the bridge.

With the concept phase complete, the combined design can be addressed. It has different cross-sections at different positions of the bridge. This is called a non-prismatic beam. The non-prismatic beam is modelled in SCIA Engineer, a finite element software, using 1D elements. The actual actions on the structure are used in compliance with the standards, and different combinations are used to simulate different train positions. The static requirements of strength and deflections are checked based on the enveloping load diagrams. With these results, the location of the connection is determined qualitatively. Dynamics play a significant role in railway bridge design. Additionally to the static checks, a preliminary dynamical analysis is performed.

The third part contains the connection design. Theory about the calculation methods of the chosen connection is explained based on literature. A promising design option is chosen from several connection possibilities that were considered conceptually. The connection effects on the bridge are reported by implementing the connection in the SCIA model. The connection is implemented via spring stiffness values since the model consists of 1D elements.

At last, the design is assessed from the architectural perspective of ZJA. Both practical and visual improvements are suggested. The environmental impact is estimated conceptually to confirm that timber has a lower impact. A definitive design is presented that follows this investigation to answer the main research question. Two alternative approaches are suggested and discussed. Concluding remarks and recommendations for future work are given.

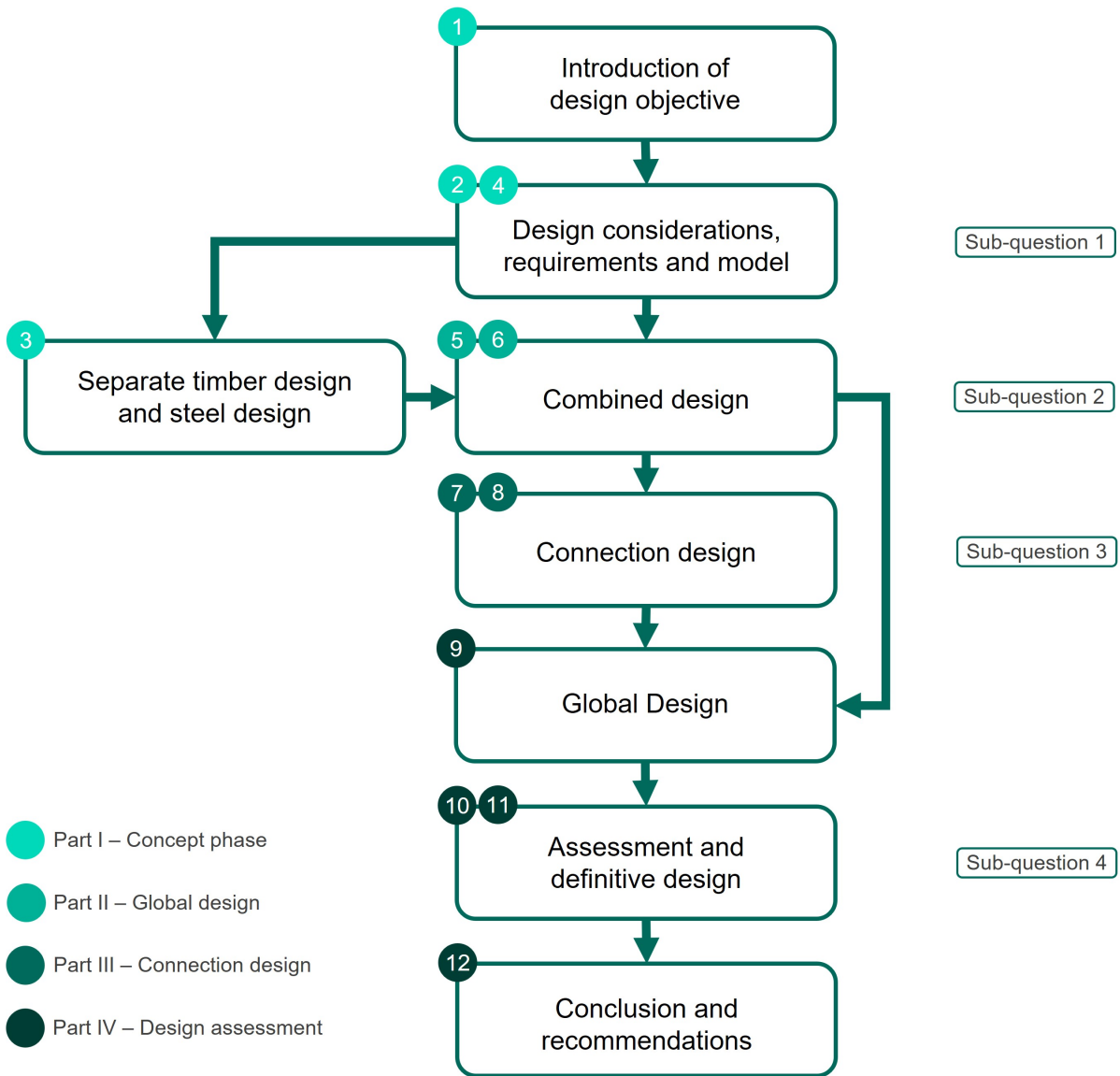


Figure 1.5: Design process of this thesis. Including colour coded chapter indication and sub-question division.

1.4. Report structure

The first chapter introduces this thesis's topic, research questions, and methodology. It contains information about the background of the project and the motivation of the objective. Research questions are constructed, and a methodology is explained in text and visual.

Part one contains chapter two, which discusses several considerations and design choices. Chapter three lists the Eurocode requirements for a railway bridge design and presents calculations for initial cross-section dimensions. The last chapter, number four, presents modelling choices and load factors and combinations to use in the second part.

In the second part, the non-prismatic bridge design is presented in chapter five. It is also called the combined or hybrid bridge. The strength and serviceability requirements are checked. Chapter six contains a preliminary dynamic analysis of the combined bridge design.

The connection is the main topic in part three. Theory from literature is explained in chapter seven. Subsequent, chapter eight discusses the connection design options, calculates the connection dimensions, and shows its effects on the global design, mainly the deflection.

Part four contains the assessment of the design. First, the design is summarised in chapter nine, and its limitations and assumptions are discussed. Chapter ten shows architectural and practical improvements from a conceptual perspective. It also considers manufacturing and handling constraints and a brief environmental impact examination. The definitive design is shown in chapter eleven. Strength and deflection checks are performed based on the new dimensions for the important instances. And two alternative design approaches are suggested.

Finally, conclusions are drawn to answer the main research question in chapter twelve. Recommendations are given for future design and research.

The bibliography containing references follows at the end. References to standards are listed separately. The appendices can be found in part five and support the main chapters, principally elaborating on calculations.

Part I

Concept phase

Design considerations

This chapter presents and discusses considerations, assumptions, and choices for the design to determine the scope.

2.1. Structural model

A structure can be modelled in many ways. The most commonly used model for a stringer bridge is a beam on supports. A beam model is a 2D representation of reality and is proven to be very accurate for bridges. Supports are considered rigid, hinged, or rollers, each with displacement and rotation constraints in different directions.

The bridge has a total length nearing a kilometre and uses recurring spans of 50 m. In Figure 2.1 three different options of beam models are shown. Simply supported will split the total bridge into a number of simply supported bridges, Figure 2.1a. The disadvantage is large bending moments at midspan. A second option, Figure 2.1b, shows a continuous beam. The bending moments at midspan are reduced whilst introducing bending spans at the support. It is advantageous since the extreme bending moment is reduced. It does lead to higher cross-sectional forces at the support. The last model, Figure 2.1c, is a mechanism. If the hinges have some rotational capacity, the bending moment at midspan will be almost zero. It becomes two cantilever beams that are connected at midspan. The large deflection of the hinge is far from ideal.

The continuous structural model is ideal for this project. It reduces extreme moments and has more favourable deflection values. The steel cross-section above the support must resist shear force and a hogging bending moment. The timber only requires to withstand a large sagging moment at midspan, though this is much lower compared to the simply supported model.

2.2. Span length

The total length of the bridge is around a kilometre. The architect desires a repeating span length of 50 m. The bridge length and the specific span layout will influence the design. Temperature and the outer span length are factors that influenced this choice.

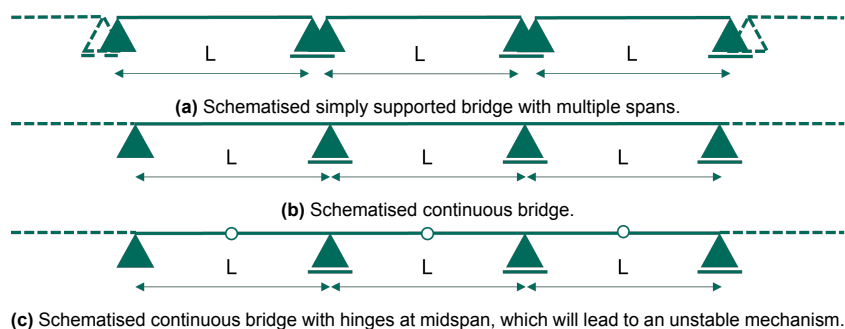
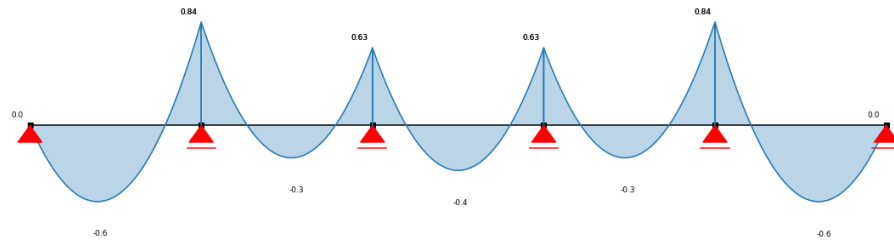
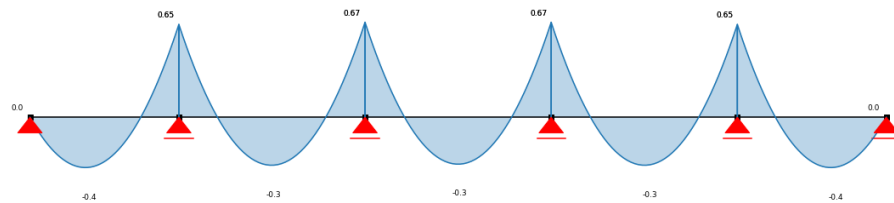


Figure 2.1: Different schemes of a bridge structure.



(a) Moment distribution of five span continuous beam with equal spans.



(b) Moment distribution of five span continuous beam with 0.8L outer spans.

Figure 2.2: Moment distribution for constant stiffness and distributed load in terms of $qL^2/8$.

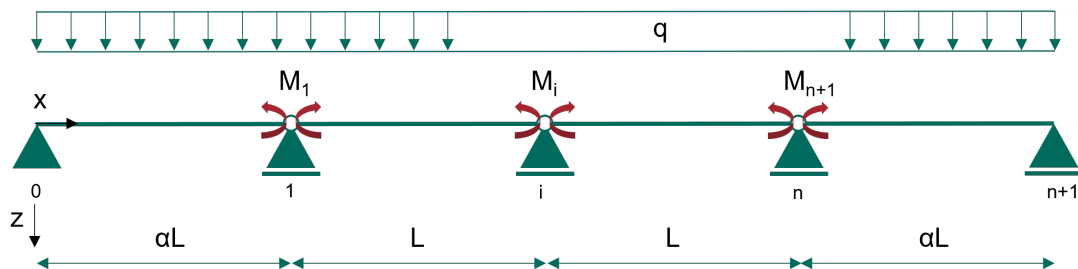


Figure 2.3: Continuous beam with introduced hinges and unknown moments.

2.2.1. Outer span length

At the outer two supports, the bending moment is zero. In Figure 2.2a the bending moment diagram of five equal spans with constant stiffness and distributed load is presented. Clearly visible is the larger hogging and sagging moment in the outer spans. There are two options: constant construction height and a repetitive design. The first is to change the outer span length. This leads to a bending moment distribution in which the extreme values are similar for each span. The second option is to have a semi-rigid outer support. Such a support is difficult to make and often expensive. For this thesis, the latter option has been disregarded.

Analytical and numerical tools are used to determine the outer span length to achieve less deviation between extreme bending moments. The structure is indeterminate and can be solved with the force method. This method transforms an indeterminate structure into a determinate structure with additional unknowns, shown in Figure 2.3. To solve for the unknowns, boundary and compatibility conditions are used. In Appendix A.2 the analytical derivation is shown. The additional variable α is introduced, representing the non-dimensional outer span length dependent on the main span length.

It is desired to find a value for α that leads to a minimal deviation between each sagging bending moment and each hogging bending moment. For many values of α , the analytical solution is calculated using Python. The result is shown in Figure 2.4. It shows that a value of approximately 0.8L results in equally large hogging moments at all intermediate supports. Equally big sagging moments occur in the outer and main spans also at approximately 0.8L. The value of 0.8L is chosen. A representation of the bending moment diagram with this outer span length is shown in Figure 2.2b.

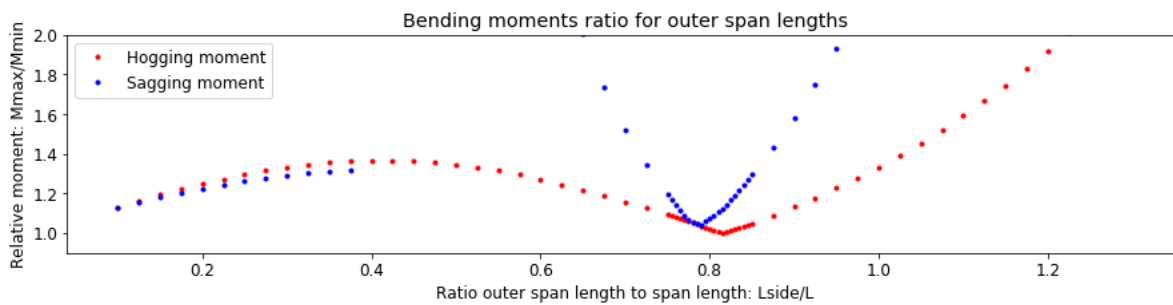


Figure 2.4: Bending moment ratio with different outer span ratios.

2.2.2. Temperature effect

Materials expand and contract due to temperature changes over time. The temperature has a significant influence on the axial deformation of long bridges. Expansion joints are necessary and are a critical detail for track design. Maurer guided cross-tie railway expansion joint is an example that is specifically designed to close up to 1600 mm railway gaps (Maurer, 2015). In Spain, rail expansion joints for long bridges are available (Garcia-Sanchez et al., 2021), common for concrete bridges. Expansion joints in China for high-speed rail can cover displacements up to 1000 mm (Guo et al., 2018).

The axial deformation for a kilometre long steel bridge when assuming 40 °C change in temperature can be up to 266 mm. The calculation can be found in Appendix A.1. There are expansion joints that can span this potential gap. To limit the complexity and costs of the expansion joint, the bridge can be divided into several parts to have several independent bridges in sequence. ZJA states that dividing the bridge into several parts would be more architecturally appealing if it were an odd number.

The difference between modelling 8 or 21 spans is negligible. However, modelling fewer spans will be computationally less expensive.

2.2.3. Span distribution

The bridge is modelled using eight spans, of which the two outer spans have a length of 0.8L. This leads to three bridge parts with smaller outer spans but a different number of intermediate spans to reach the required kilometre length. To be precise, two parts have five intermediate spans, and one has six intermediate spans.

2.3. Cross-section

Several considerations have to be taken into account for the cross-section. The type and geometry, for example. These considerations and their justification and impact are presented in the following sections.

2.3.1. Type

Railway bridges have a higher ratio of live-to-dead loads than pedestrian or road traffic bridges. There are two tracks with a specific position that introduce the large loads. Two types of steel beam bridges exist—a box girder and a plate girder. Since the live load is large, eccentricities can lead to substantial torsional effects. A box girder can resist torsion much better than a plate girder bridge.

The double-track could rest on a single box girder. However, the torsional loads from a single train crossing the bridge would be immense, especially since the eccentricity is very large to have sufficient spacing between the tracks. An initial design attempt seemed not feasible to resist such high torsional stresses with timber. It is chosen to have two separate box girders. From a structural point of view, these are considered to be not connected regarding calculations.

Timber cross-sections are often parallel beams or large solid cross-sections. Although no examples have been found of timber box girders, Aicher and Stapf (2014a) shows box girder block glulam sections that follow from DIN 1052-10:2010. The reason to not find box girder timber bridges is, most likely, their low shear strength. A large shear area is required to resist the loads at the support.



Figure 2.5: Concrete railway bridge examples with varying construction height. Specifically the Zeelandbrug and the Xiangbahe Railway Bridge

Connecting a timber and steel cross-section is expected to be beneficial when both have a similar cross-section. The steel section takes the high shear loads so that the timber section can reduce its shear area. This thesis continues with a box girder type bridge where both materials have a box girder cross-section.

2.3.2. Width

In the previous study (Zweistra, 2020) a required total width of 12 m was determined. This included the tracks, spacing between the tracks, and non-public footpath space. The cross-section is now split into two sections that carry a single railway track. There is some space required between the two box girders. This space can accommodate a link between the box girders for stability and a maintenance or inspection path. It is not considered in the design part of the thesis but highlighted in the final part. The two box girders thus only require to carry the tracks and moving trains. The width of a single box girder is chosen to be 4 m.

2.3.3. Height

The construction height can be optimised in bridges to, for example, reduce the amount of material. In Figure 2.5 two concrete bridge examples are shown using this optimisation. Such an optimisation would improve very little for this bridge while increasing its deflection. A constant construction height is preferred from the design perspective. This also adds to the continuity and repetitive visual appearance.

2.3.4. Web distance

The train loads are introduced via the rails and transferred via a track structure to the bridge. The webs are the main shear force resisting parts of the cross-section. Logically the webs would benefit from being precisely underneath the tracks. This limits the transverse bending of the deck.

2.4. Steel

Steel is one of the most used construction materials alongside concrete. Advantageous qualities are its high strength and high strength-to-weight ratio, ductile behaviour, and stiffness. Its high strength can resist high loads and result in, often, visually pleasing slender designs. Ductile behaviour is the ability to deform under load without breaking, especially ductile failure is desired in engineering since it gives users a warning before failure. Stiffness is the main contributing factor considering deflections, rotations, and dynamic behaviour. Especially important in railway engineering such that trains will not derail. The material is isotropic, behaving the same in every direction.

Commonly and most used construction steel is S355, although higher strength steels (hss) have increased in popularity in both research and construction (Ban & Shi, 2018; Bjorhovde, 2004; Miki et al., 2002; Shi, 2012). Higher grade steels lead to even more slender designs and carry a higher load while contributing less to the self-weight. The disadvantage of hss is its reduced ductility at peak stress and its buckling governed design. Another disadvantage is its lower fatigue strength, leading to S355 being the highest grade often used in steel railway bridge design (Iles et al., 2004, Chapter 8).

The timber cross-section is already expected to be larger than the steel cross-section. Having higher grade steel would only increase the difference. For this reason and its fatigue strength, S355 is chosen in this thesis.

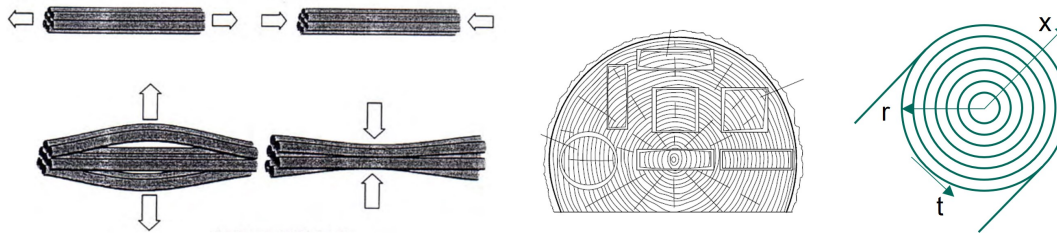


Figure 2.6: Anisotropy of wood explained via multiple figures. Behaviour of wood fibres (left, Angst et al. (2008)), different locations of planks (middle, Angst et al. (2008)), and the main directions, x is axial, r is radial, and t is tangential, of wood (right).

2.5. Wood

Wood is a natural resource and a collective term for an abundant set of species worldwide. It is divided into two groups, softwood and hardwood. This division is based on their cellular structure. Softwood has a simple structure, and hardwood a more complex. In most cases, softwood is weaker than hardwood. This thesis does not present an in-depth explanation of wood at a microscopic level as it is not required for a design. More information on wood and its cellular structure can be found in books such as *Handbook 1 Timber Structures* by Malo (2016) and *Timber Engineering - Principles for Design* by Blass and Sandhaas (2017).

2.5.1. Properties

The fibre distribution is not equal in each direction. Therefore the properties of wood are dependent on the direction. It is an orthotropic material. Wood grows primarily vertical but also outward. It has three directions in which the properties are different. The axial, radial, and tangential directions are shown in the right of Figure 2.6. For engineering practice, a reasonable approach is to consider radial and tangential properties the same, especially for glued laminated timber, which consists of a combination of planks that have an arbitrary radial and tangential direction, visualised in Figure 2.6. The axial directions are defined as parallel-to-grain and the other two as perpendicular-to-grain, of which the latter is the weakest direction.

Naturally grown wood has defects. Branches from the tree's main stem result in a local change of direction of the fibres, thus a change of grain. A cut-down tree sawn into a beam will randomly scatter these defects along the beam. The defects are called knots and are weak points. The amount and size of knots and other imperfections determine the strength class of timber when visually graded.

Wood can have a significant variation in properties, even within single species. A member's strength decreases when its size increases. This phenomenon has been the topic of wood research for almost a century. Bohannon (1966) developed a theory for a size-strength relationship for wood, explicitly bending. The theory was based on the weakest link theory, also called brittle fracture theory, of Weibull (1939). The larger a beam, the higher the probability of weak elements that can start failure. An example to explain this phenomenon is having a wooden beam divided into tiny elements. Each element has individual properties based on a distribution, for example, strength. The larger the beam, the more elements there are, and thus a higher probability for an element to have low strength. Buchanan (1990) also uses this theory to argue that the tensile strength in bending is larger compared to pure tension. A smaller part is in tension, thus a lower probability that the weakest element is situated in the tensile zone. Therefore the bending strength is larger than the tensile strength for wood and thus for timber. This has been proven to be true in several research studies.

Madsen and Buchanan (1986) gathered over 17 000 tests to determine the influence of parameters such as length, load configuration, depth, stress distribution, breadth, length in series, and grading. It quantified values for different size effects. These size effects are used in design standards.

2.5.2. Time-dependent influences

As wood is an organic material, its properties are dependent on the environment it is in. It also has time dependencies.

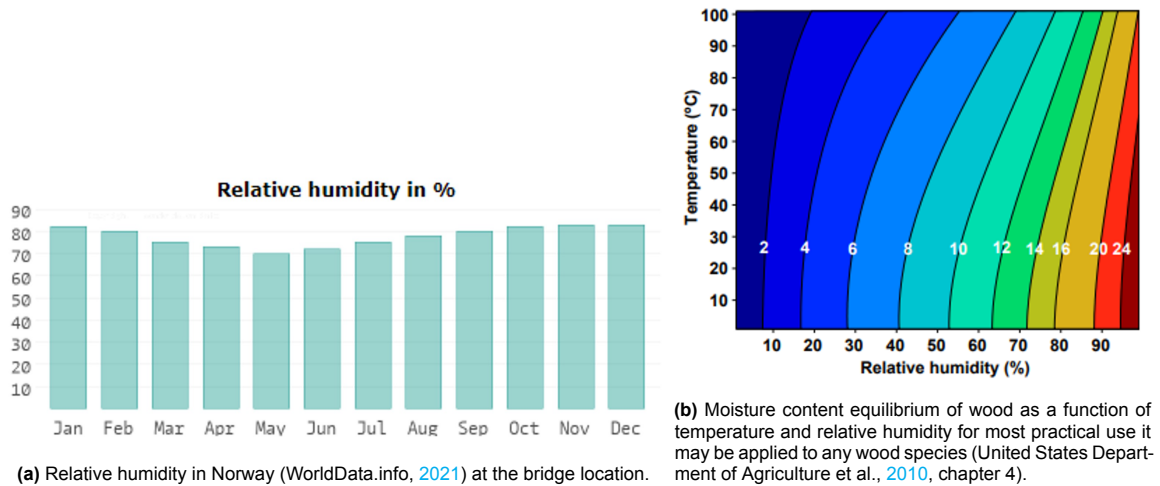


Figure 2.7: Graphs to determine expected moisture content equilibrium of timber.

Moisture content

Moisture content (MC) is one of the main contributing factors that change material properties. For an explanation on a microscopic level, see Blass and Sandhaas (2017, chapter B2). From an engineering perspective, it is important to know that an increase in MC leads to a decrease in stiffness, increase in creep deformation, and increase in the risk of fungal infection. A critical MC of 20% is used as a boundary value. Above this limit, wood degrades fast, which should be avoided.

In Norway the maximum average relative humidity is almost 85%, shown in Figure 2.7a, and its average temperature is -5°C in winter and 20°C in summer (WorldData.info, 2021). Extracting the equilibrium MC from Figure 2.7b gives an MC of less than 20%. Protective measures are not required, if the elements are not directly exposed to water.

Suitable protective measures used to be chemical preservatives such as creosote, which has protected many timber structures (Ritter, 1990). Although currently, it is undesirable to use chemical protection (Blass & Sandhaas, 2017). Another protective measure is to structurally protect timber elements, which is essential to compete with alternative building materials according to Liuzzi et al. (2020) and Simon and Koch (2016).

In addition to the effect on wood properties, it also affects the size of wood. Wood is a hygroscopic material; shrinkage and swelling occur when the MC changes. Structural timber has an MC between 8 and 20% (Blass & Sandhaas, 2017).

Each direction has a different coefficient of moisture expansion and contraction (CME & CMC). Tangential and radial directions have larger coefficients than longitudinal directions. The shrinkage in the tangential direction is around 1.5 times more than in the radial direction (United States Department of Agriculture et al., 2010, chapter 4). Glulam has an arbitrary orientation of tangential and radial direction and thus has an average transverse coefficient. An extensive experimental study of shrinkage and swelling of glulam showed that the CME and CMC in the transverse direction was an order of magnitude larger than in longitudinal direction (Chiniforush et al., 2019).

Creep

Sustained loading during a structure's service life leads to a deflection that increases over time in. Dependent on the material a significant additional deformation can occur. The tendency of a material to deform under sustained loading is called creep. It is effected by moisture content, duration of loading, temperature, and level of stress (Blass & Sandhaas, 2017). The first two factors are covered by the use of the creep factor k_{def} in EC5, the latter two have a lower impact.

Permanent loads on the structure are the sustained loading under which creep will occur. In bridge design a precamber is often used to nullify creep deflections and immediate permanent load deflections.

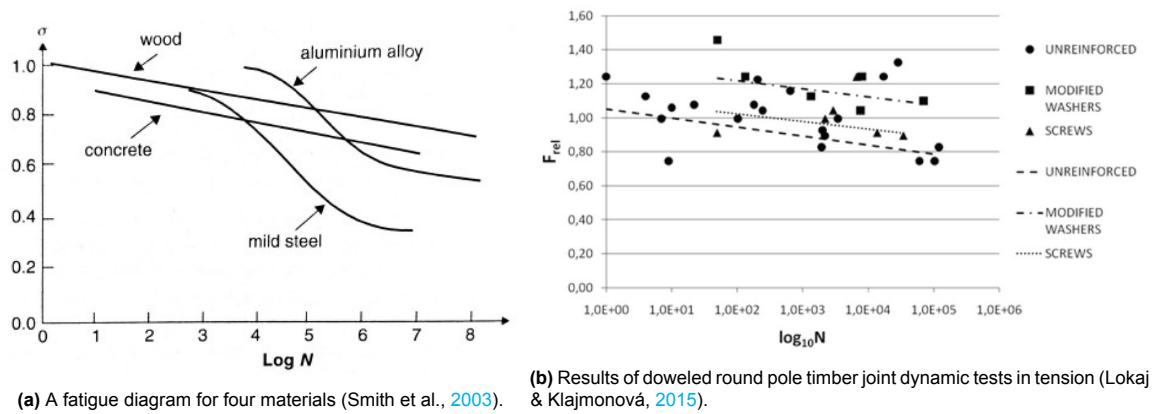


Figure 2.8: Fatigue diagrams.

Fatigue

A material that undergoes cyclic loading will suffer from fatigue. Fatigue is the crack initiation and propagation that follows from cyclic loading that results in stresses less than the tensile strength. It is possible for a material to resist a single load close to its strength, but to fail after millions of cycles of a very low load. Many repetitions of loads closer to the material's strength can also lead to fatigue failure. For steel bridge design, fatigue is a concern and often governing in design.

Wood is much better suited to resist high repetitions of loads (Jutila, 2003). Figure 2.8a shows fatigue curves for four different materials. It is important to note the logarithmic scale on the horizontal axis. While mild steel has a significant drop between ten thousand and one hundred thousand cycles, wood linearly decreases.

Connections in timber are critical. There is research into fatigue on different timber connections, but this is by far not as extensive as for steel. An experimental research to a doweled connection loaded in tension (Lokaj & Klajmonová, 2015) does show a similar trend as plain wood, see Figure 2.8b. Research on glued-in GFRP rods (Madhoushi & Ansell, 2008a, 2008b), on CLT structures (Gavric et al., 2015), and a bolted connection with cracks (Zhang et al., 2021), focus partly on the energy dissipation under cyclic loading. This is primarily important for earthquake design. Eurocode 5 does not contain any methods to calculate fatigue for timber connections of the current structure scale.

The result of cyclic loading tests of slotted-in steel plates observed that the initial stiffness drops quickly after the first few cycles and then a steady state is reached (T. Reynolds et al., 2014; T. P. Reynolds et al., 2018). This was also found in an experimental research on steel cross-beam to timber girder connection. After a few hundred thousand cycles the connection stiffness reduction was negligible (Gocál & Odrobiňák, 2019).

T. Reynolds et al. (2014) specifically looked at a reversal and two non-reversal states, $R=-1$, $R=1.2$, and $R=10$. R-ratio is the maximal loading force over the minimal loading force. The tests represented in-service structural vibration and were done with peak loads of 20% and 40% of the predicted yield load according to EC5. It was concluded that the Eurocode method to calculate stiffness underestimates the stiffness of non-reversal loading states. Damage due to the cyclic loading was not considered, and fatigue strength was not investigated.

Fatigue is touched upon in this thesis to a limited extent for two reasons: the lack of knowledge of fatigue in timber connections and the focus on the connection under the assumption the steel section can be designed to comply with the requirements for there is sufficient knowledge to design steel to not fail in fatigue. In Chapter 5 steel details are checked with a fatigue calculation.

2.6. Timber

Timber is wood that is manufactured to be used in structural applications. It has been used for centuries as a building material. With the introduction of concrete and steel, timber has been replaced as a building material. Most bridges that have been built in the past few decades have been made with



Figure 2.9: An example of a trestle bridge, the Kinsol trestle in Victoria, Canada.

concrete and steel, even though timber bridges can be competitive, especially for small spans. The project DuraTB (Pousette et al., 2017) states that recent interest in timber bridges has risen by increasing environmental awareness. Though, there always has been a significant amount of timber bridges in use in Scandinavian countries (Aasheim, 2019) and the United States (Ou & Weller, 1986). There are many design guides for timber bridges (Malo, 2016; Ritter, 1990).

Typically timber bridges were constructed with sawn wood, limiting the size and load-bearing capability. But with the development of engineered timber products, like glued laminated timber (glulam) and laminated veneer lumber (LVL), these limitations have changed for the better. Four typical structural elements in timber bridge design are glulam members, stress laminated decks, slotted-in steel plates, and steel cross girders (Aasheim, 2019). Glulam members provide the main load-bearing structure, while slotted-in steel plates connect the different members with dowels or bolts. CLT decks, or stress laminated decks, have good performance for smaller point loads such as pedestrians and low-speed road traffic.

Small timber bridges can be built using main beams, crossbeams, and a deck. For longer spans, glulam trusses or glulam arches are viable options, as shown in Figure 1.1. Spans of almost a hundred meters can be achieved with trusses (Gilham, 2015). There are plenty of examples of current road traffic and pedestrian bridges, though not for rail traffic. In North America, many trestle bridges have been built in the past. The downside of this design is the limited clearance, the lower allowed speeds, and labour intensive execution, as can be imagined seeing Figure 2.9.

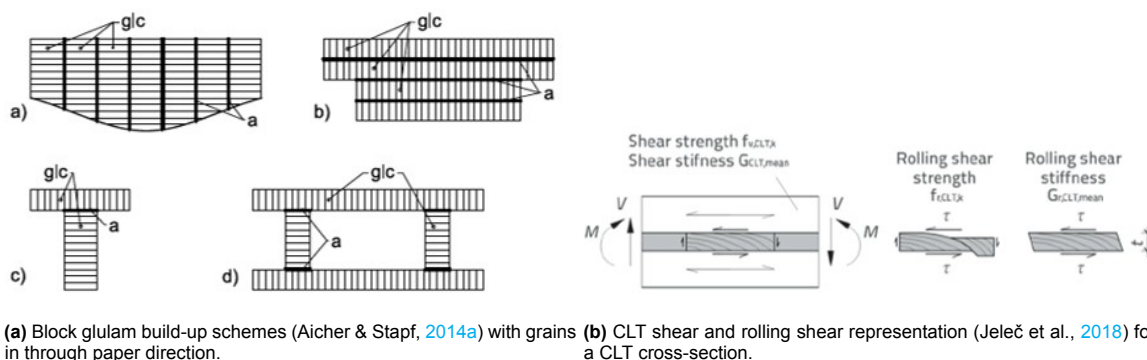
2.6.1. Engineered Wood

A wide variety of wood products exist. Engineered wood comes in all shapes, sizes, strengths, stiffness, etc. A benefit of engineered wood is the possibility of removing defects and creating shapes and sizes that do not occur naturally. It also provides means to increase mechanical properties in weak directions by specific arrangement.

Most commonly used in structural engineering are glulam, cross-laminated timber (CLT), and LVL. Glulam is used to form block glued laminated timber, see Figure 2.10a, to create bigger cross-sections. The lamella size cut from trees limits glulam size. Each product combines wood and an adhesive.

Glulam

Glulam consists of wooden planks, called lamellae, that are finger-jointed together to create longer planks. Lamella size is limited by tree size. A maximal thickness of 280 mm can be achieved, generally. Beams are formed by stacking and glueing individual lamella. All planks are stacked such that the grains are in the axial direction. It is primarily used in long spans since it has an excellent bending



(a) Block glulam build-up schemes (Aicher & Stapf, 2014a) with grains (b) CLT shear and rolling shear representation (Jeleč et al., 2018) for in through paper direction.

Figure 2.10: Block glulam cross-sections and rolling shear in a CLT cross-section.

moment resistance in one direction. It is produced with softwood, though interest is increased to create glulam with hardwood to form stronger elements (Morin-Bernard et al., 2021). Finger jointing hardwood lamellae together pose a challenge for hardwood glulam (Aicher & Stapf, 2014b; Tran et al., 2016). The finger joint strength becomes governing due to the higher tensile strength of hardwoods. Current models are not sufficient for high strength hardwoods.

CLT

CLT is built similarly to glulam, though plates are created instead of beams. The lamellae are stacked, alternating their grain direction. The strength and stiffness of such a plate are (almost) equal in both plate directions. Generally, it is used as floors and walls in buildings. But in bridge design, it can be used as a deck. The cross-layers introduce an additional failure mechanism, rolling shear, shown in Figure 2.10b. Rolling shear strength is dependent on the perpendicular-to-grain shear strength, which is even lower than normal timber shear strength.

LVL

LVL is used to create both beams and plates. It is built of veneer sheets and also glued together. The veneer sheets are very thin. It is a cheap alternative and used in a variety of situations. It is less often used for large structures as it is made in standard sizes smaller than glulam.

2.6.2. Timber selection

All three engineered products are stronger than sawn timber, mainly because defects get cut out. Additionally, these products can be used to form non-standard cross-sections. Glulam is often used in larger constructions. It performs better than LVL in terms of exposure to the environment. CLT is advantageous for plated structures. The cross-section will consist of plates arguably. However, it is reasonable to assume that it predominantly acts as a beam structure. Therefore the cross-section will be chosen to be made of only glulam.

2.6.3. Glulam properties

The properties of different glulam strength classes are found in EN14080. Table 2.1 shows the characteristic values for homogeneous glulam members. The shear strength and stiffness values do not differ per strength class. Shear is not often governing in timber design due to the fact relatively wide members are used (André & Kliger, 2009). Although shear is often considered conservative, these values are used in the design. The assumed strength class to be used in this design is GL30h.

The table shows clearly the much lower values for perpendicular-to-grain and shear properties. These are very important in design, as they are often the limiting factor.

2.7. Tracks and speed

An additional component in the design of a railway bridge is its track structure. Aside from the vast loads, more strict requirements, dynamic limitations, and increased complexity, the track structure requires specialists to design. The track system consists of rail beams, sleepers, ballast or slab, and fasteners.

Property	Symbol	GL20h	GL22h	GL24h	GL26h	GL28h	GL30h	GL32h	
Bending	$f_{m,g,k}$	20	22	24	26	28	30	32	MPa
Tensile	$f_{t,0,g,k}$	16	17.6	19.2	20.8	22.3	24	25.6	
Compression	$f_{t,90,g,k}$				0.5				
	$f_{c,0,g,k}$	20	22	24	26	28	30	32	
Shear	$f_{c,90,g,k}$				2.5				
	$f_{v,g,k}$				3.5				
Rolling shear	$f_{r,g,k}$				1.2				
E-modulus	$E_{0,g,mean}$	8400	10500	11500	12100	12600	13600	14200	MPa
	$E_{0,g,0.5}$	7000	8800	9600	10100	10500	11300	11800	
	$E_{90,g,mean}$				300				
	$E_{90,g,0.5}$				250				
G-modulus	$G_{g,mean}$				650				
	$G_{g,0.5}$				540				
Rolling shear modulus	$G_{r,g,mean}$				65				
	$G_{r,g,0.5}$				54				
Density	$\rho_{g,k}$	340	370	385	405	425	430	440	kg/m ³
	$\rho_{g,mean}$	370	410	420	445	460	480	490	

Table 2.1: Glulam strength class properties copied from table 5 in EN14080.

Several different systems exist to use for the track structure. Ballast track is the most commonly used system, while a non-ballast track is often considered in special cases.

2.7.1. Ballast track

Ballast track consists of rail beams connected to sleepers, sleepers embedded in ballast material, and a layer between the ballast and the subgrade. The subgrade is the soil on which the railway needs to rest. The ballast ensures a transfer of forces of the rail beam, via the sleepers, to the subgrade, such that the subgrade will not fail. The main upside of ballast track is its cheap production and installation (Colla et al., 2002), but also the good damping effects, good drainage behaviour, and easy maintenance (Esveld, 2005).

Maintenance also proves to be a costly downside. Annually between 100.000 and 200.000 sleepers require replacement in the Netherlands. In the United States, Canada, Germany, and Australia, millions more require replacement each year (Silva et al., 2017). Although research presents new and better sleeper options, with a longer service lifetime (Manalo et al., 2010; Senaratne et al., 2020; Silva et al., 2017), the main reason for the maintenance is the degradation of the ballast material (Esveld, 2001), not the sleeper quality.

2.7.2. Non-ballast track

There are several non-ballast track systems of which slab-track is most often used. The rail beam is connected to sleepers that are either connected to a concrete slab or embedded in this slab. Advantages compared to conventional ballast track are its weight, increased service life with less maintenance, and low construction height. It has a higher initial cost, but during its service life, costs are significantly reduced. Silva et al. (2017) concluded that the lower life-cycle costs are the main reason slab track is more cost-effective.

Slab track for high-speed rail in Germany uses RHEDA systems (Esveld, 2003). These systems are a product of RAIL.ONE. The RHEDA2000 system, shown in Figure 2.11, is the current non-ballast track that is used in Europe and Asia (Rail One, 2011). It performs very well for high-speed rail. It is the track system chosen for this project. Only its weight is considered, which is estimated in Appendix B.1.

2.7.3. Train speed

This thesis has little information on the use of this rail line or its allowed speeds. The Norwegian government has a new National Transport Plan, which invests in railroads. The plan is to have multiple

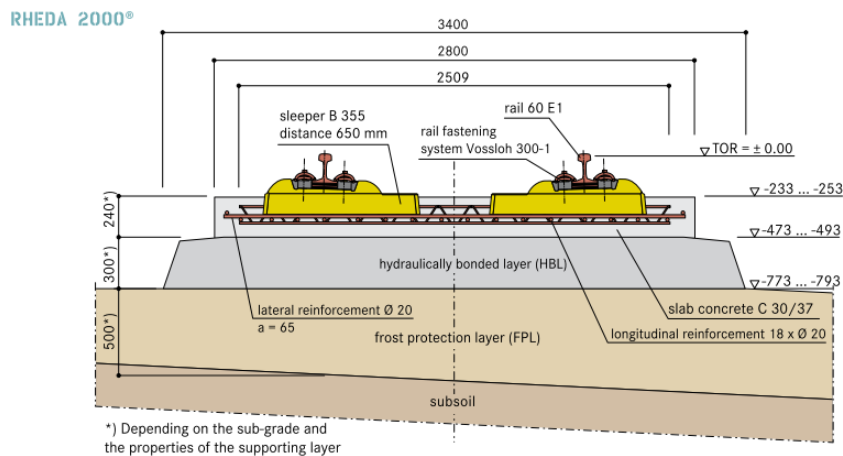


Figure 2.11: RHEDA2000 system cross-section drawing (Rail One, 2011).

railroads which can allow high speeds up to 250 km/h (Global Railway Review, 2018). Currently passenger trains and freight traffic are slow in Norway, average speeds are under 100 km/h (Kalstad, 2017). High-speed rail traffic is subjected to more strict dynamic and deflection requirements to prevent derailment. The bridge and train dynamics are explained and addressed in Chapter 6. The strict deflection requirement for passenger comfort is chosen for a design speed of 250 km/h.

2.8. Loading

Structures are subjected to all kinds of different loads. A railway bridge is no exception. EC1 presents all sorts of loads and how to determine their value. This section only discusses the loads that are considered in the design. The value determination can be found in Appendix B, and the combination of loads and their factors are presented in Chapter 4.

Train traffic

Traffic loads on bridges are specified in EN1991-2. There are several loading models for different loading situations. The most used and basic, and therefore also most conservative, are the load models LM71, SW/0, and SW/2. These load models are used for strength and serviceability design. SW/0 is used for continuous bridges, although it is not stated that LM71 can be neglected in that case. The SW/2 load models represent heavy train traffic. All three should be used to determine the static effect for regular track in Europe.

HSLM-A and HSLM-B are separate load models for railway bridges to model high-speed trains. These are specifically used for the dynamic analysis of railway bridges.

In the case of fatigue calculation, multiple fatigue load models can be found in the annexe of EN1991-2. These models can be used to achieve less conservative results compared to the standard three load models. LM71, SW/0, and SW/2 are also allowed for fatigue but generally result in higher fatigue stresses.

At last, the models are allowed to be real trains if specified for the project. When specific information about the use of the track and what trains are allowed on it, these models suffice.

This project does not specify any train traffic or load models to use. For this preliminary design, the three standard load models are used. The dynamic load models HSLM-A and HSLM-B are not considered since the dynamics is assessed more simplistically in Chapter 6. The fatigue load models are not used so that the fatigue train loads will be conservative.

Each train model, LM71, SW/0, and SW/2, has accompanying horizontal and axial loads. Horizontal loads consist of a small nosing force. The centrifugal force in curved bridges has not been considered. The bridge is assumed to be straight. Axial loads occur due to either acceleration or braking of the train. There are maximum values for the braking and traction force. It depends on the length of the load model, and while LM71 has an infinite length, SW/0 and SW/2 do not. Thus the axial force from

those models is always smaller. Therefore calculations are performed conservatively with the maximum value for the axial force according to the LM71 model.

Wind

Wind forces are exerted on a structure by means of pressure differences. Horizontal wind loading does not require an explanation, vertical wind loads however, do. Due to turbulence, wind can act on a bridge under an angle. This leads to possible downward and upward loading. This turbulence can also induce vibrations. However, the bridge has relatively small spans compared to its cross-section, so wind-induced vibrations are neglected in this thesis.

Temperature

Loading due to temperature change has two effects. The first is axial and already explained in Section 2.2. This load is not considered since the structure is free to move in axial direction. The fact a continuous beam is used restricts the free movement of the structure due to a change in temperature through the cross-section. The top of the cross-section will heat up while the bottom stays cooler. The bridge bends upward and is restrained, thus introducing additional bending moments.

Snow

In Norway, snow loads can become quite large. According to the standard, snow loads on bridges do not need to be combined with trainloads. Since the snow load is smaller than the trainloads, a load case with only snow is expected to result in much lower forces and thus not governing. There was no available national standard of Norway to deviate from this general approach.

Non-public footpath

Variable loads on non-public footpaths were not considered in the loading analysis, as it would not be safe to have persons walking next to a track with active trains. In the case of an evacuation a train and passengers will be simultaneously loading the structure. However, the load will not increase when passengers evacuate the train, it will only shift.

3

Single material design

This chapter presents three cross-section designs that satisfy limit states stated by the Eurocode. These designs are the backbone for the actual design. Each cross-section is checked by use of hand calculations that follow from EC. The first section addresses loading to get a single distributed load value. It also presents the global limit states of the design. The following three sections show what cross-section can satisfy the limit states. A single timber box girder and two steel box girder sections are calculated. Loads are expected to be conservative. Local checks are disregarded, except for a class 4 section. The goal is to have a cross-section that complies with the limits.

3.1. Loading and limit states

A single distributed load is determined to get a simplistic approximation of the cross-sectional forces. The determination of the loads can be found in Appendix B.

- 40 kN/m self weight estimate;
- 45 kN/m weight of track structure, estimate of RHEDA2000 system weight;
- 8 kN/m downward wind force, resultant of 4 m width;
- 22 kN/m sideways wind force, resultant at track rail level of 4 m bridge and 4 m train;
- 133 kN/m SW/0 train load, with an eccentricity of 80 mm see Appendix B.2;
- 80 kN/m LM71 train, necessary for specific SLS;
- 6000 kN maximal possible horizontal forces from traction or braking according to EN1991-2

Several limit states require different loading combinations and have different safety and load combination factors. The factors are presented in Section 4.2. For ultimate limit state (ULS), a safety factor, a train weight factor, and a combination factor are used. There are three combinations to consider in the serviceability limit state (SLS). The characteristic, quasi-permanent, and frequent combination. Normal deflection is checked with the characteristic and creep deflection with the quasi-permanent combination. A frequent load combination without permanent loads and only LM71 is used for the passenger comfort limit in accordance with clause A2.4.4.3.2 (2) EN1990. The train weight factor can also be ignored in the frequent combination.

	perm		live wind		live train			
$q_{z,uls}$	=	1.15 * 85	+	1.13 * 8	+	1.93 * 133	=	363 kN/m
$q_{y,uls}$	=			1.13 * 22			=	25 kN/m
$q_{t,uls}$	=			1.13 * (22 * 2 + 8 * 1)	+	1.93 * 133 * 0,08	=	70 kNm/m
$N_{x,uls}$	=					1.93 * 6000	=	11 580 kN
$q_{z,sls}$	=	1.00 * 85	+	0.75 * 8	+	1.33 * 133	=	268 kN/m
$q_{z,passcomf}$	=			0.50 * 8	+	1.00 * 80	=	84 kN/m
$q_{z,quasi}$	=	1.00 * 85			+	1.33 * 133	=	262 kN/m

To check ULS, the cross-sectional forces are calculated using a beam model with two supports. In Figure 3.1 two beam models are shown with their bending moment and deflection formulae. A continu-

ous beam can be simply modelled as one of these models depending on the loading situation. Model A3 can be used when loading is present at each span. Model A2, on the other hand, is used when a span is loaded and the next is not, which can be the case for a train passing the bridge. The permanent load is present at each span, and thus model A3 is used. However, this will be conservative since flanking spans will bend and resist part of the load. It is fine for this preliminary design. The box girder is assumed to be supported by two bearings, such that torsion is restricted at each support. The cross-sectional forces for ULS are presented in Table 3.1.

	At support	At midspan
$M_{y,Ed}$	113.44 MNm	63.81 MNm
$M_{z,Ed}$	7.81 MNm	4.39 MNm
$M_{T,Ed}$	1.98 MNm	0 MNm
$V_{z,Ed}$	9.08 MN	0 MN
$V_{y,Ed}$	0.63 MN	0 MN
$N_{x,Ed}$	11.58 MN	11.58 MN

Table 3.1: Cross-sectional forces of single distributed load for ULS.

Deflection

Only vertical deflection, which will be the governing one, is considered in this phase. Due to permanent and live loads, bending deflection uses a different mechanics model requiring a different formula. In addition to bending deflection, shear deflection is also accounted for. Shear deformation can be calculated using Equation (3.3), irrespective of the models.

$$w_{EI,perm} = \frac{q_{perm}L^4}{384EI} \quad (3.1) \quad w_{EI,live} = \frac{2 \cdot q_{live}L^4}{384EI} \quad (3.2) \quad w_{GA} = \frac{qL^2}{8GA_{eff}} \quad (3.3)$$

There are three SLS deflection limits, of which each checks a different loading combination. The deflection from the characteristic loading combination should not exceed a limit of $L/600$ according to EC0 clause A2.4.4.2.3 (1). The limit for creep deflection is the same, but it checks the quasi-permanent loading. The passenger comfort limit can be calculated using Figure 3.2 and clause A2.4.4.3.2 (5) in EN1990. It results in a value of $L/(1900 * 0.9)$ for train speeds up to 250 km/h. The frequent loading combination deflection is checked against this limit.

A general deflection limit of $L/600$ according to EC0 clause A2.4.4.2.3 (1). It should account for all permanent and live loads with the characteristic load combination. The creep deflection limit is the same but requires the quasi-permanent loading combination. The difference with the characteristic combination is the use of ψ_2 instead of ψ_0 , which is generally a smaller number. In the case of train traffic, however, a note in EC0 states that a value of 1 should be used for ψ_2 . The creep deflection is the normal deflection plus a time-dependent part that multiplies the normal deflection. A simplified calculation method is presented in section 2.2.3 in EC5. The factor k_{def} is used.

The deflection should be increased according to the simplified calculation method in section 2.2.3 in

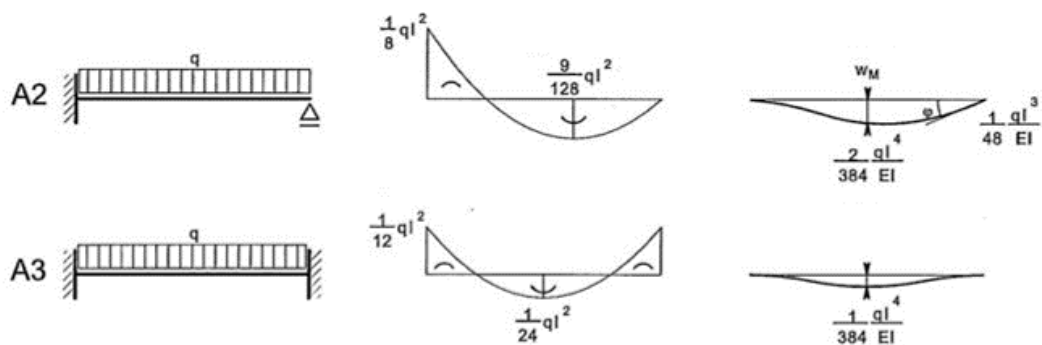


Figure 3.1: Mechanics scheme for bending moment and deflection for a beam with two rigid supports and a rigid plus roll support.

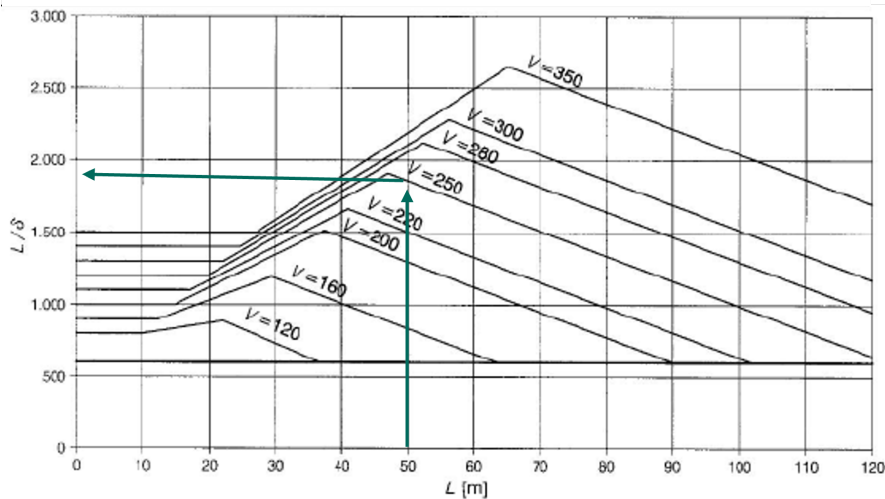


Figure 3.2: Deflection limit for passenger comfort, figure A2.3 in EN1990.

EN1995-1-1. k_{def} is used for permanent and live loads and ψ_2 only for live loads. Train traffic is required, when considering deflection, to use $\psi_2 = 1$ instead of zero.

w_{lim}	$\frac{L}{600}$	83.33 mm
$w_{lim,passcomf}$	$\frac{L}{1710}$	29.24 mm

Table 3.2: Deflection limits in SLS.

Equations (3.4) to (3.6) present the deflection calculation for each case. With a precamber that matches the permanent loads, the characteristic deflection only requires bending and shear deflection from the live loads. The creep deflection uses two additional factors. The deflection can be calculated using a simplified method presented in section 2.2.3 in EN1995-1-1. A creep factor k_{def} is used to simulate additional deflection from creep. Train traffic is required, when considering deflection, to use $\psi_2 = 1$ instead of zero. The passenger comfort deflection uses the same approximation as characteristic deflection but with another load. Figure 3.3 visually supports these formulae.

$$w_{sls} = \left(\frac{2L^4}{384EI} + \frac{L^2}{8GA} \right) q_{sls,live} + 0 \tag{3.4}$$

$$w_{quasi} = \left(\frac{2L^4}{384EI} + \frac{L^2}{8GA} \right) q_{sls,live}(1 + \psi_2 k_{def}) + \left(\frac{L^4}{384EI} + \frac{L^2}{8GA} \right) q_{sls,perm}(0 + k_{def}) \tag{3.5}$$

$$w_{passcomf} = \left(\frac{2L^4}{384EI} + \frac{L^2}{8GA} \right) q_{sls,LM71} + 0 \tag{3.6}$$

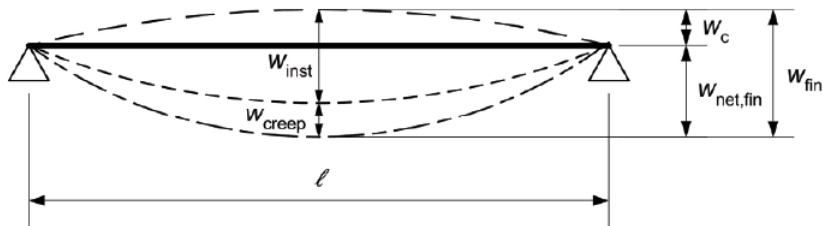


Figure 3.3: Individual contributions to total deflection, figure 7.1 in EN1995-1-1.

3.2. Timber design

The cross-section type is a box girder. A symmetric cross-section is used for simplicity in this preliminary design. A drawing and its cross-section properties are shown in Table 3.3 and Figure 3.4 respectively.

Timber	
A	9.32 m ²
$A_{z,eff}^{1)}$	5.78 m ²
$A_{y,eff}^{2)}$	4.48 m ²
I_y	16.72 m ⁴
W_y	8.36 m ³
I_z	11.10 m ⁴
W_z	5.55 m ³
A_m	4.94 m ²

1) webs and half of flange

2) only flanges

Table 3.3: Timber cross-section properties.

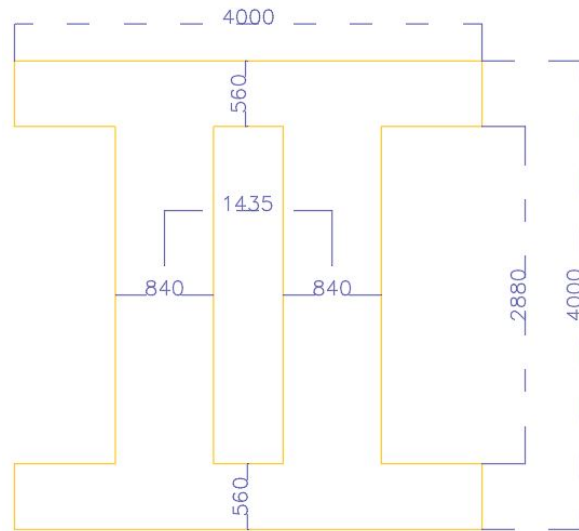


Figure 3.4: Timber cross-section.

3.2.1. Material properties

The properties of GL30h can be found in Table 3.4. The timber is assumed to be under service class 2 and undergoes short loading. Consequently the timber modification value k_{mod} is 0.9. The creep reduction value k_{def} , dependent on the service class, equals 0.8 and the safety factor used for glulam γ_M is 1.25. All three values can be found in EN1995-1-1.

Timber - GL30H					
		γ_M	1.25		
		k_{mod}	0.9	k_{def}	0.8
f_{mk}	30 MPa	f_{md}	21.6 MPa		
$f_{t,0,k}$	24 MPa	$f_{t,0,d}$	17.3 MPa		
$f_{t,90,k}$	0.5 MPa	$f_{t,90,d}$	0.28 MPa		
$f_{c,0,k}$	30 MPa	$f_{c,0,d}$	21.6 MPa		
$f_{c,90,k}$	2.5 MPa	$f_{c,90,d}$	1.76 MPa		
f_{vk}	3.5 MPa	f_{vd}	2.52 MPa		
E_{mean}	13 600 MPa	E_d	10 880 MPa	$E_{mean,fin}$	7556 MPa
G_{mean}	650 MPa	G_d	520 MPa	$G_{mean,fin}$	361 MPa

Table 3.4: Material properties of GL30h.

3.2.2. ULS

The timber Eurocode compares stresses to material strength to get unity checks. Normal force and biaxial bending induce normal stresses. Axial tension and compression can occur, though tension always governs over compression. This leads to Equation (3.7) that should be satisfied. The k_m factor is 1 for every cross-section not rectangular. It is a factor that is applied to have less conservative results in the case of rectangular cross-sections, which has $k_m = 0.7$.

Shear stresses are addressed separately. EC5 does not have a combined shear and bending check, but factor k_{cr} is introduced to account for it. It reduces the cross-section by a third to account for cracks due to bending. The effective area is calculated and shown in Table 3.3. It is assumed that this reduction replaces a reduction of k_{cr} . Torsion and shear stresses are not combined in EC5, but the

shear strength should not exceed the combined shear and torsion stress. This check is added in the German DIN, resulting in Equation (3.8).

$$\frac{\sigma_{t,0}}{f_{td}} + \frac{\sigma_{m,y}}{f_{md}} + k_m \cdot \frac{\sigma_{m,z}}{f_{md}} < 1 \quad (3.7)$$

$$\frac{\tau_z}{f_{v,d}} + \frac{\tau_{t,z}}{f_{v,d}} \text{ OR } \frac{\tau_y}{f_{v,d}} + \frac{\tau_{t,y}}{f_{v,d}} < 1 \quad (3.8)$$

Stresses are calculated by dividing the force or moment by its appropriate cross-section property. The flange and web experience different torsional shear stress since these have different thicknesses. These are calculated using thin-walled theory. The shear stresses are governing, which is expected for a box girder cross-section. It should be noted that the unity check is above 1. This is no problem since the combined design will have lower shear and torsional stresses.

Resistance		Effect at support		Unity check	Effect at midspan		Unity check
f_{md}	21.60 MPa	$\sigma_{m,y}$	13.57 MPa	0.78	$\sigma_{m,y}$	7.63 MPa	0.47
		$\sigma_{m,z}$	1.41 MPa		$\sigma_{m,z}$	1.00 MPa	
f_{td}	17.28 MPa	$\sigma_{t,0}$	1.24 MPa	1.03	$\sigma_{t,0}$	1.24 MPa	0.00
		τ_z	2.36 MPa		τ_z	0.00 MPa	
f_{vd}	2.52 MPa	$\tau_{t,z}$	0.24 MPa	0.22	$\tau_{t,z}$	0.00 MPa	0.00
		τ_y	0.21 MPa		τ_y	0.00 MPa	
		$\tau_{t,y}$	0.36 MPa		$\tau_{t,y}$	0.00 MPa	

Table 3.5: Unity check timber cross-section for each stress at the support and midspan.

3.2.3. SLS

The beam deflection formula, the SLS loading, and the limits have been presented in Section 3.1. The bending and shear stiffness can be calculated with the values presented in Tables 3.3 and 3.4. The shear stiffness used for shear deflection is the shear modulus times the effective area.

$$EI_y = 227 \times 10^3 \text{ MNm}^2$$

$$GA_{z,eff} = 3756 \text{ MN}$$

$$EI_z = 119 \times 10^3 \text{ MNm}^2$$

$$GA_{y,eff} = 2912 \text{ MN}$$

The permanent loading deflection is already excluded from Equations (3.4) to (3.6),

$$w_c = q_{perm} \left(\frac{L^4}{384EI_y} + \frac{L^2}{8GA_{z,eff}} \right) = 13.16 \text{ mm}$$

The other three deflections are shown in Table 3.6. The shear and bending parts are separately calculated to show the percentage of shear deformation, which turns out to be significant. The deflections are calculated using Equations (3.4) to (3.6) that already accounts for the precamber for w_{sls} and w_{quasi} . The shear deflection is significant due to the low shear stiffness and the small web area. It is also highly dependent on the structural model. For a continuous beam the bending deflection can be a factor five lower while the shear deflection stays the same and thus increasing its contribution to the total deflection.

	Bending	Shear	Total	w_{GA}/w_{EI}	UC
w_{sls}	26.21	15.22	41.43	37%	0.50
w_{quasi}	50.49	32.16	82.65	39%	0.99
$w_{passcomf}$	12.03	6.99	19.02	37%	0.65

Table 3.6: Deflection check timber cross-section for each combination in mm with a significant contribution of the shear deflection due to the low shear stiffness, the small web area, and the chosen structural model.

3.3. Class 2 steel design

The first steel design aims to have a cross-section that will not locally buckle. Steel sections often use thin plates, and when the plates become too large, the resistance is reduced due to buckling. To satisfy the limit states, thick webs and flanges are chosen with an appropriate cross-section height. The cross-sectional properties and cross-section sketch are shown in Table 3.7 and Figure 3.5. The cross-section is reduced for shear lag effects in the compression and tension zone. It is a class 2 cross-section, for which bending around the major axis is used since this is the main loading direction. The calculation of it can be found in Appendix C.1.

Steel	
A_{eff}	0.461 m ²
$A_{z,eff}^{1)}$	0.171 m ²
$A_{y,eff}^{2)}$	0.290 m ²
$I_{y,eff}$	0.536 m ⁴
$W_{y,eff}$	0.433 m ³
$I_{z,eff}$	0.321 m ⁴
$W_{z,eff}$	0.259 m ³
A_m	3.509 m ²
$m_{s,cl2}$	3690 kg/m

1) only webs

2) only effective flanges

Table 3.7: Effective cross-sectional properties due to shear lag.

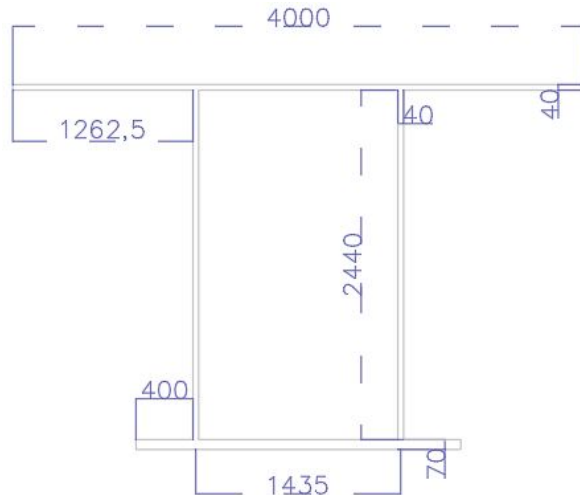


Figure 3.5: Steel cross-section with thick plates such that it is class 2.

3.3.1. Material properties

The cross-section is made of strength grade S355. It uses a safety factor γ_M for steel equals to 1. For thick plates the strength has a lower value that can be found in table 3.1 in EN1993-1-1.

Steel - S355

	$t \leq 40$ mm	$t \leq 80$ mm
f_y	355 MPa	f_y 335 MPa
γ_M	1.00	
E	210 000 MPa	

Table 3.8: Material properties S355.

3.3.2. ULS

The cross-section is only checked above the support. This is the location where the highest cross-sectional forces occur. The effective cross-sectional properties are used to determine its resistances. Loading cases will lead to a combination of stresses such that combined unity checks are required. The individual unity checks for each force are presented in Table 3.9. The combined bending and tension unity check and the combined shear and torsion unity check are shown and are just within limits.

$$UC_{M,N} = \frac{M_{y,Ed}}{M_{y,Rd}} + \frac{M_{z,Ed}}{M_{z,Rd}} + \frac{N_{x,Ed}}{N_{x,Rd}} = 0.95 \quad UC_{V,T} = \frac{V_{z,Ed}}{V_{z,Rd}} + \frac{V_{y,Ed}}{V_{y,Rd}} + \frac{T_{Ed}}{T_{Rd}} = 0.31$$

	Effect	Resistance	Unity check
$M_{y,Ed}$	113.44 MNm	$M_{y,Rd}$ 144.97 MNm	0.78
$M_{z,Ed}$	7.81 MNm	$M_{z,Rd}$ 86.86 MNm	0.09
$V_{z,Ed}$	9.08 MN	$V_{z,Rd}$ 33.10 MN	0.27
$V_{y,Ed}$	0.63 MN	$V_{y,Rd}$ 56.05 MN	0.01
$N_{x,Ed}$	11.58 MN	$N_{x,Rd}$ 154.41 MN	0.07
T_{Ed}	1.98 MNm	T_{Rd} 82.28 MNm	0.02

Table 3.9: Unity check steel class 2 cross-section per individual force.

3.3.3. SLS

A larger cross-sectional property reduction from shear lag is required for SLS. The necessary cross-sectional properties are shown in Table 3.10. These differ from the cross-sectional properties used in ULS. The bending and shear stiffness can be derived from the properties. The deflection is calculated using the methods presented before in Section 3.1. The normal deflection limit is not governing, even if a precamber is neglected.

$$EI_y = 101.3 \times 10^3 \text{ MNm}^2 \quad GA_{z,eff} = 13.9 \times 10^3 \text{ MN}$$

$$EI_z = 49.4 \times 10^3 \text{ MNm}^2 \quad GA_{y,eff} = 20.8 \times 10^3 \text{ MN}$$

Steel	
$A_{z,eff}^{1)}$	0.171 m ²
$A_{y,eff}^{2)}$	0.256 m ²
$I_{y,eff}$	0.483 m ⁴

1) only webs
2) only effective flanges

Table 3.10: Effective cross-section properties due to shear lag for SLS.

	Bending	Shear	Total	w_{GA}/w_{EI}	UC
w_{sls}	72.43	6.04	78.47	8%	0.94
$w_{passcomf}$	26.98	1.89	28.87	7%	0.99

Table 3.11: Deflection check steel thick cross-section for two combinations in mm without precamber reduction. The creep combination with quasi-permanent loads is not necessary since steel has negligible creep.

3.4. Class 4 steel design

The class 2 design has a much smaller height than the timber design. A more slender design will have a more similar cross-section height, such that, when combined, a more fluent conversion of steel to timber is possible. Additionally, a more slender cross-section can utilise class 4 plates to reduce material. Handling and manufacturing become more complex due to stiffeners and more welding. These two aspects are not addressed in this phase.

Class 4 cross-sections require plate buckling checks for each conceivable plate. The calculation methods and procedures can be found in EN1993-1-5. A separate calculation for each cross-sectional force is required to determine the reduced cross-sectional properties for that specific load case. The effective cross-section properties are only calculated to address the governing major bending moment and the deflection limit. These are the main factors that determine the dimensions in this preliminary stage. The goal was to achieve a similar unity check for the major bending moment as the class 2 section.

The mass per length is determined to compare the class 4 and the class 2 design. Stiffeners for the bottom flange follow from the reduced cross-sectional property calculation of the major bending moment. A calculation to determine the reduced properties for the web and top flange following the shear and normal force has not been done. For comparison reasons interpolation is used to get a fictitious area and consequently mass for these plates. The area ratio of the stiffened web and top flange to the stiffened bottom flange is assumed to be equal to the area ratio of the web and top flange to the bottom flange of the class 2 section. The calculation is presented in Appendix C.2 and is expected to lead to a conservatively large mass.

The cross-section with only the stiffened bottom flange is shown in Figure 3.6. The web and stiffener distances are centre-to-centre, while the height includes flange thicknesses. Only the effective properties of interest can be found in Table 3.12.

The effective properties calculation can be found in Appendix C.2. It checks the stiffeners, bottom flange, and web for local and global plate buckling and shear lag. Local plate buckling only occurs to the web. The stiffener plates and bottom flange plates, split by the stiffeners, are class 3 and don't require local buckling reductions. The stiffened bottom flange is reduced for the combined effect of equivalent orthotropic plate behaviour and column buckling of individual stiffeners. The effective area is calculated by multiplying the gross area by the plate buckling reduction and the shear lag reduction as per clause 4.5.1 (7) in EN1993-1-5. An effective width is calculated to match this effective area and can thus be used for the effective first and second moment of area.

Steel	
$I_{y,eff,uls}$	0.611 m ⁴
$W_{y,eff,uls}$	0.404 m ³
$A_{z,eff,sls}$	0.138 m ²
$I_{y,eff,sls}$	0.498 m ⁴
$m_{s,cl4}^*$	3132 kg/m

$m_{s,cl4}^*$ is the fictitious mass

Table 3.12: Reduced steel cross-section properties.

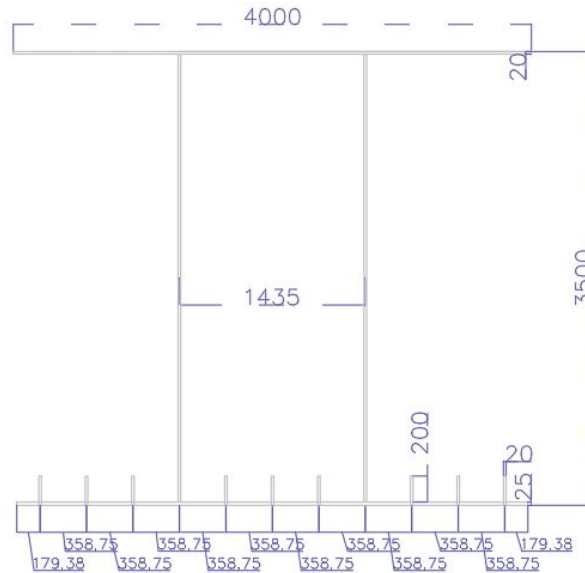


Figure 3.6: Steel cross-section for class 4 design with only stiffeners at the bottom flange.

3.4.1. ULS

Only the major bending moment is considered in ULS. It is assumed that, under the assumption that stiffeners are introduced at the web and top flange, the other cross-sectional forces will have similar unity checks as for the thick design. Thus, the goal is to have a section that has a similar unity check for the major bending moment to the class 2 section. The unity check is shown in Table 3.13.

	Effect	Resistance	Unity check
$M_{y,Ed}$	113.44 MNm	$M_{y,Rd}$ 143.59 MNm	0.79

Table 3.13: Unity check steel slender cross-section for major bending moment.

3.4.2. SLS

Bending and shear stiffness are straightforwardly calculated for SLS only accounting for shear lag. The deflection is calculated similar to the class 2 steel section, by use of Equations (3.4) and (3.6). No precamber is assumed since normal deflection is not governing. And a different deflection formula is used for live and permanent loads as explained in Section 3.1. It can be observed that the unity checks in Table 3.14 are very similar to the ones of the thick steel section in Table 3.11.

$$EI_{y,eff,sls} = 105 \times 10^3 \text{ MNm}^2$$

$$GA_{z,eff} = 11.2 \times 10^3 \text{ MN}$$

	Bending	Shear	Total	w_{GA}/w_{EI}	Unity check
w_{sls}	70.19	7.48	77.67	11%	0.93
$w_{passcomf}$	26.15	2.34	28.49	9%	0.97

Table 3.14: Deflection steel slender cross-section for two combinations in mm without precamber.

3.5. Concluding remarks

The timber cross-section has a larger construction height than the steel section, as expected. The single rail track decision leads to a smaller timber section size, which is an improvement to the previous study. The shear resistance is not sufficient. However, the timber section will experience lower shear forces, for it will not be located at the support position. Shear force decreases linearly with its distance to the closest support.

The slender class 4 section weighs around 15% less, even with the conservative assumption of adding stiffener area based on the area ratio. While the mass decrease is beneficial, the welding length substantially increases.

To form the non-prismatic beam bridge, it is the aim to have a fluent conversion. This implies that the construction height of the timber and steel sections should be very close. The slender steel section and a reduced timber section is used for the architectural and practical assessment in part four. The reduced timber section has a height of 3.5 m. It is expected that such a height is still feasible when using more realistic loading values and considering that lower cross-sectional forces occur at 3 to 7 metres from the support, which contains the position of the connection.

4

Model and loading

This chapter describes the modelling approach in SCIA Engineer of the combined timber and steel railway bridge. SCIA Engineer is a finite element (FE) program. It also presents the loading combinations and factors.

4.1. Model

A 1D beam element model is used to determine cross-sectional forces and deflection of the non-prismatic bridge structure. SCIA Engineer offers the opportunity to generate results for more complex systems and cross-sections. Three complementary features to the regular SCIA license are used in this thesis. The first feature is a general cross-section editor to enable SCIA to work with the custom-made cross-sections. The moving load feature is the second. It allows the automatic generation of a loading model at varying positions along the track. Lastly, the dynamics feature is used to calculate the eigenfrequencies of the girder.

The bridge is modelled with beam elements and has six spans of 50 m and two of 40 m. One support has is hinged, so it cannot move. All other supports can only move in the longitudinal direction, making them rolling supports. It is assumed that there will be two bearings at each support under each web. This is modelled by restricting any torsional rotations for each support. Bending in the vertical and horizontal plane is possible. Figure 4.1 shows part of the model and its nodes. Additional nodes are added to change the cross-section for a specific part easily. These nodes do not influence the result since they are rigidly connected.

A single plate element is rigidly connected to all beam elements. The plate is small and thin to have a negligible influence on the result. A plate element is required to use the moving load feature. A load lane is defined, as well as different load models. Consequently, it can generate many load cases to simulate train load models at various locations.

The loading inputs are the load cases and combinations defined in Section 4.2. Each train load case is exclusive, such that only a single train can occupy the track at once. The loading scheme comprises the vertical train load and the horizontal nosing and braking or traction force. A standard linear calculation method of SCIA is used to calculate the effects of these loads. Cross-sectional forces and deflections are gathered from the output.

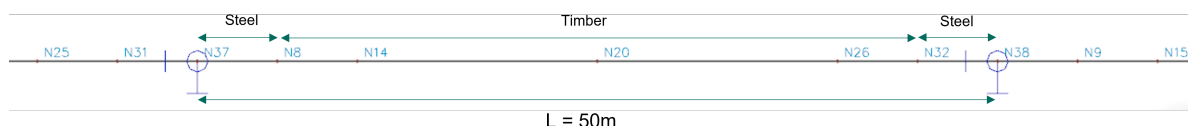


Figure 4.1: SCIA model screenshot of part of the model to show each span is divided into multiple beam elements that can have different cross-sections. The two elements next to the support have a size of 5 m, while the middle two have a size of 20 m. The nodes have numbers starting with a letter 'N'. There are additional nodes that are not necessary but do not influence the result because they have no finite stiffness.

Creep effects have been calculated with the simplified calculation method in EN1995-1-1 for the timber railway bridge in Chapter 3. The total deflection was multiplied with the creep factor k_{def} . This is conservative for the combined girder since part of the beam is steel. A more general approach is used to model creep, as suggested in EN1995-1-1. The stiffness of the timber material is reduced by Equation (4.1) in the model.

$$E_{mean,fin} = \frac{E_{mean}}{1 + k_{def}} \quad (4.1)$$

To model the connection in Chapter 8, rotational springs can be introduced. These are defined at the end of a beam element. This thesis defines the rotational spring at the end of the timber element since the connection is situated inside the timber section. The springs are given a rotational stiffness value for bending around the major and minor axis.

The dynamics feature enables the calculation of eigenfrequencies of the structure. The track structure is modelled as a distributed mass. SCIA handles the self-weight of the structure by itself.

4.2. Load factors and combinations

The different loads are already specified in Section 2.8 and their values presented in Appendix B. This section only determines the factors with which the loads are supposed to be multiplied for different limit states. There are several factors to consider.

For a safe design, the Eurocode applies the partial factor method. For both actions and resistance, partial safety factors must be included in design calculations. These factors account for negative deviations of loading effects, variability in material properties, and uncertainties in resistances. These effects are combined in single γ factors to convert characteristic values to design values. Both the actions and the resistance have their own γ factor.

Combination factors ψ are introduced to avoid conservative loading situations. Partial safety factors account for the probability of failure for each load. Combining these extreme probabilities leads to a higher probability of failure than necessary. Combination factors reverse this extremely low probability to avoid over-conservative design. The standard also allows the removal of nonsense combinations and even states to ignore particular combinations.

Specifically for railway traffic actions, two additional factors are required according to EN1991-2. An α factor to cover more frequent and heavier railroad use. And a dynamic factor Φ , which includes dynamic effects in case no dynamic analysis is required. See Chapter 6 for further explanation.

4.2.1. Factors

These values can be found in two standards, EN1990 and EN1991-2. The values are gathered and presented in tables. Each factor is addressed separately.

Partial safety factor

The characteristic load values must be reduced by a partial safety factor only in ULS. Favourable and unfavourable loads have different factors. For this design, the live load is assumed to be governing and lead to safety factors presented in Table 4.1. SLS requires no partial safety factors.

Load	variable	factor
Permanent load	γ_G	1.15
LM71 & SW/0	γ_Q	1.45
SW/0	γ_Q	1.2
Wind & Temperature	γ_Q	1.5 ¹⁾

1) This value is used for all general variable loads

Table 4.1: Partial safety factors for loads, based on table A2.4 in EN1990

Rail traffic factor

This factor is found in EN1991-2 as part of the rail traffic load model section. It is a factor between 0.75 and 1.46 with a standard value of 1. When a railroad is used very frequently and with larger or heavier trains, this factor can represent the increased loading that comes from it. The Dutch national annex advises using 1.21.

In a presentation Tschumi (2012) presents a map in which Norway uses a value of 1. It is recommended by UIC Leaflet 702 to use 1.33 for all future railroad projects, such that all of Europe uses an identical factor. This is especially important for international rail traffic. Sweden uses a factor of 1.33 according to the presentation's map. Its recommendation is used for this design.

$$\alpha = 1.33$$

Dynamic factor

A simplified approach can be used to account for dynamic effects by introducing a dynamic amplification factor Φ . It is highly dependent on the span length. In section 6.4.5.2 of EN 1991-2, this factor is determined using one of the following two equations.

$$\Phi_2 = \frac{1.44}{\sqrt{L_\Phi} - 0.2} + 0.82 \quad 1 \leq \Phi_2 \leq 1.67$$

$$\Phi_3 = \frac{2.16}{\sqrt{L_\Phi} - 0.2} + 0.73 \quad 1 \leq \Phi_3 \leq 2$$

where:

L_Φ = determinant length

The determinant length is taken from table 6.2 in EN1991-2. Case 5.2 is chosen from that table. It can be used for continuous girders over multiple spans. Both equations result in a factor of 1. See Chapter 6 for further elaboration regarding bridge dynamics.

Load combination factor

A separate combination factor is used for each load in a different design situation. The load combination factors applicable to this design are presented in Table 4.2.

Load	ψ_0	ψ_1	ψ_2
Rail traffic group	0.8	0.8	0 ¹⁾
Wind	0.75	0.5	0
Temperature	0.6	0.6	0.5

1) in case of deformation this value is 1

Table 4.2: Load combinations factors, table A2.3 in EN1990.

Load groups

Trains will lead to actions in several directions. To combine these for all possibilities is useless. Therefore Eurocode has created predefined load groups. These load groups are defined in table 6.11 in EN1991-2. This design has four load groups of interest, but these can be limited to two groups.

- gr11 and gr12 will lead to the maximal vertical actions with LM71 or SW/0 while having a different maximal horizontal direction
- gr16 and gr17 are equal to gr11 and gr12 but use load model SW/2

Horizontal loads are not governing. Therefore, it is decided to account for all horizontal loading without reducing their value for this preliminary design phase.

Loads	Load combinations			
	gr11	gr12	gr16	gr17
LM71 or SW/0	1	1	0	0
SW/2	0	0	1	1
Horizontal longitudinal	1	0.5	1	0.5
Horizontal transverse	0.5	1	0.5	1

Table 4.3: Load group factors for rail traffic taken from table 6.11 in EN1991-2.

4.2.2. Combinations

Both ULS and SLS have different load combinations. In the case of ULS, two fundamental equations are used to find the largest cross-sectional forces. These are 6.10a and b and can be found in EN1990. Since rail traffic loads are higher than all dead loads, only Equation (6.10b) is used. The quoted plus signs mean 'in combination with'.

$$\gamma_G \cdot \xi \cdot G_k \text{ " + " } \gamma_{Q,1} \cdot Q_{k,1} \text{ " + " } \sum \gamma_{Q,i} \cdot \psi_{Q,i} \cdot Q_{k,i} \quad (6.10b)$$

For SLS, there are three basic combinations: characteristic, frequent, and quasi-permanent. These are used for the irreversible limit states, reversible limit states, and long-term effects respectively. Section 3.1 has mentioned these loading combinations already. Each is used for a different limit.

$$\sum G_{k,j} \text{ " + " } Q_{k,1} \text{ " + " } \sum \psi_{0,i} Q_{k,i} \quad (6.14b)$$

$$\sum G_{k,j} \text{ " + " } \psi_{1,1} Q_{k,1} \text{ " + " } \sum \psi_{2,i} Q_{k,i} \quad (6.15b)$$

$$\sum G_{k,j} \text{ " + " } \sum \psi_{2,i} Q_{k,i} \quad (6.16b)$$

The characteristic combination (6.14b) is used to check the deflection limit.

The frequent combination (6.15b) is used to check the passenger comfort deflection limit. However, only LM71 is used, and the permanent loading is neglected since the latter does not influence passenger comfort.

The quasi-permanent combination (6.16b) is used to check the creep deflection limit. The effect of creep is introduced via a reduction of stiffness, not an increase in loading. The ψ_2 factors represent the long term effect of variable loads.

4.2.3. Final load multiplier

Combining these factors results in seven combinations that use different factors and load models to comply with different limit states. The combination values are shown in Table 4.4. Two additional combinations are presented with a reduced combination factor for rail traffic actions with a quasi-permanent case.

As stated in Table 4.2 the combination factor ψ_2 for rail traffic in case of deflection is required to be 1. This factor represents the long term effect of variable loads and is thus included in the creep combination. However, trains are not permanently occupying the tracks, thus including the total live load effect as creep is illogical from an engineering perspective.

Creep deflection is a result of sustained loading and train live loads are not sustained loading. Background documentation on this requirement of the Eurocode has not been found. It potentially is an additional limitation to lower the risk of derailment as creep leads to larger deflections and thus influences track straightness. However, the creep deflection limit is the same as the normal deflection limit. Essentially meaning that normal deflections adhere to an even stricter limit. The Eurocode is not equipped for the design of timber railway bridges, thus it is possible that this combination factor is too conservative for timber creep.

To show the effect of lowering this limit Chapter 5 also shows a final load multiplier that has a value of 0.5 for ψ_2 . In the next chapter the creep deflection unity check for this half effective train live load is shown next to the EC limit.

Loads	ULS		SLS		Pass comf	Creep		Creep 0.5 ¹⁾ $\psi_{2,train} = 0.5$	
	CHAR <i>gr11/12</i>	CHAR <i>gr16/17</i>	CHAR <i>gr11/12</i>	CHAR <i>gr16/17</i>		FREQ <i>gr11/12</i>	QUASI <i>gr11/12</i>	QUASI <i>gr16/17</i>	QUASI <i>gr11/12</i>
Permanent	1.15	1.15	1.00	1.00		1.00	1.00	1.00	1.00
LM71 or SW/0	1.93		1.33		1.00	1.33		0.67	
SW/2		1.20		1.00			1.00		0.5
Wind	1.13	1.13	0.75	0.75	0.50				
Temperature	0.90	0.90	0.60	0.60		0.50	0.50	0.50	0.50

1) reduction of factors by use of a lower value for ψ_2 .

Table 4.4: Load multiplier for several loading combinations specified in EN1990. Combining factors to get a single final factor for the loads.

4.2.4. Fatigue loading

Loading combinations to assess fatigue cannot be categorised under SLS or ULS. Stress ranges must be known to check the fatigue resistance. In this preliminary stage hand calculations based on nominal values are used to calculate fatigue. The nominal values for wind, LM71, and SW/0 follow from the model. These are used to determine the stress range for several fatigue load configurations. Specific fatigue train load models, supposedly less conservative, are not used for this preliminary design.

It is assumed that 50% of the train traffic is heavy, and thus LM71 and SW/0 both account for 50% of the cycles. The total number of train passes is assumed to be two million. That is slightly over two trains each hour each day. The normal force from braking or acceleration is not considered under the assumption that this only happens occasionally and thus has negligible cycles.

Wind actions also have a cyclic behaviour. The wind speed design value is 25 m/s, see Appendix B. Examining weather data near the bridge location, the wind distribution appeared to have much lower wind speeds. The weather data can be found in Appendix B.4. Taking the large values of the average wind speed range and doubling these leads to the assumed distribution in Table 4.5. It is assumed to be in accordance with the design wind speed value and a train combination reduction. Fifty two million cycles are considered, as if the wind has minute cycles.

	percentage	wind speed	factor
W1	45%	5 m/s	0.2
W2	50%	10 m/s	0.4
W3	5%	20 m/s	0.8

Table 4.5: Wind distribution for fatigue loading.

To determine the stress range, cross-sectional forces are determined based on the characteristic train and wind loading that follow from the model. No partial safety factor is considered, like in SLS, and the train weight alpha factor is neglected. The fatigue damage is calculated by determining the stress range at an appropriate detail category and dividing the occurring number of cycles by the max number of cycles possible for that stress range, see Equation (4.2). The calculation is performed in the next chapter with the detail categories from EN1993-1-9.

$$D_d = \sum_i^n \frac{n_{Ei}}{N_{Ri}} \quad (4.2)$$

where:

D_d = damage during a structures service life

n_{Ei} = number of cycles with design stress range σ_i

N_{Ri} = endurance value for design stress range σ_i

Part II

Global design

5

Combined timber-steel design

This chapter provides the next step in the design process. Cross-sections have been calculated for a complete timber and a complete steel railway bridge. The objective is to have a steel section above the support and the remaining part made of timber. In this chapter, the position of the connection is determined by analysing the cross-sectional forces and deflections for several locations.

5.1. Implementation

The model described in Section 4.1 is used. Four locations of the connection are considered, at three, five, seven, and ten metres distance from the support. In Figure 5.1 the different models that it results in are shown. This section describes the modelled cross-sections and addresses the difference between the loading in hand calculations and the load modelling.

5.1.1. Timber section

To match the height of the steel and timber section, a timber section with a height of 3.5 m was chosen. It is expected that this height should suffice to resist forces at the position the timber cross-section begins. These forces, as mentioned before, should be lower because of the location and the modelling of more realistic loading.

5.1.2. Steel section

A problem arises when the steel class 4 section is loaded with the general cross-section feature. The effective properties can be calculated by hand, but SCIA cannot perform the required reduction. It can reduce cross-sectional properties for predefined cross-sections but not for a general orthotropic user-defined cross-section. Either every property is defined by hand, or a similar section that requires no reduction is chosen.

A numeric cross-section can be used in SCIA to define every property by hand. It bypasses the 2D FEM analysis that determines the cross-section properties. This numeric cross-section does not allow the use of temperature loads, rendering it useless.

Modelling a cross-section that has equal effective as nominal properties which is similar to the effective properties of the class 4 section could be sufficient. The class 2 steel section is designed to resist the same design loads and can be modelled with temperature loading. It does have a slightly lower bending stiffness but a larger shear stiffness.

No exact results will be obtained by using a different cross-section. However, for this preliminary phase, the effect of realistic loading and the non-prismatic beam can nonetheless be observed.

5.1.3. Load

SCIA determines the self-weight load case. The permanent load uses the same value as before. The moving load feature has generated a few hundred load cases with different train positions. An interval of 5 m is used. Load models SW/0 and SW/2 have a finite length. It is not specified for LM71. A length of 400 m is chosen to cover the total model. The braking and traction force are a distributed horizontal load with a limited length not to exceed the maximal value given by the standard.

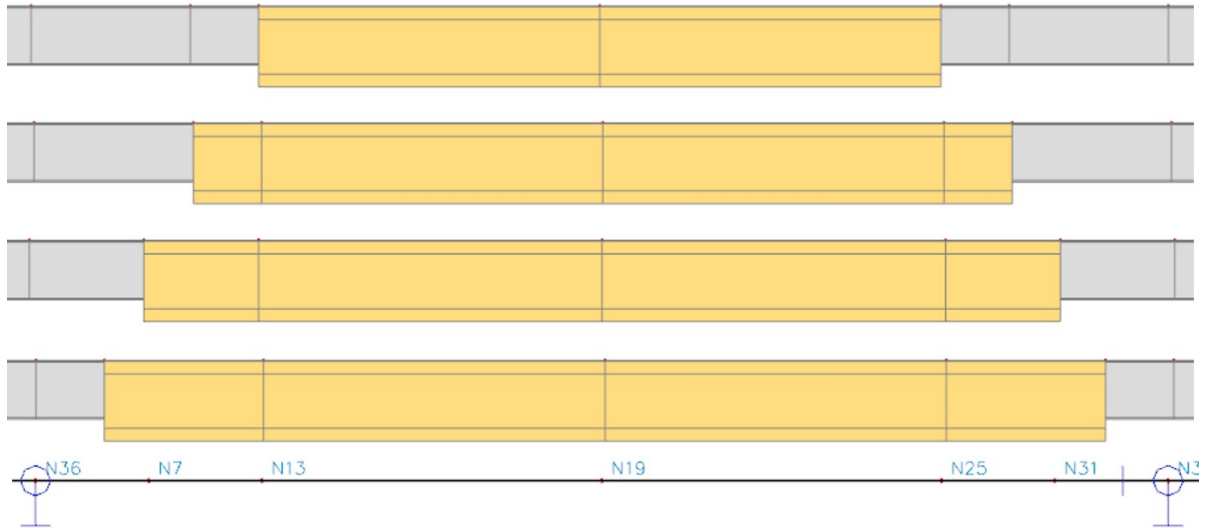


Figure 5.1: Renders of the beam models with 3, 5, 7, and 10 meter steel section and the beam model in SCIA.

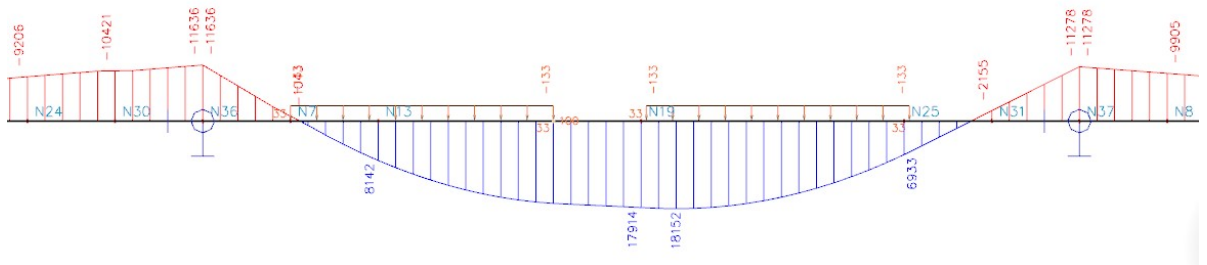


Figure 5.2: Snapshot of an SW/0 load with its bending moment diagram.

5.2. ULS

The hogging bending moments, see Table 5.1, have lower extreme values than the simplified loading model. Sagging bending moments have not reduced as much. This can be assigned to the lack of temperature loading and the simplification of the length of SW/0. Temperature loading increases a downward bending moment due to heating of the deck and constraining supports of the continuous beam. SW/0 only acts on a single span. The flanking spans are not loaded and are free to move upward. This results in a bending moment distribution between a simply and a rigidly supported beam. It can be seen in Figure 5.2

	Hand	Model				
		3 m	5 m	7 m	10 m	
Maximal hogging	-113.44	-55.62	-54.95	-54.56	-54.39	MNm
Maximal sagging	63.81	53.20	53.87	54.30	54.56	MNm

Table 5.1: Maximal hogging and sagging moment values present in structure with hand calculation and from the model for different connection positions.

5.2.1. Connection forces

The maximal cross-sectional forces of the four connection locations are compared. Generally, the cross-sectional force becomes smaller the further away the connection is located. However, the extreme bending moment around the major axis will switch signs at some point. This can be observed in Figure 5.3. The smallest extreme bending moment is best for the connection.

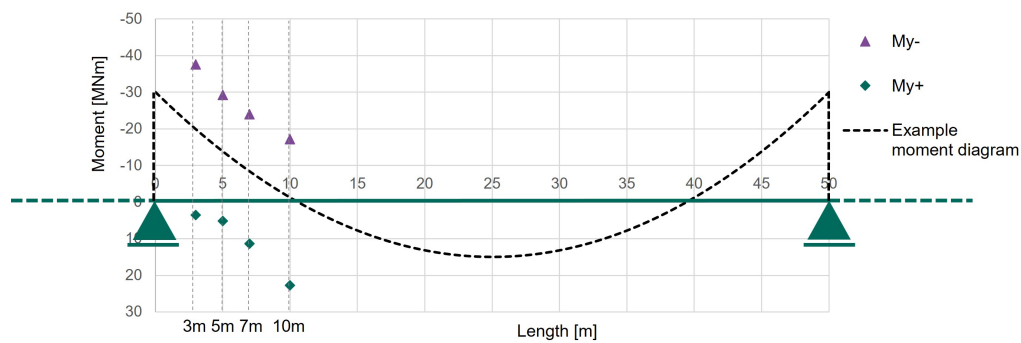


Figure 5.3: An example bending moment diagram from the SCIA model together with the positive and negative moments of the envelope of the ULS combinations gr11, gr12, gr16, and gr17 for four different connection locations.

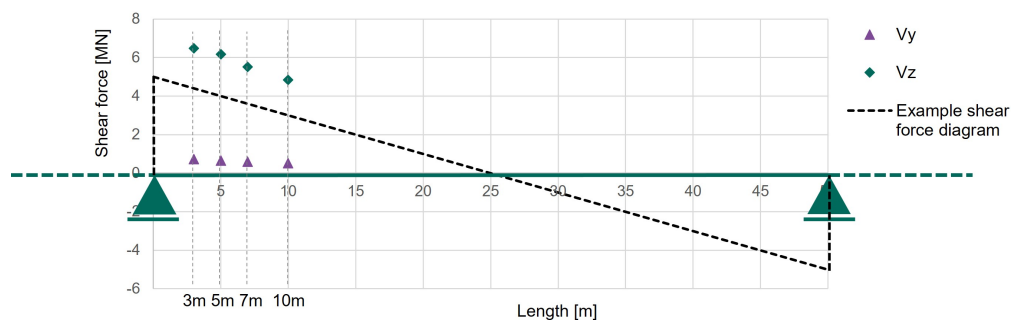


Figure 5.4: An example shear force diagram from the SCIA model together with the vertical and horizontal shear forces of the envelope of the ULS combinations gr11, gr12, gr16, and gr17 for four different connection locations.

	3 m	5 m	7 m	10 m
$M_{y-,Ed}$	-37.617 MNm	-29.298 MNm	-24.022 MNm	-17.167 MNm
$M_{y+,Ed}$	3.583 MNm	5.202 MNm	11.344 MNm	22.689 MNm
$M_{z,Ed}$	7.480 MNm	6.284 MNm	5.223 MNm	4.509 MNm
$M_{x,Ed}$	1.418 MNm	1.29 MNm	1.196 MNm	1.014 MNm
$V_{z,Ed}$	6.477 MN	6.171 MN	5.521 MN	4.835 MN
$V_{y,Ed}$	0.721 MN	0.654 MN	0.605 MN	0.512 MN
N_{Ed}	11.062 MN	10.988 MN	10.915 MN	10.803 MN

Table 5.2: Cross-sectional forces at the connection for four different positions.

A similar figure is constructed for the shear forces, Figure 5.4. In this case, the horizontal and vertical shear forces are shown, noted that the horizontal shear force can be both negative and positive. It can be observed that horizontal forces are much lower than vertical. The lower the shear force, the easier a connection can be designed.

The torsional moment and normal force are not visualised in a figure. The torsional moment acts like a shear force. It becomes smaller the closer it is to midspan. The normal force is highly dependent on the size of the train and its location. A conservative approach is always to consider the maximal possible value.

5.2.2. Resistance

The timber cross-section is chosen such that the construction height of steel and timber sections are aligned, which is 3.5 m. This section is smaller than the one that is checked in Chapter 3 and thus must be rechecked. The new properties are presented in Table 5.3. The unity checks that follow are shown in Table 5.4. While shear is still governing, the bending UC at the position of the connection has become smaller than the midspan bending UC.

Timber							
A	8.48 m ²						
$A_{z,eff}^{1)}$	4.94 m ²						
$A_{y,eff}^{2)}$	4.48 m ²						
I_y	11.69 m ⁴	3 m	5 m	7 m	10 m	midspan	
W_y	6.68 m ³	0.42	0.35	0.30	0.28	0.50	$\sigma_{M_y} + \sigma_N$
I_z	8.27 m ⁴	0.86	0.82	0.73	0.64	0.00	$\tau_{V_y} + \tau_T$
W_z	4.13 m ³						
A_m	4.22 m ²						

- 1) webs and half of flange
2) only flanges

Table 5.4: Unity checks of timber section starting at different positions.

Table 5.3: Timber cross-section properties for a construction height of 3.5 m.

5.3. SLS

SLS has several limits to comply with that are listed in EN1990 A2.4.4.1. The deflection limits already have been calculated in Section 3.1 and can be found in Table 3.2. The vertical acceleration of the deck is addressed in Chapter 6, as well as horizontal frequency limits. Other limits are unhindered uplift at the bearings, end of deck rotation, longitudinal displacement, and horizontal deformation.

5.3.1. Deflection

The model assumes a rigid connection. Even though a connection will have a finite stiffness, the effect of using partly steel and partly timber is investigated for now. Both the steel and timber section had deflection unity checks near 1, while the timber assumed a precamber and the steel section not.

Figure 5.5 shows deflection unity checks at different connection locations for the three deflection limits. The values are also summarised in Table 5.5. In this table, both precambered and non-precambered unity checks are presented. The deflection from the creep combination is governing both with and without precamber. Although the passenger comfort limit becomes governing when a reduced creep impact of train traffic is considered. This issue has been discussed and in Chapter 9 it is reiterated.

Increasing the amount of steel results in less deflection. Although the bending stiffness of the steel section is lower, the difference in shear stiffness is relatively larger to reduce the deflection. Using the smaller timber section does have a large impact on the stiffness, but the steel section can counter this.

$$\begin{aligned}
 EI_{y,timber,4m} &= 227 \times 10^3 \text{ MNm}^2 & GA_{z,eff,timber,4m} &= 3756 \text{ MN} \\
 EI_{y,timber,3.5m} &= 159 \times 10^3 \text{ MNm}^2 & GA_{z,eff,timber,3.5m} &= 3210 \text{ MN} \\
 EI_{y,steel} &= 101 \times 10^3 \text{ MNm}^2 & GA_{z,eff,steel} &= 13\,863 \text{ MN}
 \end{aligned}$$

	Without precamber				Precamber of 12 mm			
	3 m	5 m	7 m	10 m	3 m	5 m	7 m	10 m
w_{sls}	0.73	0.72	0.70	0.68	0.59	0.57	0.56	0.53
w_{freq}	0.77	0.75	0.72	0.68	-	-	-	-
w_{creep}	1.19	1.13	1.07	1.00	1.05	0.98	0.93	0.86
$w_{creep,0.5}$	0.75	0.71	0.67	0.62	0.60	0.56	0.53	0.48

Table 5.5: Deflection unity checks of the combined girder with and without a precamber, left and right values respectively. The precamber value is the deflection of a rounded down value of the deflection under all permanent loads with the connection position at 5 m. The $w_{creep,0.5}$ uses a ψ_2 of 0.5 for rail traffic. The frequent combination only accounts for live loads, so a precamber has no effect on these values.

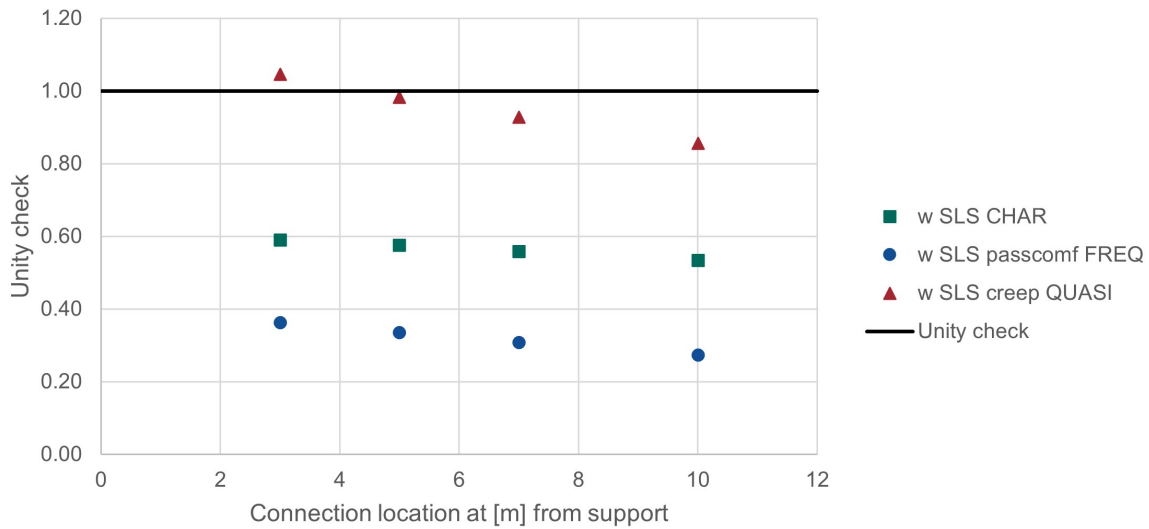


Figure 5.5: Deflection unity checks of the combined girder including a precamber of 12 mm for the three limits for four different connection positions. Different connection positions mean a different steel and timber cross-section amount.

5.3.2. Unrestrained uplift

Specific loading combinations can lead to tensile forces at the support. Bearings are often not designed to resist tensile forces and the unrestrained uplift can lead to premature failure. The bridge comes loose from the bearing and can impact the bearing when the loading changes. To check this a specific ULS combination is considered. Permanent loads act favourable and thus should use a factor of 0.9. The wind force can occur such that an upward wind action is present.

$$0.9 \cdot G_{perm} \quad "+" \quad 1.93 \cdot Q_{k,train} \quad "+" \quad 0.9 \cdot Q_{k,temp} \quad "+" \quad - 0.75 \cdot Q_{k,wind,z}$$

This combination leads to tensile forces at the outer supports. However, it is assumed that the permanent track structure will continue to connect the bridge to the land and such lead to additional downward loading. It is expected there will be no uplift due to this.

5.3.3. Deck twist

Torsional loading leads to deck rotations that enlarge the risk of derailment. The limit depends on the speed and is presented in Table 5.6. Deck rotation ϕ_x is calculated by the model and has an extreme value at midspan. The SLS characteristic load combination for the case of a connection at 5 m results in a value of 2.1 mrad.

$$t = \tan(2.1 \text{ mrad}) \cdot 1435 \text{ mm} = 3\text{mm}/25\text{m} = 0.36\text{mm}/3\text{m}$$

Speed range km/h	limit mm/3m
$V \leq 120$	$t \leq 4.5$
$120 < V \leq 200$	$t \leq 3$
$V > 200$	$t \leq 1.5$

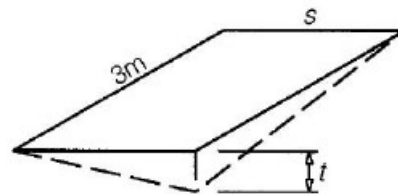


Table 5.6: Deck rotation limits for different train speeds, table A2.7 in EN1990.

Figure 5.6: Definition of deck rotation t with track width S of 1435 mm, figure A2.1 in EN1990.



Figure 5.7: Definition of angular rotations, figure A2.2 in EN1990.

5.3.4. End-of-deck rotation

Rotation about the transverse axis at the end of each deck or the rotation between two decks is limited to reduce rail stresses, uplift forces on rail fastening systems, and angular discontinuity at expansion devices. Illustrated in Figure 5.7. In case of a ballasted railway bridges the limits are implicit in EN1991-2 6.5.4, which is a section on track-bridge interaction. This interaction is not part of the preliminary design. For a non ballasted bridge requirements ought to be specified in the national annexe, though the Dutch annexe does not specify any limits for the non ballasted bridge.

5.3.5. Longitudinal displacement

Standards provide limits for longitudinal deck displacements to limit stresses in the steel tracks. When such a limit is exceeded, measurements must be taken. Thermal expansion joints have been discussed and will be necessary. It is assumed there is free movement possible in the longitudinal direction. The steel tracks are part of the track structure, which is out-of-scope.

5.3.6. Horizontal deformation

Deformation in the horizontal plane can be divided into horizontal deflection and horizontal rotation. Limits for the horizontal rotation ensure that horizontal deformations are not exceeded. These limits also depend on the allowed speeds, see Table 5.7. The maximal horizontal rotation also follows from the model. The same model, the one for the deck rotation, is used to find ϕ_z .

	Speed range	limit
	km/h	mrad
$\phi_z = 0.3 \text{ mrad}$	$V \leq 120$	$a_1 \leq 3.5$
	$120 < V \leq 200$	$a_2 \leq 2.0$
	$V > 200$	$a_3 \leq 1.5$

Table 5.7: Horizontal rotation limits dependent on trains speeds, table A2.8 in EN1990.

5.4. Fatigue

Live loads lead to cyclic loading. Train loads are largest while wind loads occur most often. These loads result in stress changes from which stress ranges can be determined. Stress ranges at specific positions in the steel section should be checked with their detail categories from EN1993-1-9.

The nominal stress method is used to check fatigue. Forces are gathered from a FE model that uses 1D elements. The by hand calculated effective cross-section properties are used to get the characteristic stress value. To get the design value for fatigue Equation (5.1) is used. The product of λ_i is the equivalent damage factor.

$$\gamma_{Ff} \Delta \sigma_{E,2} = \prod_i^n (\lambda_i) \cdot \Delta \sigma \quad (5.1)$$

where:

γ_{Ff} = partial safety factor for constant amplitude stress ranges

$\Delta \sigma_{E,2}$ = the design stress range value

λ_i = damage equivalent factor

$\Delta\sigma$ = characteristic stress range

The equivalent damage factor is dependent on the type of structure. For steel bridges there are four factors. All factors can be determined using tables in section 9.5.3 in EN1993-2

- $\lambda_1 = 0.64$ = factor for the damage due to traffic and is dependent on the length. It follows from table 9.3 in EN1993-2 assuming normal train traffic.
- $\lambda_2 = 1.15$ = factor for traffic volume. It depends on the annual tonnage and is taken as the most conservative value since no tonnage volume is known.
- $\lambda_3 = 1.00$ = factor dependent on the service life. For 100 years the value is one.
- $\lambda_4 = 1.00$ = factor for the load bearing element that carries more than one track. Since the bridge only carries one track this value is considered one. For multiple tracks the value can be decreased.

The combined factor cannot exceed a value of 1.4.

$$\lambda = \prod_{i=1}^4 (\lambda_i) = 0.74$$

To check the fatigue strength, stresses at specific locations need to be calculated, dependent on the detail categories. Since there are different stress ranges, a damage during service life is calculated and should not exceed 1.

5.4.1. Detail categories

There are many standard details listed in EN1993-1-9 of which only a few occur in this design. The most evident is to check the parent material of the welded profile. It depends on the weld quality and process what category it is. It is assumed to be automatically welded without start and stop positions, at least the the support position where the fatigue strength is checked. The difference between the detail categories in Figure 5.8 is the one- or two-sided welds. The stress range comes from normal stresses due to bending, the major component of the train live load.

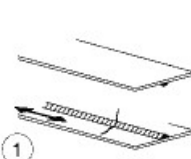
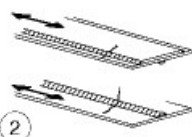

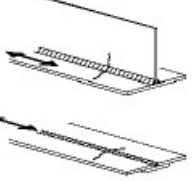
125	 	<p>Ononderbroken langlassen:</p> <p>1) Automatisch of volledig gemechaniseerd gelaste stompe lassen, uitgevoerd aan beide kanten.</p> <p>2) Automatisch of volledig gemechaniseerd gelaste hoeklassen. De uiteinden van aangelaste opdik-platen zijn getoetst via detail 6) of 7) in tabel 8.5.</p>	<p>Details 1) en 2): Start/stop-posities zijn niet toegelaten tenzij het herstel is uitgevoerd door een specialist met aansluitende inspectie ter verificatie van de goede uitvoering van het herstel.</p>
112	 	<p>3) Automatisch of volledig gemechaniseerd gelaste hoeklassen of stompe lassen, uitgevoerd aan beide kanten maar met start/stop- posities.</p> <p>4) Automatisch of volledig gemechaniseerd gelaste stompe lassen, uitgevoerd aan slechts één kant, op een ononderbroken onderlegstrip, maar zonder start/stop-posities.</p>	<p>4) Indien dit detail start/stop- posities bevat, moet categorie 100 zijn gebruikt.</p>

Figure 5.8: Combined welded profiles class one to four from table 8.2 EN1993-1-9.

At the support, and at the connection, transverse stiffeners are welded. These are important to resist plate buckling and to transfer all the loads to the support. The difference between category 80 and 71 is the thickness of the transverse welded plate in Figure 5.9. No calculations have been made for this part, but it is assumed that it will not exceed a thickness of 50mm. It is rather likely to have two transversely welded plates instead of a very thick one.

The stress range is, again, the normal stress in longitudinal direction. Therefor satisfying this detail automatically results in a sufficient fatigue strength for the parent material detail.

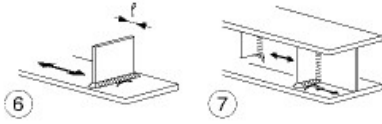
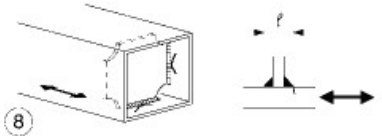
80	$\ell \leq 50 \text{ mm}$	 <p>6) Gelast op een plaat. 7) Verticale verstijvingen, gelast aan een profiel of een plaatligger.</p>	<p><u>Aangelaste platen in de dwarsrichting:</u></p> <p>6) Gelast op een plaat. 7) Verticale verstijvingen, gelast aan een profiel of een plaatligger. 8) Tussenschotten in gelaste kokerprofielen, gelast aan de flens of de lijfplaat. Dit kan onmogelijk zijn bij kleine buisprofielen.</p> <p>De waarden zijn eveneens geldig voor ringvormige verstijvingen.</p>	<p><u>Details 6) en 7):</u></p> <p>De uiteinden van de lassen zijn zorgvuldig zijn geslepen om mogelijk aanwezige randinkartelingen te verwijderen.</p> <p>7) $\Delta\sigma$ berekend met hoofdspansingen indien de verstijving aan de lijfplaat stopt, volgens linker kant.</p>
71	$50 < \ell \leq 80 \text{ mm}$	 <p>8) Tussenschotten in gelaste kokerprofielen, gelast aan de flens of de lijfplaat. Dit kan onmogelijk zijn bij kleine buisprofielen.</p>	<p>De waarden zijn eveneens geldig voor ringvormige verstijvingen.</p>	

Figure 5.9: Welded stiffeners class six to eight from table 8.4 EN1993-1-9.

This next detail considers cracks in welds between longitudinal stiffeners and cross girders. Normal and shear stresses in the cross girder occur due to a secondary bending moment and shear force to transfer the loading from the deck to the main girders. However, the current design has webs immediately under the loaded rail tracks. It is also assumed that the bearings are situated right under the webs at the support. Therefore it is expected that the stresses are very low in the cross girder if these are designed with proper dimensions. The detail categories in Figure 5.10 are therefore not considered in the calculation.

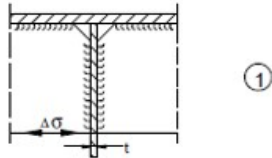
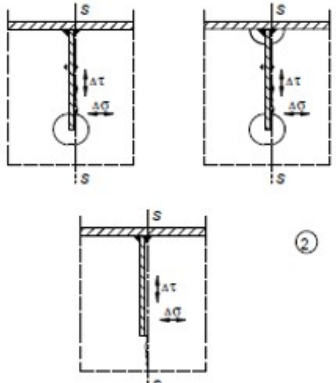
80	$t \leq 12 \text{ mm}$	 <p>1</p>	1) Verbinding van langsverstijver aan de dwarsdrager.	1) Toetsing gebaseerd op het normaalspanningsinterval $\Delta\sigma$ in de langsverstijver.
71	$t > 12 \text{ mm}$			
56		 <p>2</p>	<p>2) Verbinding van doorgaande langsverstijver aan de dwarsdrager.</p> $\Delta\sigma = \frac{\Delta M_s}{W_{net,s}}$ $\Delta\tau = \frac{\Delta V_s}{A_{w,net,s}}$ <p>Toets eveneens het spanningsinterval tussen de langsverstijvers, die zijn gedefinieerd in EN 1993-2.</p>	<p>2) Toetsing gebaseerd op de combinatie van het schuifspanningsinterval $\Delta\tau$ en het normaalspanningsinterval $\Delta\sigma$ in het lijf van de dwarsdrager, als een equivalent spanningsinterval:</p> $\Delta\sigma_{eq} = \frac{1}{2} \left(\Delta\sigma + \sqrt{\Delta\sigma^2 + 4\Delta\tau^2} \right)$

Figure 5.10: Orthotropic deck open stiffeners from table 8.9 EN1993-1-9.

5.4.2. Design stresses

The characteristic stresses can be collected from the SCIA model that is used in the previous sections. A passing train will have several stress ranges in one stress cycle. These are determined by collecting the bending moment at a position for several train load positions. In Figures 5.11 and 5.12 a single cycle is shown for LM71 and SW/0 respectively. In Figure 5.11 two different locations at a support are plotted to their respective distance to the loading. A connection location is also plotted, the green circles line. This shows that the highest moments are indeed at the support.

For LM71 it is assumed that one cycle contains three stress ranges. In case of SW/0 two stress ranges are identified. However, the small stress range does occur three times. The stress ranges are estimated based on the reservoir cycle counting method. In Table 5.8 the bending moment and the resulting stress is shown. The section modulus of the slender steel design is used.

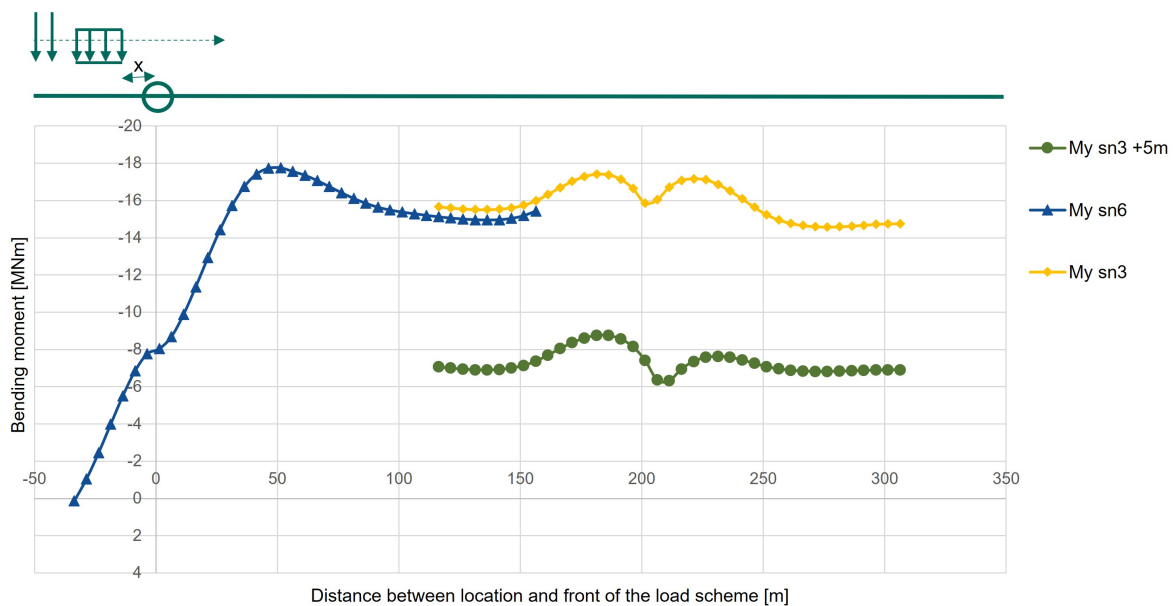


Figure 5.11: Bending moment at three positions for several LM71 positions. The horizontal axis represents the relative distance between a location and the front of the train load scheme. Sn3 and sn6 are the third and sixth support respectively, at a distance of 90 and 260 meter from the outer support. The graph suggests that similar locations will experience the same stress ranges.

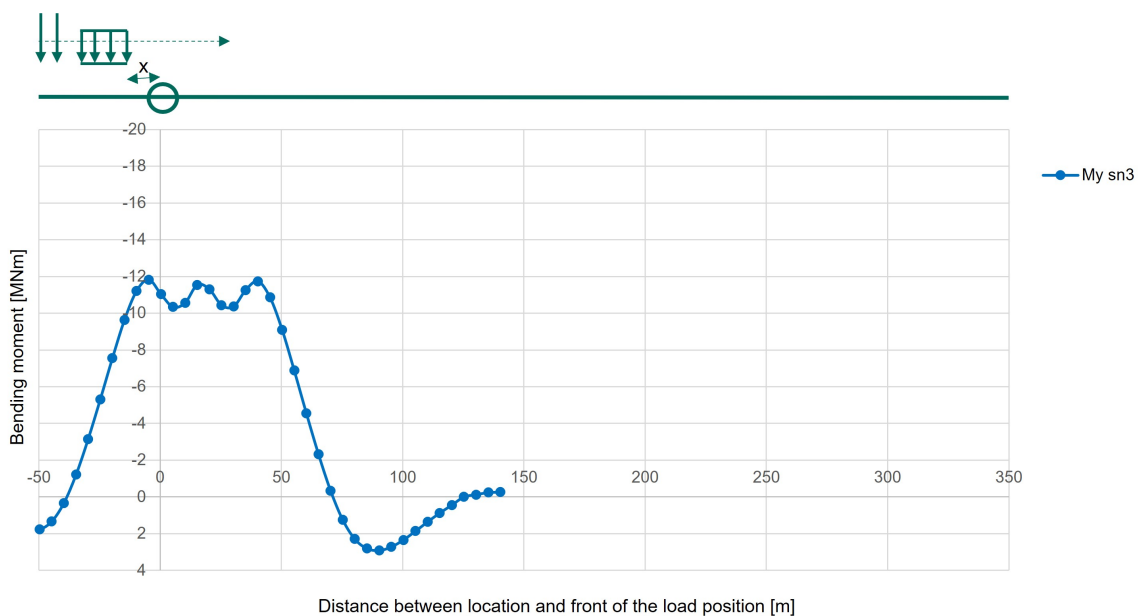


Figure 5.12: Bending moment at sn3 for several SW/0 positions. The horizontal axis represents the relative distance between location sn3 and the front of the train load scheme. Sn3 is the third support. Another location will show a similar result.

$$W_{y,eff,uls} = 0.404 \text{ m}^3$$

	Bending moment MNm	Stress range ¹⁾ MPa
Wind	2.155	5.33
Wind + Wind train	4.31	10.67
LM71.1	17.88	88.53
LM71.2 ²⁾	3	14.85
LM71.3 ²⁾	1.5	7.43
SW/0.1	14.74	72.97
SW/0.2 ²⁾	1.9	9.41

1) based on $W_{y,eff,uls}$ in Table 3.12

2) estimated based on graph

Table 5.8: Characteristic stress ranges from SCIA model.

The distribution in Table 4.5 presents the wind distribution. It is assumed that all train passes have the same wind distribution interaction. Resulting in eighteen stress ranges of which the damage can be calculated. The damage can be calculated with Equation (4.2). The endurance of the design stresses is dependent on the detail category.

The governing detail category is the welding of the cross girder, or transverse stiffener, to the main section. It is category 80. With help of the SN-curve the endurance can be calculated. SN-curves are shown in Figure 5.13. The constant amplitude fatigue limit and the cut-off limit must be calculated.

$$\Delta\sigma_C = \frac{\Delta\sigma_c}{\gamma_{Mf}} = 59.3 \text{ MPa}$$

$$\Delta\sigma_D = \frac{2^{1/3}}{5} \cdot \Delta\sigma_C = 43.7 \text{ MPa}$$

$$\Delta\sigma_L = \frac{5^{1/5}}{100} \cdot \Delta\sigma_D = 24.0 \text{ MPa}$$

The endurance limit can be calculated with the known SN-curves.

$$N = \begin{cases} 0 & \Delta\sigma_{E,2} \leq \Delta\sigma_L \\ \frac{\Delta\sigma_D^5 \cdot 5e6}{\Delta\sigma_{E,2}} & \Delta\sigma_L < \Delta\sigma_{E,2} \leq \Delta\sigma_D \\ \frac{\Delta\sigma_C^3 \cdot 2e6}{\Delta\sigma_{E,2}} & \Delta\sigma_D < \Delta\sigma_{E,2} \end{cases}$$

From Table 5.9 it can be observed that the low stress ranges that occur during a cycle do not contribute to the fatigue check. The stresses are below the cut-off limit and can be neglected. Fatigue damage due to stresses from only wind actions can also be disregarded. Removing all wind stresses in the stress range calculations would result in a cumulative damage of 1.04.

The high live loads from passing trains are, as expected, the main influencing parts for fatigue strength. Constructing the transverse stiffeners a few decimetres from the midpoint of the support would possibly reduce the stresses sufficiently. The fatigue load models are less conservative than the standard load models used currently, and thus will also reduce the stresses. Therefore, it can be expected that the structure should be able to meet fatigue design requirements.

Loading	$\Delta\sigma$	$\Delta\sigma_{E,2}$	n_{Ei}	N_{Ri}	D_d
W1	1.07	0.79	2.37E+07	0.00E+00	0.00
W2	2.13	1.57	2.63E+07	0.00E+00	0.00
W3	4.27	3.14	2.63E+06	0.00E+00	0.00
LM71.1 + W1	90.66	66.73	4.50E+05	1.40E+06	0.32
LM71.1 + W2	92.80	68.30	5.00E+05	1.31E+06	0.38
LM71.1 + W3	97.06	71.44	5.00E+04	1.14E+06	0.04
LM71.2 + W1	16.99	12.50	4.50E+05	0.00E+00	0.00
LM71.2 + W2	19.12	14.07	5.00E+05	0.00E+00	0.00
LM71.2 + W3	23.39	17.21	5.00E+04	0.00E+00	0.00
LM71.3 + W1	9.56	7.04	4.50E+05	0.00E+00	0.00
LM71.3 + W2	11.69	8.61	5.00E+05	0.00E+00	0.00
LM71.3 + W3	15.96	11.75	5.00E+04	0.00E+00	0.00
SW/0.1 + W1	75.10	55.28	4.50E+05	2.46E+06	0.18
SW/0.1 + W2	77.24	56.85	5.00E+05	2.27E+06	0.22
SW/0.1 + W3	81.50	59.99	5.00E+04	1.93E+06	0.03
SW/0.2 + W1	11.54	8.49	1.35E+06	0.00E+00	0.00
SW/0.2 + W2	13.67	10.06	1.50E+06	0.00E+00	0.00
SW/0.2 + W3	17.94	13.20	1.50E+05	0.00E+00	0.00

1.18

Table 5.9: Service life damage. The loading combinations, stress range, and design stress range are shown in the first three columns. The design stress range includes the damage equivalent factor λ . The fourth column shows the number of assumed stress cycles, note that SW/0.2 is the small stress range that occurs three times per cycle. The last two columns calculate endurance value for the design stress range and the damage.

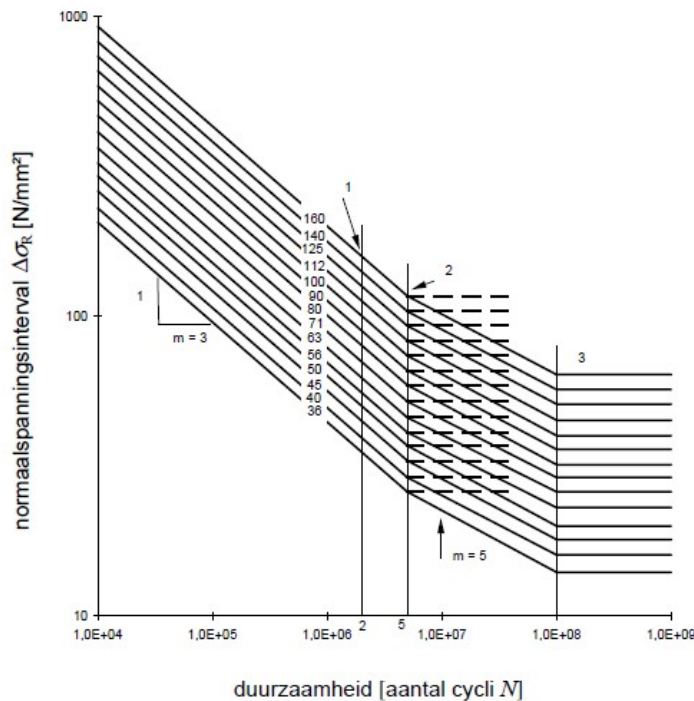


Figure 5.13: Fatigue strength curves for normal stress. Figure 7.1 in EN1993-1-9. 1) is the detail category $\Delta\sigma_C$, 2) is the constant amplitude fatigue limit $\Delta\sigma_D$, 3) is the cut-off limit $\Delta\sigma_L$.

5.5. Global design conclusions

In this chapter, cross-sectional forces have been calculated more precisely by implementing the actual loading in an FE model. The forces were slightly lower than the calculations in Chapter 3, which were expected to be conservative. This made a lower timber cross-section still satisfy ULS limits. The deflection limit was still governing, so a precamber is required. Fatigue appeared to be the governing factor of the steel section. Only the large stress ranges of the train loading were damaging. Small stress ranges from only wind, or small intermediate train loading ranges did not matter.

The position of the connection has a significant impact. It was decided to place the connection at 5 m to have mainly a timber bridge but still gain the benefits of a steel section at the support. With this location the deflection limits were still satisfied while mostly timber was used. In the next chapters, the connection will not change position. However, in future designs, the connection location can still be optimised.

6

Dynamic analysis

The dynamic response of bridges is a critical aspect to consider in railway bridge design. Trains travel at high speeds and exert large moving loads on the bridge structure. The dynamic response must not lead to large deck accelerations to prevent derailment. A preliminary assessment is performed to determine the risks for this design from a dynamic perspective. In consultation with an expert in railway engineering, prof. Z. Li, it was proposed to compare the bridge eigenfrequencies to periodic wheel loads of high-speed trains.

6.1. Induced vibrations

A moving train will exert a temporary moving force on the bridge structure, leading to vibrations in the structure. These induced vibrations will have a frequency depending on the train and its speed. Dozens of trains exist with different lengths and axle distances. The weight, and thus the force, will vary per train. The travel speed and wheel distances determine the frequency of the loading. Resonance can occur when the frequency of the load coincides with the natural frequency of the structure. This is dangerous since it causes increased deflection and leads to high structure accelerations. In an extreme case, it can become catastrophic, like the infamous Tacoma Narrows Bridge.

The periodic wheel load is the frequency at which a wheel load passes the bridge. It would be beneficial not to have a fundamental frequency that coincides with the periodic wheel load for a safe design. From the periodic wheel load and the bridge frequency, a critical resonant speed, in m/s, of the train can be determined. The derivation of Equation (6.1) is performed by Xia et al. (2006). Milne et al. (2017) supports that the most severe dynamic response occurs when a structure's frequency is close to integer multiples of the periodic wheel load.

$$v_{cr} = \frac{f_n D}{i} \quad (6.1)$$

where:

f_n = frequency of the bridge for the n-th mode

D = interval between moving loads

i = the multiplier

Table 6.1 shows ten high-speed load models that EN1991-2 defines. These models should be used for a dynamic analysis when designing high-speed rail. In this preliminary assessment, each train model is used to determine its critical speed for a variable structure frequency. Figure 6.1 show the critical train speeds for each HSLM-A train model.

The upper limit for the bridge frequency is determined for two maximal train speeds. For bridges that have a fundamental frequency above the value of those lines, there is no risk of resonance in the fundamental frequency. If the fundamental frequency is smaller than the upper limit in the graphs, resonance can occur.

Train model	Number of intermediate coaches N	Coach length D m	Bogie axle spacing d m	Point force P kN
A1	18	18	2.0	170
A2	17	19	3.5	200
A3	16	20	2.0	180
A4	15	21	3.0	190
A5	14	22	2.0	170
A6	13	23	2.0	180
A7	13	24	2.0	190
A8	12	25	2.5	190
A9	11	26	2.0	210
A10	11	27	2.0	210

Table 6.1: High-speed load models from EN1991-2 for HSLM-A.

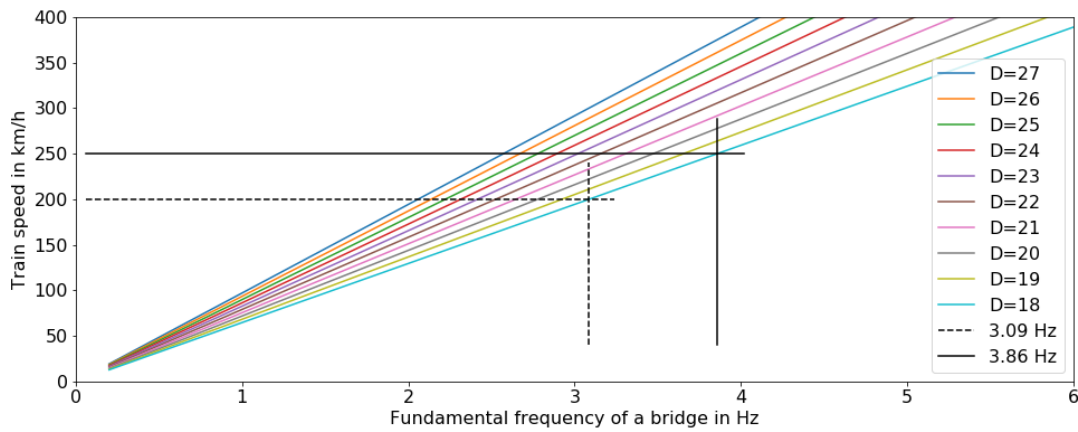


Figure 6.1: Critical train speeds of HSLM-A train models for a variable structure frequency. Determined the upper limit of the structure frequency for 200 km/h and 250 km/h.

Mode	1	2	3	4	5	6	7	8	9
Single-span	2.72	10.08							
Eight-span	2.72	2.84	3.17	3.66	4.25	4.88	5.49	5.97	10.08

Table 6.2: Vertical natural frequencies of IPE300 calculated with SCIA for a simply supported beam and a continuous beam with eight spans in Herz.

Middle aligned			Top aligned			Bottom aligned		
Mode	frequency	dir	Mode	frequency	dir	Mode	frequency	dir
1	2.23	H	1	2.02	H	1	2.04	H
2	2.62	V	2	3.57	V	2	3.64	V
3	7.95	H	3	5.87	T	3	5.96	T
4	8.42	T	4	6.06	T	4	6.02	T
5	8.698	V	5	8.63	V	5	8.66	V
6	15.29	T	6	9.74	T	6	9.90	T

Table 6.3: Eigen frequencies of non-prismatic cross-section with a construction height of 3.5 m. The section is aligned to three positions, the neutral axis, top of the section, and bottom of the section. The direction of the mode is also mentioned, H for horizontal, V for vertical, and T for torsional.

6.2. Continuous bridge

A single-span simply supported beam is a basic structure of which the natural frequencies are easily analytically calculated. For multi-span beams, this is not straightforward. Running an eigenfrequency analysis of a simply supported beam and a continuous eight span beam with a uniform cross-section showed that more modes exist for a continuous beam, see Table 6.2. In other words, continuous beams have a denser distribution of frequencies (Q. F. Gao et al., 2012; Q. Gao et al., 2015; Yau, 2001).

In general, an increase of span length, fundamental frequency, mass, or damping ratio reduces accelerations of the bridge structure Svedholm (2017). Continuous bridges also reduce the accelerations of a structure. The dynamic response of continuous beams is significantly less compared to simply supported beams (Yau, 2001). It can be explained by noticing that vibration energy can dissipate to other spans. Svedholm (2017) concludes that continuous bridges can reduce vertical deck acceleration up to 60% compared to simply supported bridges. Cervero (2017) supports this by stating that resonance problems become less severe for multi-span continuous beams.

6.3. Eigen frequency bridge

For the non-prismatic cross-sections of this design, an eigenfrequency analysis is performed with SCIA. A simply supported beam is used since the only addition of modelling the multi-span beam is a denser distribution of frequencies. For a single-span, the different modes can more easily be identified. It reuses the model with a timber section of 3.5 m and the class 2 steel section with a rigid connection at 5 m. The weight of the track structure was added as a distributed mass.

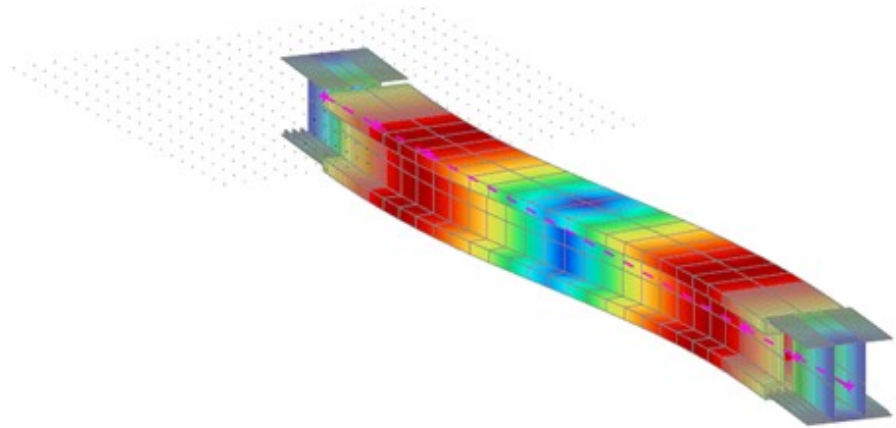
The first mode was a horizontal mode, which was expected as the cross-section has a lower transverse stiffness. The low torsional stiffness of timber results in torsional modes with frequencies close to the fundamental frequency. In Table 6.3 the eigenfrequencies are shown for the combined beam.

The bridge is supported at the bottom of the cross-section. Therefore, the eigenfrequencies with a different alignment have been calculated as well. This mainly introduces complex torsional modes with lower frequencies. An explanation for this is the fact that the top flange has more freedom to rotate out-of-plane in case of bottom alignment.

Figures 6.2a to 6.2c show a selection of the modes in Table 6.3. Figure 6.2c shows the rotation and sideways deflection of the top flange for a torsional mode.

3D displacement

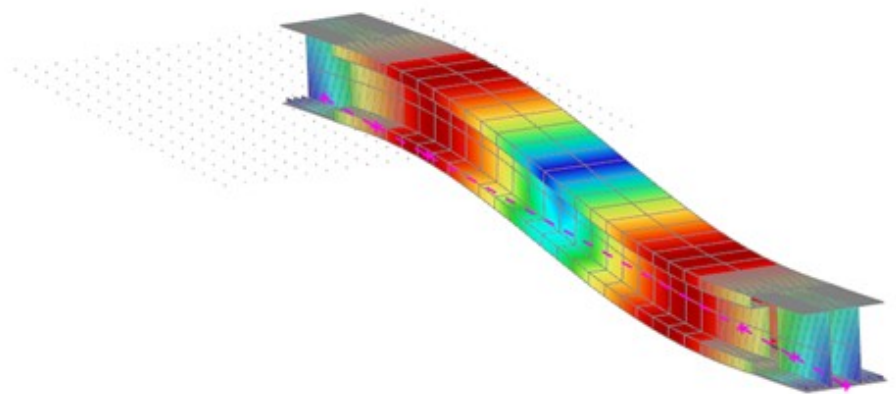
Values: U_{total}
 Modal shapes are normalized, so that the generalized modal mass of each mode is equal to 1kg.
 Mass combination: Full mass/3 - 7,95
 Selection: All
 Location: In nodes avg.. System: Global



(a) Mid aligned mode 3, second horizontal

3D displacement

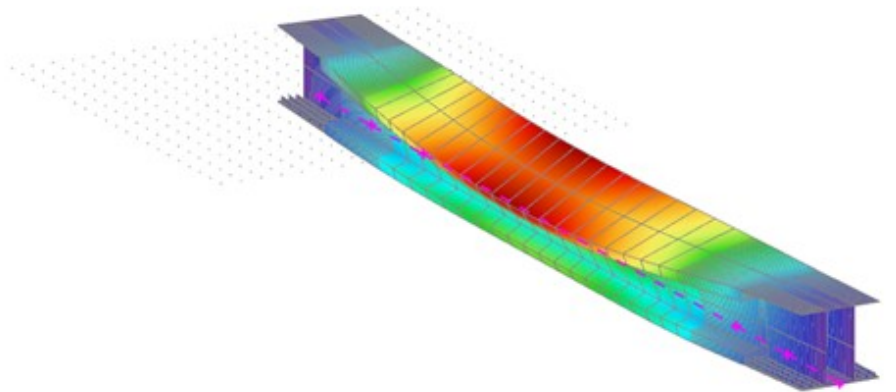
Values: U_{total}
 Modal shapes are normalized, so that the generalized modal mass of each mode is equal to 1kg.
 Mass combination: Full mass/5 - 8,66
 Selection: All
 Location: In nodes avg.. System: Global



(b) Bottom aligned mode 5, second vertical

3D displacement

Values: U_{total}
 Modal shapes are normalized, so that the generalized modal mass of each mode is equal to 1kg.
 Mass combination: Full mass/4 - 6,02
 Selection: All
 Location: In nodes avg.. System: Global



(c) Bottom aligned mode 4, second torsional

Figure 6.2: Vibrational modes of timber and steel beam SCIA model with purple=0 and red=1

6.4. Eurocode dynamics

In addition to deflection limits for static analysis, there is a vertical acceleration limit given by EN1990. For tracks with ballast, a maximal acceleration of 3.5 m/s^2 is allowed, while for slab track and high-speed rail, the maximal acceleration is 5 m/s^2 . To do a full-scale dynamic analysis is computationally expensive. It is not always necessary. Figure 6.3 shows a flowchart from EN1991-2 to determine if a dynamic analysis is required or not.

In Section 1.1 the requirement to have a maximal allowed speed of 250 km h^{-1} is stated. This originates from the Norwegian National Transport Plan (Global Railway Review, 2018). Following the flowchart for this complex structure with high speeds shows it is required to do a dynamic analysis, including torsion and bending. This analysis should show that the acceleration of the deck does not exceed the limits.

When considering maximal speeds of 200 km h^{-1} the flowchart gives a different outcome. Since it is a continuous bridge and does not exceed deflection limits, note (5), no dynamic analysis is required. Even at resonance, no check is required for acceleration or fatigue. The dynamic amplification factor sufficiently covers bridge dynamics. In Section 4.2 this factor appeared to be 1 for this design.

6.5. Remarks

This design does not have a large enough fundamental frequency to have little to no resonance risk if compared to the periodic wheel load. It is, however, a continuous beam and thus will have a lower dynamic response. The fact that the dynamic amplification factor is 1 also suggests that the span is sufficiently long for no critical dynamical problems.

The torsional modes are concerning. Concrete and steel railway bridges often have good torsional rigidity. Timber is, per definition, weak in torsion and has low torsional stiffness. Future studies should investigate the dynamic response of eccentric loading for sections with low torsional stiffness.

The first mode is horizontal and is above 2 Hz. EN1990 states that horizontal frequencies should not be smaller than 1.2 Hz. The same value is advised in the Dutch national annexe. This suggests that the horizontal modes pose no risk.

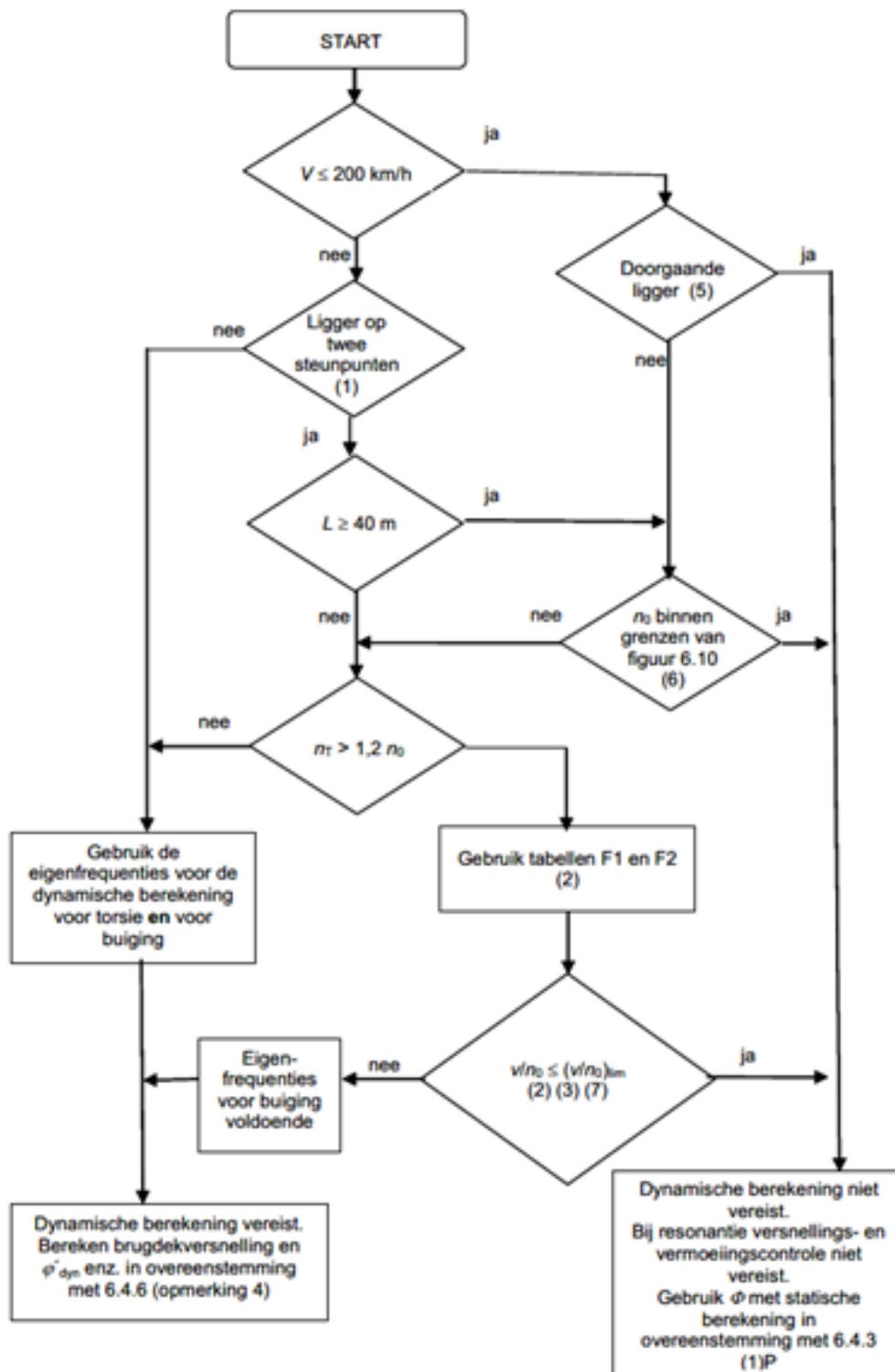


Figure 6.3: Dynamic flow chart of EN1991-2

Part III

Connection Design

Dowel-type calculation models

Different connection details exist to connect timber elements. The dowel-type connection is commonly used. Dowels, bolts, screws, and nails are all dowel-type steel fasteners. Bigger structures use dowels and bolts to connect their large elements. These are also fasteners that can connect timber to steel elements. This thesis uses slotted-in steel plates to connect the timber to the steel cross-section with dowel-type fasteners. This chapter presents background on the calculation models in EC for these timber to steel connections.

7.1. Principle

The principle of the fastener is to transfer the force between two elements. An example of a single fastener transferring a tension force between a timber element and a steel plate is shown in Figure 7.1. Each force exerted on the dowel will lead to embedment stresses in timber and bearing in steel. Figure 7.2 shows a top view of three possible failure modes of Figure 7.1. It also shows the embedment stresses configuration. The fastener transfers the loading from timber, via its shear plane, to the steel plate. Multiple fasteners can be used in an arbitrary configuration to transfer normal force, shear force, and bending moments.

Such a connection can fail in multiple manners, especially with the orthotropic nature of timber. There are two independent sets of criteria to determine how the connection will fail. These can be differentiated by defining them as local and global design criteria (Pedersen, 2002). The local criteria apply to a single fastener. To determine the strength of a single fastener is dependent on its own strength and the embedment in the timber element. Global criteria view the connection as a whole. The strength of the timber element and steel plate dictate a connection its strength.

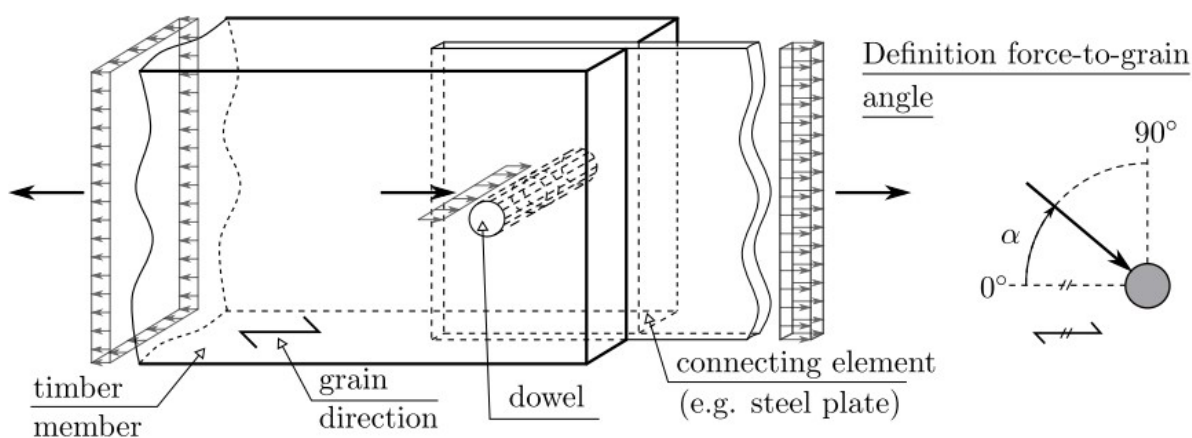


Figure 7.1: A schematic view of a dowel connection with a single fastener (Schweigler, 2013). The loading and grain direction are defined, as well as the force-to-grain angle definition. The latter is important for embedment strength of the timber.

7.2. Local criteria

The strength of a single fastener is dependent on its bending strength and the embedment strength of the timber element. Johansen (1949) found out that there are three main failure modes for timber to steel connections. The three failure modes are shown in Figure 7.2 and can be calculated using Equation (7.1). Johansen assumed that the timber elements are of the same grade and have equal width. Additionally, the plastic moment capacity was assumed to be the yield moment capacity of the fastener. The single fastener and timber are assumed to behave in an ideal plastic way. The single-fastener acts rigidly.

In the case of a steel plate, the two plastic hinges form on both sides. It is assumed that the steel plate undergoes no extension (Pedersen, 2002). This can be true for experimental tests but can often not be realised in real constructions. Pedersen argues that the Eurocode formulation, which is based on the Johansen equations, is optimistic. However, many tests show that the Eurocode equations are rather conservative (Cabrero & Yurrita, 2018; Misconel et al., 2016; Sandhaas, 2012; Yurrita & Cabrero, 2021; Yurrita et al., 2019).

The three modes in Figure 7.2 each have a different timber width that changes the dowel slenderness. The dowel slenderness determines which mode is governing.

- **Mode I:** The fastener is stiff and strong such that the timber embedment strength fails.
- **Mode II:** A plastic hinge forms in the dowel on both sides of the steel plate.
- **Mode III:** Two plastic hinges on each side of the middle element occur.

$$F_y = \begin{cases} tdf_h & \text{for } t < \sqrt{\frac{2M_y}{df_h}} & \text{Mode I} \\ \left(\sqrt{2 + 4\frac{M_y}{t^2df_h}} - 1\right) tdf_h & \text{for } \sqrt{\frac{2M_y}{df_h}} \leq t < \sqrt{\frac{16M_y}{df_h}} & \text{Mode II} \\ \sqrt{4M_ydf_h} & \text{for } t \geq \sqrt{\frac{16M_y}{df_h}} & \text{Mode III} \end{cases} \quad (7.1)$$

where:

t = thickness of outer element, timber

d = diameter of fastener

f_h = embedment strength of timber, dependent on angle-to-grain

M_y = yield moment of fastener

The Eurocode, Equation (7.2), has slightly adjusted Johansen equations, but the theory still holds. The model is often called the European Yield Model (EYM). In mode III, a factor of 2.3 appears, which represents the $\sqrt{4}$ in Equation (7.1) multiplied with a factor to account for the difference in the partial safety factor for timber and steel. This way a single partial safety factor can be used for timber connections. The rope effect is included via $F_{ax,Rk}$. This effect is the result of the pull-out strength of the dowel-type fastener. Bolts and screws have increased strength due to this.

$$F_{v,Rk} = \min \begin{cases} f_{h,k}t_1d & \text{Mode I} \\ f_{h,k}t_1d \left[\sqrt{2 + \frac{4M_{y,Rk}}{f_{h,k}dt_1^2}} - 1 \right] + \frac{F_{ax,Rk}}{4} & \text{Mode II} \\ 2.3\sqrt{M_{y,Rk}f_{h,k}d} + \frac{F_{ax,Rk}}{4} & \text{Mode III} \end{cases} \quad (7.2)$$

where:

$f_{h,k}$ = embedment strength of timber, dependent on angle-to-grain

t_1 = thickness of timber element

d = dowel diameter

$M_{y,Rk}$ = characteristic yield moment of fastener

$F_{ax,Rk}$ = characteristic axial pull-out force of the fastener according to the rope effect

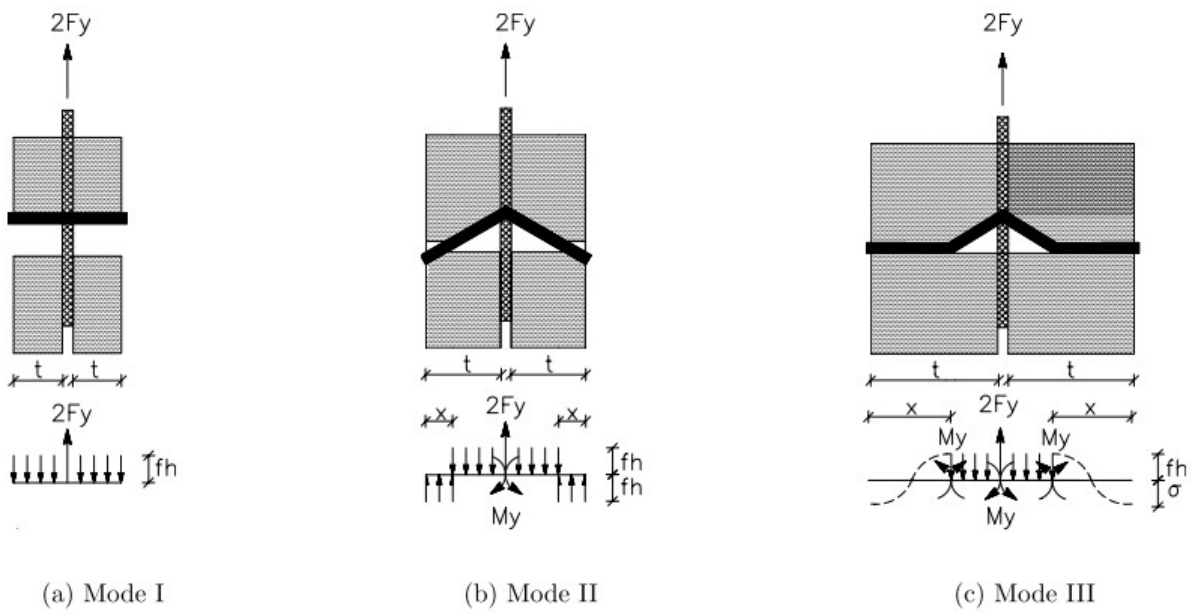


Figure 7.2: Three main plastic failure modes for a double shear connection with a dowel connecting a slotted-in steel plate Pedersen (2002). Each mode has progressively more timber of which the embedment stresses can lead to the formation of one or multiple plastic hinges in the dowel.

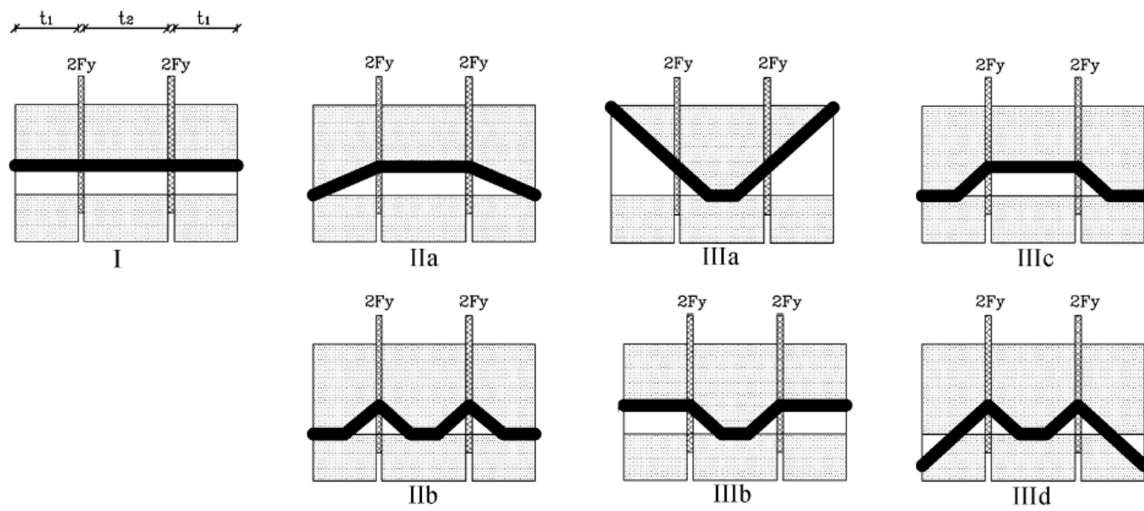


Figure 7.3: Seven failure modes for double slotted-in steel plates derived from the main failure modes (Pedersen, 2002).

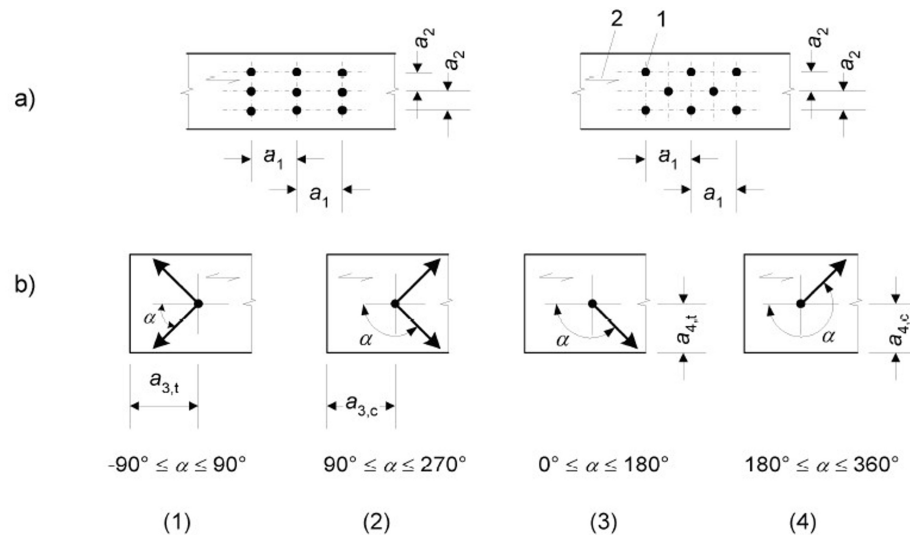


Figure 7.4: Edge distance definition of timber elements using dowel-type fasteners. Different force directions require different edge distances. The figure comes from EN1995-1-1.

Spacing and edge/end distances	Angle	Minimum spacing or edge/end distances
a_1 (parallel to grain)	$0^\circ \leq \alpha \leq 360^\circ$	$(3 + 2 \cos\alpha)d$
a_2 (perpendicular to grain)	$0^\circ \leq \alpha \leq 360^\circ$	$3d$
$a_{3,t}$ (loaded end)	$-90^\circ \leq \alpha \leq 90^\circ$	$\max(7d; 80 \text{ mm})$
$a_{3,c}$ (unloaded end)	$90^\circ \leq \alpha < 150^\circ$	$\max(a_{3,t} \sin\alpha d; 3d)$
	$150^\circ \leq \alpha < 210^\circ$	$3d$
	$210^\circ \leq \alpha < 270^\circ$	$\max(a_{3,t} \sin\alpha d; 3d)$
$a_{4,t}$ (loaded edge)	$0^\circ \leq \alpha \leq 180^\circ$	$\max([2+2\sin\alpha]d; 3d)$
$a_{4,c}$ (unloaded edge)	$180^\circ \leq \alpha \leq 360^\circ$	$3d$

Table 7.1: Minimal distances for bolts/dowels based on the definition in Figure 7.4 from EN1995-1-1.

7.2.1. Spacing limitations

The stress distribution around the steel fastener is very complex. For a fastener to develop its full potential, there should be sufficient timber to redistribute the stress through the timber element. Otherwise, the timber fails preemptively. For this reason, spacing limitations are introduced. These are dependent on the force direction since timber has different strengths depending on the force to grain angle. The distance definition and limitations for a timber element can be found in Figure 7.4 and Table 7.1. For the steel element, the spacing of bolts in steel is allowed to be much smaller and thus not governing. They can be found in EN1993-1-8.

7.2.2. Multiple shear planes

For larger structures, multiple fasteners are required, but multiple shear planes can also prove beneficial. The same theory can be used for the double shear plane of a single fastener and single plate. The combination of different failure modes leads to seven modes, shown in Figure 7.3. Sawata et al. (2006) performed tests on glulam and found good results comparing tests to the EYM approach. It showed a strong relationship between the number of slotted-in steel plates, the distance between plates, and the edge distance.

Pedersen (2002) derived the formulae for these failure modes. Extra capacity is gained compared to the EC method. Failure mode IIb is similar to mode III in EC5. The additional capacity from introducing the partial safety factors for steel and timber is not included by Pedersen.

$$F_y = \min \begin{cases} \frac{1}{4} (2t_1 + t_2) df_h & \text{Mode I} \\ \left(-\frac{1}{2}t_1 + \frac{t_2}{4} + \sqrt{\frac{1}{2}t_1^2 + \frac{M_y}{df_h}} \right) df_h & \text{Mode IIa} \\ \sqrt{4M_y df_h} & \text{Mode IIb} \\ \left(\frac{1}{2}t_1 + \frac{1}{2}\sqrt{t_1^2 + \frac{2M_y}{df_h}} \right) df_h & \text{Mode IIIa} \\ \left(\sqrt{\frac{M_y}{df_h}} + \frac{1}{2}t_1 \right) df_h & \text{Mode IIIb} \\ \left(\sqrt{\frac{M_y}{df_h}} + \frac{1}{4}t_2 \right) df_h & \text{Mode IIIc} \\ \left(-\frac{1}{2}t_1 + \sqrt{\frac{1}{2}t_1^2 + \frac{M_y}{df_h}} + \sqrt{\frac{M_y}{df_h}} \right) df_h & \text{Mode IIId} \end{cases} \quad (7.3)$$

where:

t_1 = thickness of outer timber element

t_2 = thickness of inner timber element

d = fastener diameter

f_h = timber embedment strength, similar to $f_{h,k}$ in Equation (7.2)

M_y = Yield moment of fastener, similar to $M_{y,Rk}$ in Equation (7.2)

7.2.3. Multiple fasteners in a row

Larger forces require more fasteners. However, the number cannot be linearly increased to match the increased force. When there are multiple fasteners in a row, the connection resistance should be reduced by considering only the effective number of fasteners. A row of fasteners is parallel to the force. A formula in EC5 is given to calculate this, Equation (7.4). The formula is empirical.

$$n_{ef} = \min \left\{ \begin{array}{l} n \\ n^{0.9} \sqrt[4]{\frac{a_1}{13d}} \end{array} \right. \quad (7.4)$$

where:

n = number of fasteners in a row

a_1 = internal distance parallel to grain of fasteners

d = diameter of fastener

7.2.4. Stiffness

EC5 presents an empiric formula which calculates the stiffness per shear plane per stiffener. Equation (7.5) is specific for a steel to timber connection. It is dependent on the density of timber and the fastener diameter. Sandhaas (2012) argues that the stiffness of a connection should also be reduced for the effective number of fasteners in a row. EC5 does not include such a reduction.

$$K_{ser} = 2 \cdot \rho_m^{1.5} \frac{d}{23} \quad (7.5)$$

7.3. Global criteria

Failure of the timber or steel element should be avoided, which is the global criteria. It is already known that spacing limitations will not lead to the failure of the steel plate. The failure of the steel plate is not discussed since it is assumed a sufficient thickness is chosen. The timber element can fail in undesirable brittle manners. There are four modes: tension splitting, plug shear, group tear-out, also called block shear, and net tension, shown in Figure 7.5. Figure 7.6 shows the stresses that occur around a fastener and illustrate the tension stresses that lead to tension splitting.

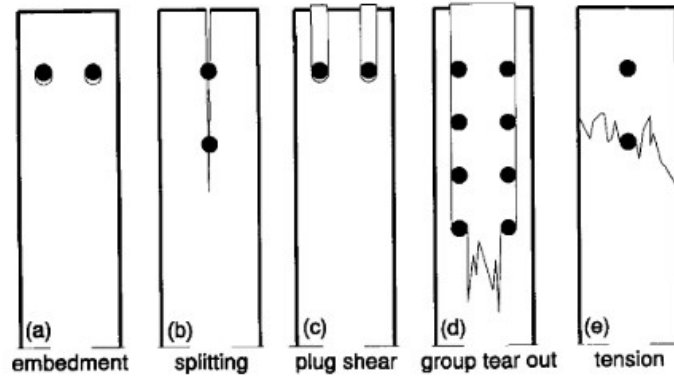


Figure 7.5: Failure modes for a connection with multiple dowel-type fasteners (Jorissen, 1998).

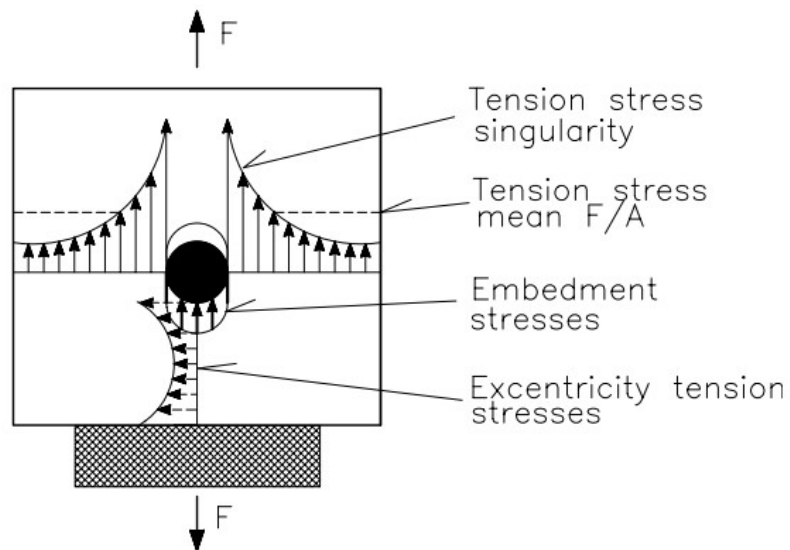


Figure 7.6: Schematic representation of stresses around fastener with the focus on tensile stresses (Pedersen, 2002).

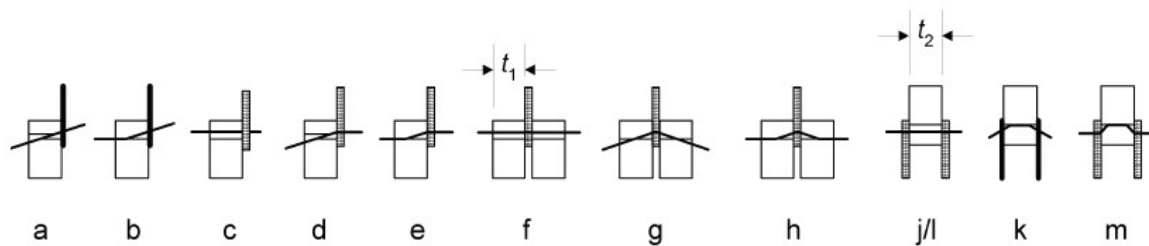


Figure 7.7: Dowel failure modes for steel-to-timber connections from EN1995-1-1.

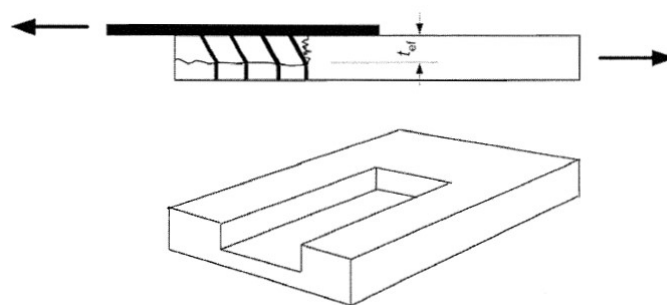


Figure 7.8: Example of one-sided shear plug with multiple fasteners, figure A.2 in EN1995-1-1.

Tension splitting can occur in two manners for a force parallel-to-grain. Splitting due to tension stress singularity is caused by stresses parallel to the grain. The dowel pushes the timber in front of it away, as if it was a wedge. Perpendicular-to-grain tensile stresses caused by eccentricity tension stresses, shown in Figure 7.6, is the second manner.

Only splitting caused by the stress singularity next to the dowel can occur when loaded perpendicular-to-grain. The spacing requirements capture this brittle failure. When complying to these limitations, tension splitting will not occur.

Plug shear is a failure when the material in front of the dowel is pushed away. It is a shear failure of the timber. The figure shows plug shear for a single fastener, but it can also occur for multiple fasteners in a row. Figure 7.8 shows a single-sided connection that fails in shear plug. It can only occur when failure mode d, e, g, or h in Figure 7.7 is governing.

Block shear is a type of shear plug but for all failure modes not specified for plug shear. It combines shear stresses along a row of fasteners and tension stresses on the net cross-section. Originally, it was not considered in the pre-standard of EC5. After a glulam roof truss collapsed in Finland, this inadequacy was met with a supplement for block shear in Finland (Ranta-Maunus & Kevarinmäki, 2003). In the case of the roof truss it was found that the capacity was only 50% of the expected characteristic strength.

In the current EC5, block shear (and plug shear) is an informative appendix. The resistance of a connection is the maximal value of either the tensile part resistance, or the shear part resistance.

Net tension is a brittle tensile failure mode. It excludes the lost material for the dowel holes and the cuts for the steel plates.



Connection

This chapter discusses several connection possibilities to connect the timber box section to the steel section. The most promising option is selected for the current design, and its strength is calculated. The connection effect on the global behaviour is modelled with the rotational spring in SCIA.

8.1. Connection options

Eurocode 5 contains a chapter dedicated to timber connections with metal fasteners. For bridges, not all connections are allowed. According to EN1995-2, axially loaded nails, stapled connections, and punch metal plate fasteners must not be used. This originates most likely because these fastening methods use small and thin steel elements. Bridges are large structures that require appropriate strong steel fasteners. Figure 8.1 shows connection principles that have been considered for the design.

8.1.1. Glued steel plates

This connection is built by cutting into a timber element, filling it with glue, and positioning a steel plate in it. The glue-line is the interface between timber and steel and will transfer the force over a large area. It has to be made in a controlled environment like a factory. Timber and steel act differently on temperature and moisture. The difference in size changes is expected to lead to brittle failure in the glue. When the interface fails, no force can be transferred anymore.

8.1.2. Pretension bolts

Bolts require to be pretensioned in steel railway bridges. This enables force transfer via friction between the steel elements and is required for fatigue reasons. The nut and head exert high compression forces perpendicular to the grain, so additional steel plates would be necessary to spread the forces. Another disadvantage is the loss of pretension force due to creep of timber under sustained loading. A spring could postpone the need to tighten the bolt. This connection is still high maintenance.

8.1.3. Steel joist hanger

These connections are often used in timber buildings to connect timber beams. The timber rests on the steel joist to transfer the force. The joists is connected to the steel section. The connection introduces too many hinges in the continuous beam, resulting in an unstable mechanism.

8.1.4. Dowel-type

A steel plate with holes is inserted in cuts in the timber elements. Steel fasteners can be placed in the holes through timber and steel. The force transfer is via shear in the steel fasteners. Embedment of the material resists the displacement of the fastener. Screws and nails loaded in shear are dowel-type fasteners with a small diameter. Bolts and dowels can have diameters up to 30 mm.

8.1.5. Gradual transition

A gradual connection can be created by combining the steel joist and dowel-type principles. Dowels can resist the bending moment, and the joist can transfer most of the shear force. This would lead to a semi-rigid connection that even can have an appealing effect from an architectural point of view.

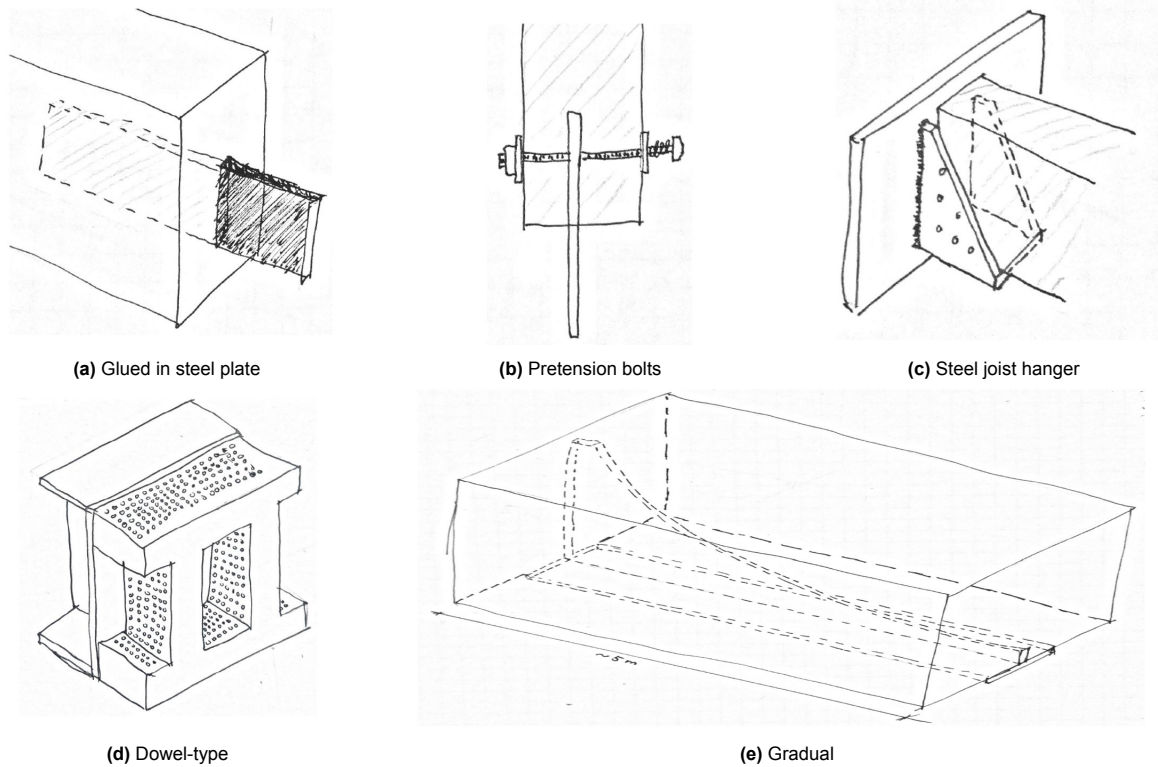


Figure 8.1: Connection examples sketches

8.1.6. Connection choice

The dowel-type connection is most promising. The disadvantages of glued-in steel plates, pretensioned bolts, and steel joists have already been stated. The gradual connection is a complex combination of the dowel-type and steel joist principles. Without knowledge on the dowel-type connection, this gradual connection is disregarded. The dowel-type connection is chosen with dowels because of the novelty of the connection application. Additional strength for using bolts is only necessary when the fasteners are governing. Figure 8.2 shows an impression of the connection at scale.

8.2. Resistance

The strength of a connection is the resistance of the weakest failure mode. For the dowel-type connection, there are several possible failure modes. As discussed in the previous chapter there are global and local criteria that lead to different failures. First, the local criteria are checked by checking the fastener strength. Then, the steel and timber material is checked as the global criterion.

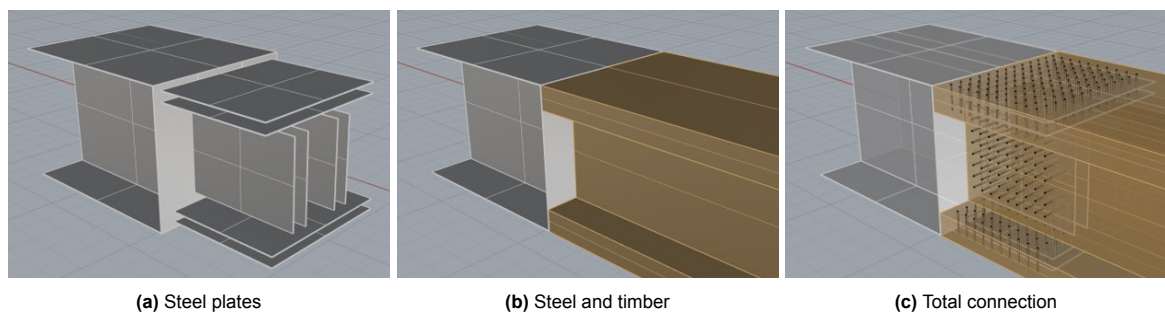


Figure 8.2: Dowel-type connection drawing made in Rhino. Double slotted-in steel plates inserted in the timber box girder connected with many dowels. The drawing is to scale.

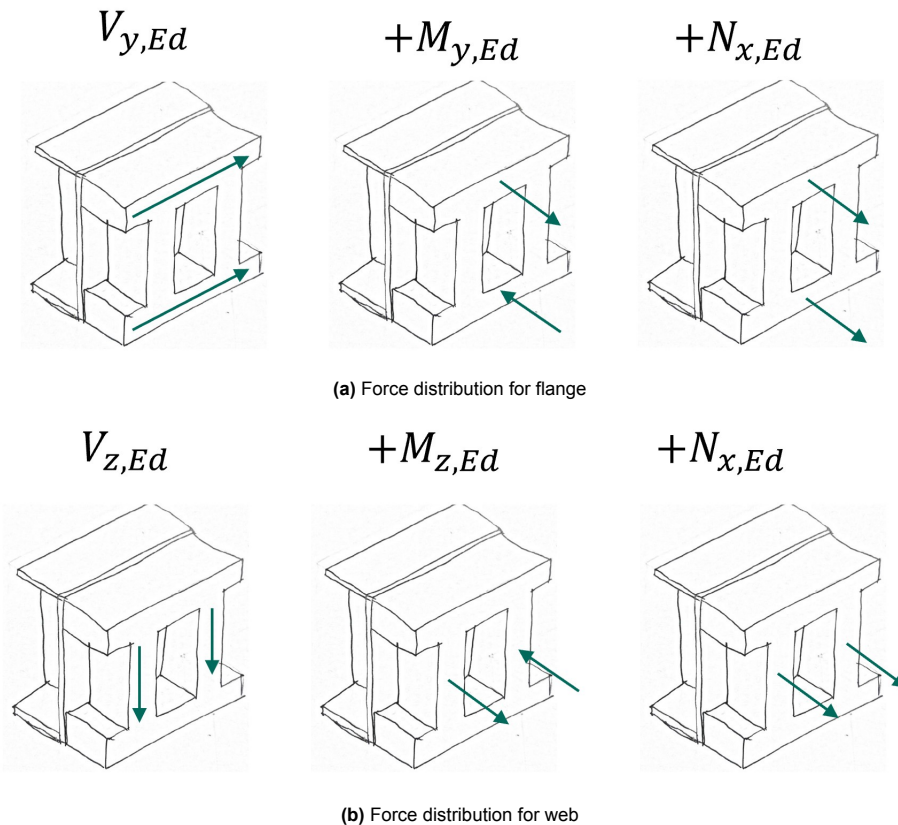


Figure 8.3: Force distribution to determine force slotted-in steel plates require to resist.

8.2.1. Fastener

To determine the connection strength regarding the local criteria, a specific procedure is followed. This procedure calculates the number of required steel fasteners to resist the cross-sectional forces that follow from the analysis in Chapter 5. As a follow-up, the number of rows and columns is chosen, and the effective number of steel fasteners in this group is determined. The number of effective fasteners must be larger than the required amount. The steps are described in more detail.

1. Calculate the characteristic resistance of each failure mode for a given timber thickness, steel fastener diameter, and embedment direction;
2. Determine the mode with the lowest resistance;
3. Distribute the cross-sectional forces as in Figure 8.3;
4. Calculate the resultant force and its angle to the grain;
5. Calculate the design resistance per fastener by multiplying the characteristic resistance of the fastener by the number of shear planes and dividing it with a partial safety factor for dowel connections, $\gamma_M = 1.3$;
6. Divide the resultant force with the design resistance per fastener to get the required number of fasteners, shown in Equation (8.1).

In reality, the major bending moment, $M_{y,Ed}$, can also be resisted by the fasteners in the web. However, it is assumed that only the flanges contribute to the bending moment resistance.

The configuration of the dowels is chosen as a square with equal fastener distances, as the dowel configuration in Figure 8.2. A row is in the longitudinal direction. A column is in the transverse direction. Multiple fasteners in a row require a reduction since the load is not equally distributed among all fasteners. Equation (7.4) is the formula to calculate the effective number of fasteners in a row. There is no reduction for multiple columns.

It is assumed that the slotted-in plates do not have the same width as the timber elements. The assumed dimensions of the steel plate in the top flange is 3.8 m and in the web 2.2 m. To acquire the number for effective fasteners for a chosen configuration of dowels is described in detail.

1. Choose the size of the slotted-in steel plate;
2. Choose the edge and internal distance, complying to spacing limitations;
3. Calculate the maximum amount of possible fasteners in a column;
4. Choose the number of fasteners per row and column;
5. Calculate the number of effective fasteners in a row;
6. Multiply number of columns by effective number of rows to get effective number of fasteners.

The calculation and intermediate values that follow from both these procedures can be found in Appendix D. The cross-sectional forces that the connection requires to resist are shown in Table 8.1. Table 8.2 shows the resultant force and the angle to the grain.

Connection at 5 m		Flange	Web
$M_{y,Ed,5m}$	29.3 MNm	F_x	13.5 MN
$M_{z,Ed,5m}$	6.3 MNm	F_y	0.6 MN
$V_{z,Ed,5m}$	6.2 MN	α_F	2.54 °
$V_{y,Ed,5m}$	0.65 MN	F_{res}	13.5 MN
$N_{x,Ed,5m}$	11 MN		7.3 MN
$T_{Ed,5m}$	1.3 MNm		

Table 8.1: Cross-sectional forces.

Table 8.2: Resultant forces.

The required number of fasteners follows from Equation (8.1). F_v is dependent on the grain angle due to the dependency of the embedment strength of timber on the grain angle.

$$n_{req} = \frac{F_{res}}{F_v(\alpha)/\gamma_M} \quad (8.1)$$

To determine the effective number of fasteners the type has to be chosen. A dowel with a diameter of 30mm and strength grade S355 is chosen. Both single and double slotted-in steel plates of 20 mm are considered. This thesis investigates the feasibility of the bridge structure, not the optimisation of this connection. Therefore the edge distance is set as $7d$ and the internal distances as $9d$ to ensure sufficient timber material to transfer the stresses. It is decided that the maximal number of fasteners geometrically possible in the transverse direction is used. Consequently, only the number of rows can be changed to get the required number of fasteners.

Table 8.3 shows the required amount of dowels required, the distribution that results in a sufficient amount of effective dowels, and the effective dowels. Having a smaller internal distance to reduce the cross-section size will lead to more dowels since n_{ef} reduces with a smaller internal distance. Introducing a second steel plate leads to a lower amount of dowels required.

	Single shear plane			Double shear plane		
	n_{req}	col x row	n_{ef}	n_{req}	col x row	n_{ef}
Flange	140	13x16	143.78	85	13x10	94.25
Web	84	7x18	86.1	48	7x10	50.75

Table 8.3: Required number of dowels for single and double slotted-in steel plates and the distribution of chosen dowels to meet the requirement when accounting for the effective row reduction.

8.2.2. Timber section

Of the global criteria presented in Section 7.3, the tensile splitting failure is covered by complying with the spacing limitations. Block shear and plug shear should be checked using the informative annexe of EN1995-1-1. The net tension section is checked separately.

Another failure mode is tension between the web and flange perpendicular-to-grain due to shrinkage or expansion. This failure can occur when the moisture content of timber changes. Steel does not change in size from moisture and therefore restricts timber shrinkage or expansion.

Block shear

The formulae from the informative annexe result in unrealistically large resistance values. The shear length is multiplied by the tension length in equation A.3 in EN1995-1-1. This seems to lead to erroneous results. Contrary to the fastener formulae, in which the minimum of a set of resistances must be taken, the maximum of the tensile area resistance and the shear area resistance results in the block shear resistance. This is counter intuitive for engineers.

A calculation for block shear based on the block shear calculation method for steel is performed to check the resistance. The slotted-in steel plates and the dowel holes reduce the shear and tension area. The timber design strength is used to determine the design block shear strength. The partial safety factor, $\gamma_M = 1.3$, for timber connections is not used since the design strength partial safety factor is much lower, around 1.8.

$$F_{b,Rd,fl} = A_{net,t,fl} \cdot f_{t,0,g,k} + A_{net,v,fl} \cdot f_{v,g,k} = 1.5 \cdot 16.8 + 2.7 \cdot 1.96 = 41.8 \text{ MN}$$

$$F_{b,Rd,web} = A_{net,t,web} \cdot f_{t,0,g,k} + A_{net,v,web} \cdot f_{v,g,k} = 1.15 \cdot 16.8 + 4.2 \cdot 1.96 = 37.8 \text{ MN}$$

This leads to a unity check for the top flange of 0.41 and the web of 0.24.

Net tension

The net tension section of timber is calculated straightforwardly. The slotted-in steel plates reduce the thickness and width by the number of fasteners times the dowel diameter. It is assumed that 30 mm dowels are pressed into holes of equal size.

The stresses are calculated by dividing the cross-sectional force by the reduced area. The resultant force in x- and y-direction are separately addressed. The unity checks are shown in Table 8.4. There is too little shear resistance. This is expected in hindsight since the shear resistance of the gross cross-section was already near the limit, and the area reduction is significant with this many bolts.

	Flange		Web	
A_{net}	1.877 m ²		1.736 m ²	
σ_t	6.23 MNm ²	0.36	3.23 MNm ²	0.19
τ_v	0.40 MNm ²	0.16	2.76 MNm ²	1.10

Table 8.4: Netto cross-section in tension and shear.

Shrinkage tension

Timber shrinks if its MC drops and expands if it rises. The steel part in the connection limits free deformation. Stresses are introduced when the timber cannot change in size. The value for strain per percentage of MC change is taken from a study by Chiniforush et al. (2019). An extensive set of softwood glulam was tested and appeared to have a maximal average value of 0.00259 $\epsilon/\%$. This value will indicate the impact of moisture shrinkage on stresses in the connection. The maximal average value is chosen to have a conservative result.

From Figure 2.7 it can be extracted that the MC of timber in Norway, based on the average relative humidity, varies between 13 and 16%. It is assumed that the timber is manufactured with an MC of 16%.

Figure 8.4 shows a representation of restricted deformation by the steel parts of the connection. The stress perpendicular-to-grain between the flange and web is calculated using Hooke's law.

$$\sigma_{MC} = E_{90,mean} \cdot \epsilon_{MC} = 300 * (0.00259 * 3) = 2.33 \text{ MPa}$$

This leads to a unity check of 8.32 for the design tensile strength perpendicular-to-grain is only 0.28 MPa. This is insufficient.

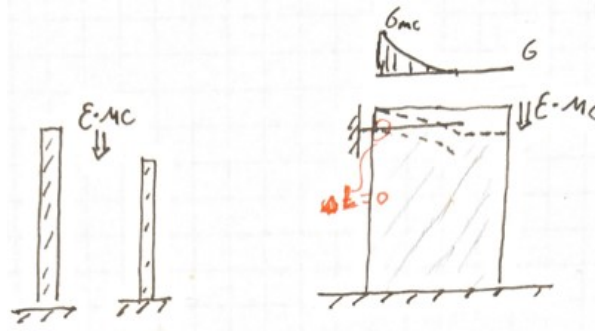


Figure 8.4: A structural model representation of timber shrinkage. Free to deform timber principle is shown on the left. The hindered deformation of the timber section by the steel slotted-in plate is shown on the right, with the occurring shrinkage stresses.



Figure 8.5: Mechanics scheme with rotational springs.

Not only the web-flange interface is affected by these stresses. Cracks will occur for every part of the timber section that experiences restricted movement.

The calculation assumes the structure to start with an MC of 16%. However, the structure can also start with a lower MC, 13%, for example. This would introduce compression perpendicular-to-grain and result in a unity check of 1.66. Although this is still insufficient, it requires less absolute deformation of the steel to lower the stresses.

8.2.3. Steel slotted-in plates

The steel plate has a thickness of 20 mm, its plate bearing strength, net section, and block shear failure modes must be checked. The block shear failure mode is neglected since the net section will always govern over it due to the dimension of the connection.

Bearing depends on the edge and internal distances. The spacing limits of steel are much less strict. This leads to a non-reduced bearing strength. The formulae can be found in table 3.4 of EN1993-1-8. The non-reduced bearing strength is calculated using Equation (8.2).

$$F_{b,Rd} = \frac{2.5f_u dt}{\gamma_{M2}} \quad (8.2)$$

The unity checks are presented in Table 8.5. It also includes the shear strength of the dowel itself.

	Flange	Web
Dowel shear	0.14	0.15
Plate bearing	0.11	0.11
Net section tension	0.49	0.40
Net section shear	0.04	0.40

Table 8.5: UC for shear strength, plate bearing, and net tension for the slotted-in steel plate.

8.3. Connection stiffness

The stiffness of the shear plane of a single fastener is calculated by Equation (7.5). A connection stiffness can have a significant effect on the structure. To model this, a rotational spring can be introduced. Figure 8.5 shows a mechanics scheme containing rotational springs at the connection positions.

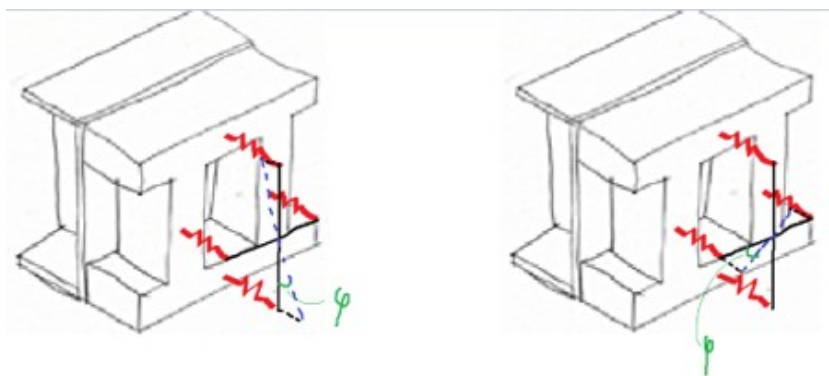


Figure 8.6: Schematising slotted-in steel plates by springs and the rotational capacity.

The stiffness of a single fastener can be multiplied by the total or the effective number of fasteners. This yields the stiffness of a flange or web. The rotational stiffness is divided similarly to the force distribution. The major axis stiffness is only dependent on the fasteners in the flange and the minor axis stiffness only on the fasteners in the web. Figure 8.6 illustrates this. Equation (8.3) is used to calculate the rotational stiffness.

$$K_r = \frac{1}{2} K_{ser,tot} h^2 \quad (8.3)$$

where:

$K_{ser,tot}$ = total stiffness of all fasteners in a plane

h = centre to centre distance of the flanges or webs

The actual rotational stiffness values are calculated for the double slotted-in steel plate. Equation (7.5) is used to calculate the stiffness per dowel. The total stiffness of all fasteners in a plane is calculated for the effective number of dowels, following the suggestion by Sandhaas (2012), and for the total number of dowels, following Eurocode procedure.

	effective	total		effective	total
K_{ser}		27.43 MN/m	K_{ser}		27.43 MN/m
$K_{ser,tot}$	10 343 MN/m	14 266 MN/m	$K_{ser,tot}$	5569 MN/m	7681 MN/m
K_r	11 175 MNm/rad	15 413 MNm/rad	K_r	1433 MNm/rad	1977 MNm/rad

Table 8.6: Connection stiffness values for flange and web.

8.3.1. Deflection effects

Without a fully rigid connection, additional deflection is inevitable. The unity check for deflection in creep is close to unity. It is expected that less rotational stiffness will result in an insufficient unity check. As the graph in Figure 8.7 shows.

The deflection increase with a stiffness following from the effective number of dowels is 15%. Accounting for all dowels the deflection is 12% larger. An increase in stiffness of 38% is achieved with the Eurocode method. However, this stiffness-deflection relationship is not linear. For a tenfold stiffness the assumption of a rigid connection is feasible.

8.3.2. Rotation effects

This finite stiffness will lead to jumps in rotations, essentially kinks in the structure. This poses a risk for derailment. There are no limits specified in the standards. As mentioned before, end-of-deck rotation is accounted for implicit by EN1991-2 6.5.4 by considering bridge-track interaction. However, this is beyond the scope. Limits mentioned in literature are in the vicinity of 5 mrad (Guo et al., 2018; Vican et al., 2015). Although the conditions were not clear.

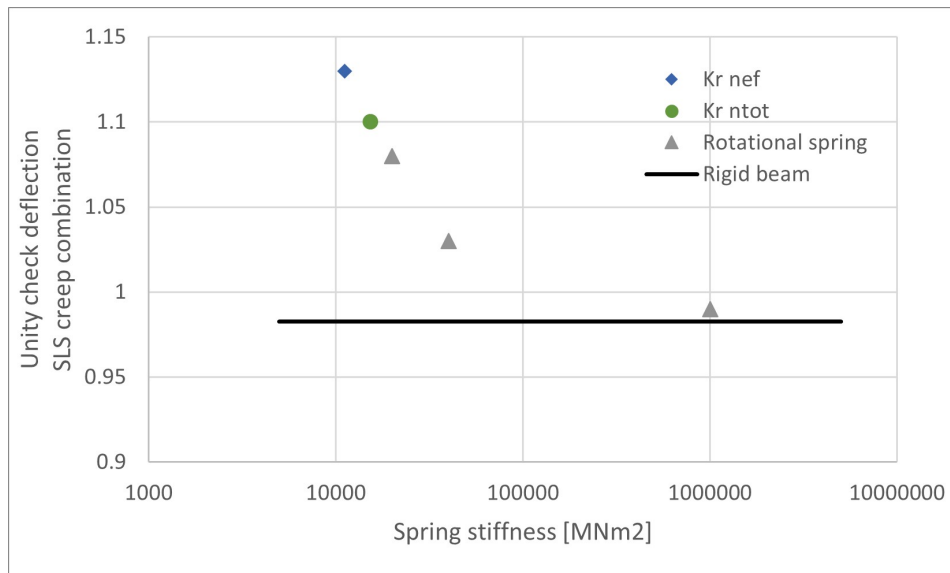


Figure 8.7: Unity check creep deflection for different rotational spring stiffness values under the SLS creep load combination. A rounded double, quadruple, and tenfold of the effective stiffness, $K_{r,nef}$, is shown to show the required stiffness to approach an ideal rigid connection.

The actual rotation this kink can have, can be calculated through dividing the bending moment by the rotational stiffness. Assuming a ULS bending moment at the connection, from Table 5.2, and the effective rotational stiffness results in a significant increase in rotation. The maximal SLS rotation in the model is 5.9 mrad.

$$\theta_{kink} = \frac{M_{Ed}}{K_{r,eff}} = \frac{30 \text{ MNm}}{11\,175 \text{ MNm/rad}} = 2.7 \text{ mrad}$$

The kink, however, is only a risk when it occurs at track level. The current calculated rotational kink is at the beam level. The top layer of 50 cm of concrete is neglected in all calculations but will provide stiffness, if it is poured continuously across the connection. This additional stiffness is expected to limit the actual kink of the track. Without values and limits no conclusions can be drawn on this topic.

8.3.3. Load distribution effects

Beam stiffness influences the bending moment distribution. A rotational spring with finite stiffness will lead to a larger bending moment at midspan. It also lowers the bending moment at the connection since it has a limited bending moment resistance. The shear force distribution is not changed since it is not dependent on the stiffness.

Part IV

Design assessment

9

Current Design

This chapter presents the complete current design with special focus on the timber and steel cross-section and the connection between the cross-sections. The results of the chapters in parts II and III are combined and translated to the railway bridge design. This hybrid design is based on multiple assumptions, which will be addressed in this chapter.

9.1. Design

In Chapter 3 several cross-section options were introduced and used in Chapter 5 to determine the cross-section design for the timber and steel sections. A shorter timber cross-section height was implemented and only shortly presented. In Figure 9.2 both the steel and timber cross-section are shown. To view the overall design a render is shown in Figure 9.1. A more elaborate explanation of the cross-sections and the necessary connection is given in the following sections. The resulting unity checks are summarised in Table 9.1 at the end of this section.

9.1.1. Cross-section

In Figure 9.2 both the timber and steel section are shown. The timber section is made from glued laminated timber and has a construction height of 3.5 m, which is used in the model and calculations in Chapter 5. It matches the height of the steel girder to have a fluent bridge superstructure.

The steel section shown in Figure 9.2b is the class 4 section presented in Section 3.4 but including the conceptual stiffeners for the webs and top flange. These stiffeners are expected to be required but not included in the calculations as they should not contribute much to the general properties.

9.1.2. Connection

Chapter 8 contains the strength and stiffness calculation of the connection after the selection of the most promising connection possibility. An impression was given, but the correct amount of dowels and spacing used in the calculations are shown in Figure 9.3.

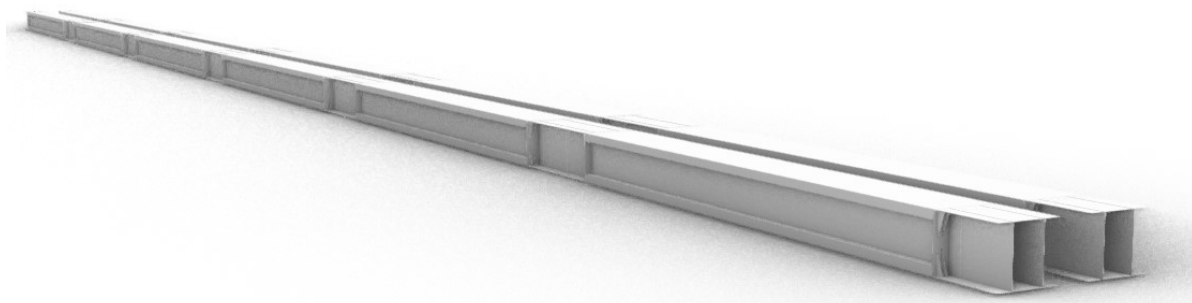


Figure 9.1: Render of the current design. Two box girders that both support a single railway track are rendered in drawing program Rhino. The cross-sections are used in the calculations in Chapter 5. The thinner sections are steel, and the thicker parts are timber, separated by a transverse steel plate.

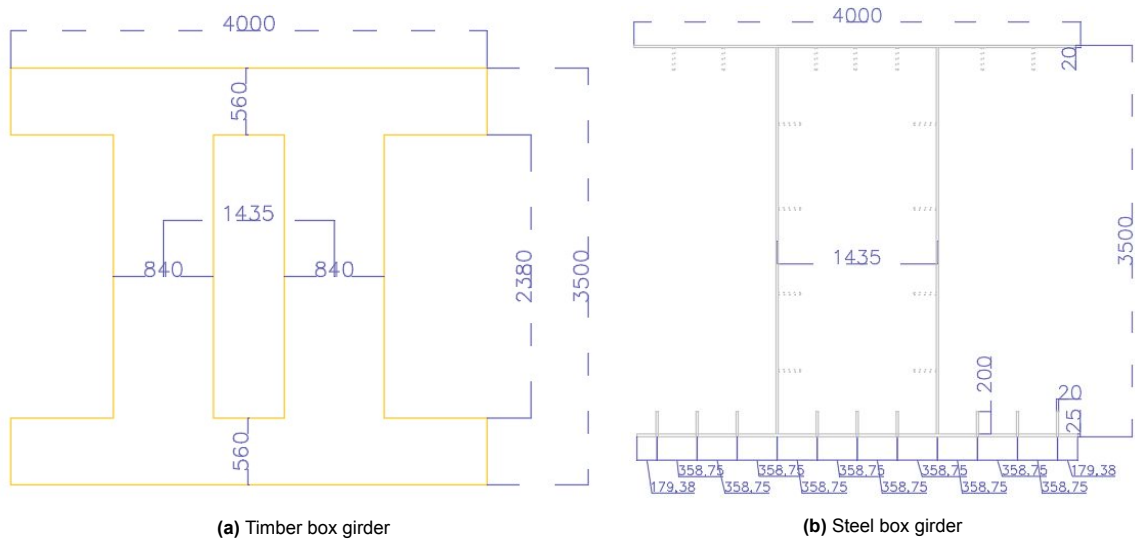


Figure 9.2: Timber and steel boxgirder of current design with a height of 3.5 m. The steel section has stiffeners that have not been calculated but will be constructed in the final cross-section design and are included in the weight calculation.

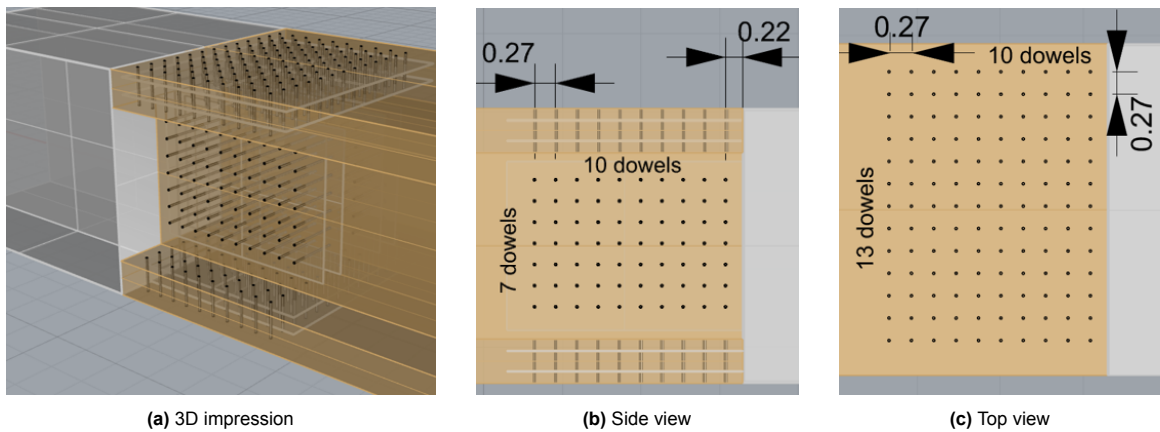


Figure 9.3: Dowel-type connection in Rhino with dimensions. Double slotted-in steel plates with the required amount of dowels and spacing.

Unity checks	
<i>At midspan</i>	
General deflection	0.57
Passenger comfort deflection	0.75
Creep deflection semi-rigid connection	1.13
Bending moment timber	0.50
<i>At support</i>	
Main bending moment class 4 section	0.38
Fatigue of transverse plates	1.18
<i>Connection at five metre</i>	
Timber combined bending moment and normal force	0.35
Timber combined shear force and torsion moment	0.82
Timber block shear flange	0.41
Timber net tension normal force flange	0.36
Timber net tension normal force web	0.19
Timber net tension shear force web	1.10
Timber shrinkage	8.32
Steel slotted-in plate in bearing	0.11
Steel net tension governing ¹⁾	0.49
Dowel shear stress	0.15

1) Governing UC of normal and shear force in flange and web

Table 9.1: Several key unity checks of the current combined girder design.

9.1.3. Unity Checks

The key unity checks of the current design are summarised in Table 9.1. It is clear that the design does not satisfy all requirements, as there are unity checks above one marked in red. However, most checks are close to unity and can be tackled by adjusting the design slightly. Only the shrinkage of timber, with a unity check of 8.32 poses a serious problem and, therefore, is addressed in detail in Chapter 11.

The unity check for creep deflection uses a conservative combination factor that includes creep from train live loads to its total extent, as aforementioned. Evaluating a 50% decrease of this factor would cause creep deflection not to govern. Such a reduction leads to a factor that is more comparable to creep deflection factors of other live loads, such as road traffic. In case of such a reduction, the creep deflection unity check would be similar to the normal deflection limit, as shown in Table 5.5. The passenger comfort limit would become governing with a unity check of 0.75.

Although deflection unity checks are quite high, it appears that the shear strength of timber is of major importance for a safe design. The unity check of the shear resistance of the timber section at the connection is 1.10. This issue can more easily be resolved by adding material to the webs or increasing the construction height. The latter also results in a larger web area to handle the shear forces and thus have lower shear stresses.

The steel section is governed by its fatigue strength, which has a unity check of 1.18. An increase of the first and second moment of area will reduce stresses, as the bending moment stresses are the main contributors to fatigue, calculated in Section 5.4. This cross-sectional property improvement also reduces stress ranges, effectively reducing the unity check of fatigue.

9.2. Discussion of design

It is important to stress that this study investigates a preliminary design. Therefore, many assumptions and simplifications are used. Calculation methods and analyses are based on the methods in the

European standards. These assumptions are discussed for both the combined girder and the connection.

9.2.1. Combined girder

The hybrid girder consists of a timber and steel cross-section. This sub-section addresses all aspects that are not related to the connection design as well as certain used assumptions.

Timber section

The strength calculations for timber are based upon methods from EC5. Many studies have contributed to the realisation of EC5 and function as background information to this standard. However, those studies have not thoroughly investigated the effects of huge cross-sections as used in this design. Therefore, two critical assumptions have been made to check the cross-section.

The first addresses size effects, as they can substantially affect the strength of a cross-section. Most research is performed on small scale test subjects. These factors are incorporated into the methods and strength values. It is essential to investigate these effects before using large cross-sections as used in the current design.

The second assumption concerns the unity checks for combined stress states. Compared to the different combinations required for steel sections, there is a lack of these in timber design, especially combinations that combine bending and shear. The Eurocode is even lacking any combined stress states for combinations of torsion and vertical loads. The German standard does present a combination, Equation (3.8), which is therefore used.

A specific example is the shear and bending combination. A combined stress state reduction factor dependent on the cross-section shape is the timber crack factor, k_{cr} . Cracks due to bending will reduce the area able to resist shear. However, for a box girder with very wide flanges, the shear stresses in the flange are much lower and contribute little to the shear resistance. Therefore, an effective shear area is used in the calculation, as shown in the cross-section properties table Table 3.3. This effective area is calculated by multiplying the web thickness by the web height plus half of the flange thickness, basically increasing the web height. Considering the current thicknesses, the area is less than the crack factor would result in. This assumption is specific to the box girder cross-section. Timber box girder sections are less frequently used because less shear area means a lower shear resistance, which can become governing.

Steel section

The design of the steel cross-section has not received priority. The steel design was assumed not to be critical. However, a steel section must have matching construction heights with the timber section resulting in a class 4 section, which is prone to buckling. Only plate buckling is considered in this thesis. Additionally, a simplified fatigue calculation is performed. Both show the importance of an adequate steel design.

These two parts can easily be addressed by increasing the construction height slightly or adding more material via increased thickness. The current preliminary design shows that the assumption not to focus on steel is justified. The unity checks for steel in Table 9.1 suffice except for fatigue. Though, this can be resolved as discussed in Section 9.1.3. It is important to note that, regarding fatigue, the standard load models were used, not fatigue load models. These are more accurate and less conservative than the standard LM71 and SW/0.

Model

The non-prismatic structure is modelled in SCIA Engineer by using 1D beam elements in a 3D space. Cross-sectional forces and deflections are calculated with a linear calculation method. A limitation in the software is the use of class 4 sections. For general sections, the effective properties cannot be calculated. Therefore the class 2 steel cross-section is used to determine the load effects. Cross-sectional properties calculated by hand were very similar but not exact. Nevertheless, for a preliminary phase, it is assumed to be sufficient.

ULS unity checks were subsequently calculated with the cross-sectional force of the model and cross-section properties calculated by hand. The properties were calculated by hand using linear elastic

mechanics and were slightly different from the sections' properties in SCIA. The cross-sectional forces were extracted from the envelope diagrams. Although the maximal hogging bending moment might not coincide with the maximal shear force, torsional moment, or normal force, the combined effect was checked. This can lead to slightly conservative checks. However, it was determined not to be overly conservative because, the largest hogging bending moment, largest shear force, and largest torsion appear in the same position, at the bearing. The unity checks sufficed, as seen in Table 9.1.

Dynamics

Every high-speed railway bridge requires an intensive dynamic analysis. A complete dynamic analysis is out of the scope of this project because it would have a sufficient amount of work to be a stand-alone thesis. A preliminary examination is performed by checking the eigenmodes with induced frequencies. It was shown that the eigenmodes are very likely to be within the range of induced frequencies at high speeds. The Eurocode does not require a dynamic analysis when train speeds are under 200 kmh^{-1} but the design speed is 250 kmh^{-1} . However, it was assumed that the dynamic response would not be a critical issue. The bridge is continuous and generally has a lower dynamic response, as discussed in Chapter 6.

Concrete slab

On top of the girder is a concrete slab, which is only considered a permanent load in this thesis. It is assumed not to contribute to the strength and stiffness of the system. However, even without any shear connection, it will most likely act additively with regard to stiffness. This would have a positive effect on deflection values and redistribute the loads in a more convenient manner.

Timber-concrete floors and bridges have been built in the last century (Wacker et al., 2017) and are proven to be effective. Combining the two materials can result in a much more effective cross-section. This concept was also suggested in a review of a timber engineer from manufacturer Hasslacher.

9.2.2. Connection

In timber engineering, details are often critical. Therefore it is essential to include the connection design between the timber and steel section already in a preliminary phase. Especially for the current structure, the connection is vital. The approach and assumptions are discussed.

Options

Hypothetically there are infinite connection possibilities to connect a steel and timber box girder. In this thesis, a limited number of options were devised and considered. Only a concise conceptual analysis was performed to choose a suitable connection. Professionals were not consulted for state-of-the-art connection possibilities. A very standard connection detail, that has received extensive research over the past decades, has been chosen, namely the dowel-type connection. As this type did not have immediate drawbacks in the conceptual analysis presented in the previous chapter.

This dowel-type connection is tested in many studies and is used in existing structures. Therefore there is much known about the failure modes and strength, which is clear in the elaborate description in EC5.

Strength

The connection in Figure 9.3 uses dowels that satisfy the local criteria. It was assumed that the webs and flanges resisted the cross-sectional forces separately. The moments and forces were divided between the webs and flanges based on the dimensions and configurations. A more detailed explanation is given in Section 8.2. Each dowel resists part of the cross-sectional forces, but not all dowels can be activated. A reduction factor is used to calculate the effective number of dowels. While adding more dowels seems a logical step to increase the strength of the connection, it can also not help at a certain point. The reduction will be severe such that adding more dowels does not improve the strength performance.

Fatigue

The steel cross-section is checked in a preliminary manner for fatigue strength. The connection detail is not considered or checked. Since the cross-sectional forces are lower at the position of the connection,

the stress range is also expected to be lower. However, the detail category is very low for welded endplates. The slotted-in steel plates are connected to an end plate, which in turn is connected to the steel section. The largest detail category for endplates is 80, which is the same as the checked detail category for the transverse stiffeners. This endplate detail category is only valid for endplates with a thickness up to 50 mm, which is larger than the expected thickness of the endplate. This category can be found in table 8.5 in EN1993-1-9.

Since the steel design received no focus, the stress range is reasonably expected to be lower, and the detail category is similar to the already checked stiffener detail, this issue is not investigated further. The exact dimensions and alignment play an essential role in a precise fatigue calculation. It is better suited to investigate fatigue in a future design phase. The alignment is conceptually discussed in the next chapter.

Stiffness

A formula from the European timber standard calculates the stiffness of a single steel fastener. A method to determine the rotational stiffness of the whole connection is not given. Based on structural mechanics theory, a model was created. The flanges were assumed to only contribute to the rotational stiffness around the major bending axis. The webs were assumed to account for rotational stiffness around the minor bending axis. By separating the flanges and webs, a conservative value is expected. Secondary effects, like load redistribution, are not considered.

The rotational stiffness is highly dependent on the number of dowels used. Eurocode does not reduce the number of dowels for a stiffness calculation. Sandhaas (2012) did advise calculating the stiffness with the effective number of dowels. The unity check in Table 9.1 considers using the effective amount of dowels.

Shrinkage

Timber shrinks and swells due to moisture content changes. The percentage change in the timber was assumed to be similar to the change in humidity of the region. Rain and temperature influence its moisture content. However, it is assumed this is very small due to a protective layer and the section size. The size of the cross-section affects the speed at which the environment can impact the moisture content of the timber. Larger sections will have minor variance in their inner parts.

The shrinkage calculation assumes that the connection to the steel section is rigid. However, the holes in the steel plate where dowels are inserted are drilled slightly bigger than the actual dowel size. Steel will also deform under loading, albeit much less than timber. Both these aspects can help or frustrate the timber in its free deformation capacity.

Practical and architectural assessment

The aim of this chapter is to express the perspective and thoughts on the design by ZJA. Despite the discussion of the limitations and the obvious strength changes that are required, the current design is assessed. During a consultation with ZJA, the current design was discussed. Figure 9.1 has shown a render of the discussed design. Firstly the inspiration or approach of ZJA is explained. Then remarks on the design are presented and divided into architectural and practical aspects. This is in line with the approach of ZJA to this project.

10.1. ZJA inspiration

The vision of ZJA for this railway bridge is that the technical possibilities determine the form and shape of the bridge. Architectural design choices should ideally come from structural improvements or positively affect the technical design. This entails that a more practical assessment of the design is desired. All suggestions for a design change come from an appealing perspective and a practical or technical perspective.

More commonly for the chosen span length are timber arch or truss bridges. The span size to construct a stringer bridge in timber is quite large compared to present examples. However, the fact that arches and trusses are used is one of the reasons to investigate this beam type bridge. The other reason is the desire to create a design that perfectly fits the surroundings. A girder bridge can have a more fluent form, including the piers, compared to a truss bridge. Figure 10.1 shows a girder and truss option to support the more fluent form of a continuous versus a truss bridge.

The length of the bridge is set. The amount of spans to cover this length has been chosen to give the bridge a rhythm. The design should have continuity to let the bridge cross the landscape but not be an eye-catcher and distract from the natural environment of the surroundings. This has been an important factor while assessing the design.

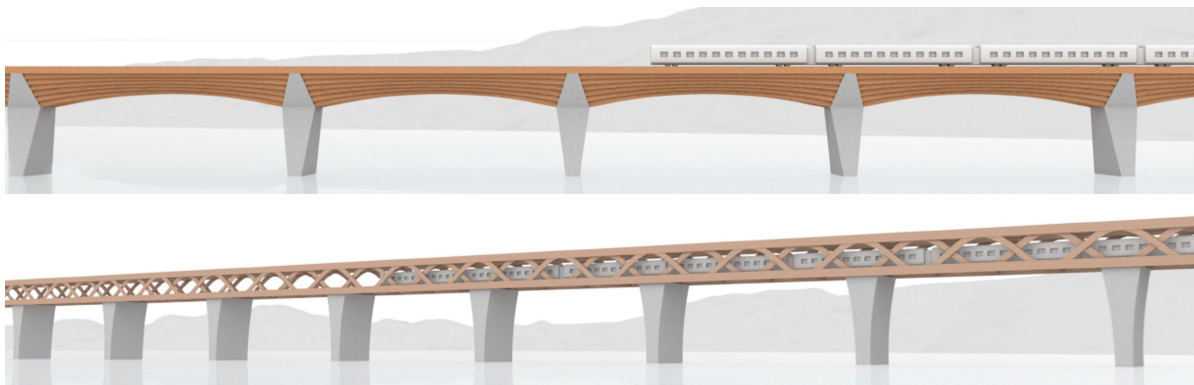


Figure 10.1: Visual designs by ZJA of an arch-beam girder and a continuous curved-truss bridge.

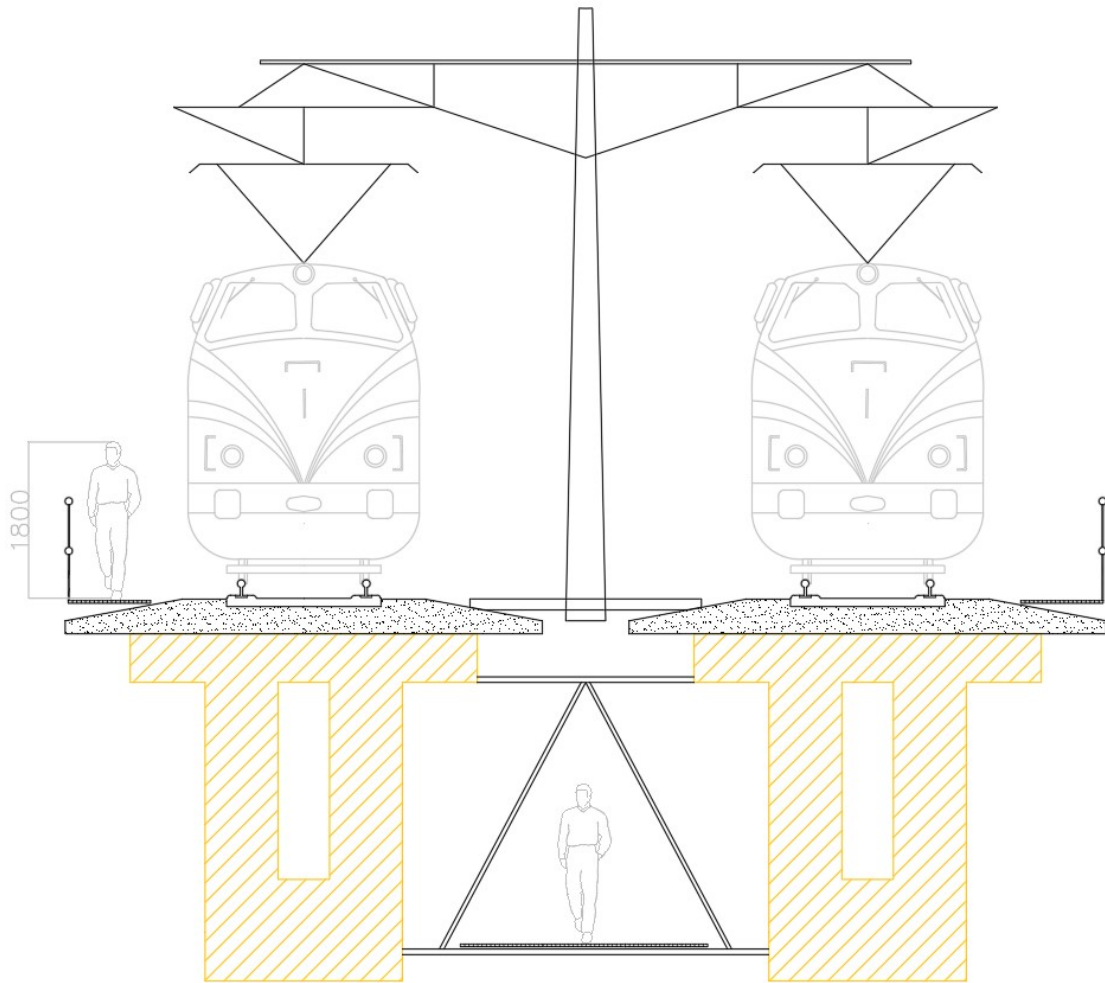


Figure 10.2: Cross-section drawing of improved box girder including additional components.

10.2. Practical assessment

The engineering approach to designing the cross-section and the connection has neglected a few components in this preliminary design phase. This section addresses these components and some practical considerations of the design. All these parts are conceptual ideas.

10.2.1. Components

Two components that are required for a railway bridge are the overhead guidance and a non-public footpath to evacuate passengers in case of an emergency or to be used for maintenance purposes. In Figure 10.2 a sketch is found that includes both these components. The footpath between tracks, mainly for maintenance, is combined with diaphragms to increase stability.

Overhead guidance

Electricity is transported via overhead guidance to charge electric trains. There are two possibilities for overhead guidance systems for this bridge. A separate box girder carries each track. On top of this box girder, portal frames can be installed to carry the electric cables. This leads to two decoupled systems that have the potential to operate independently.

The second possibility is to couple the system for both tracks. A column with two cantilevered beams can be constructed and placed between the two box girders. It will introduce additional torsional shear stresses. However, if the guidance is only placed at the columns, this effect is cancelled. For straight tracks, the portal distance in the Netherlands is around 70 m, so 50 m should be sufficient. The choice for either system is heavily dependent on the requirements set by the rail operator.

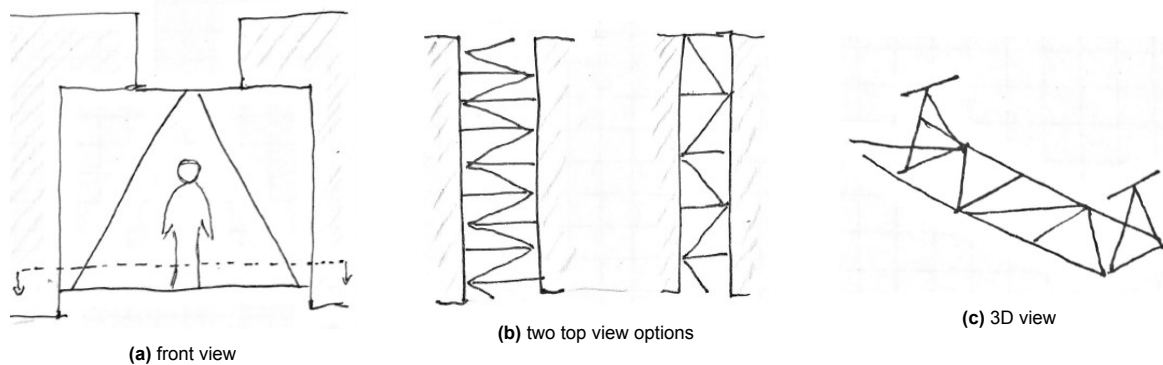


Figure 10.3: Sketches of a conceptual diaphragm structure between the box girders.

Non-public footpath

In Section 2.8 the non-public footpath loading was ignored since it was assumed to be not governing. However, it is essential to have it for maintenance and safety reasons. An emergency requires a safe evacuation. Thus the path must be located as far away as possible from the other track. The path will introduce additional torsional stresses. Designing it with lightweight material like fibre reinforced polymer or also with timber, these stresses can be very limited.

The path can also be used for maintenance and inspection. The inside also requires such a path which can be introduced at the bottom flange level. Structurally it can be combined with introducing diaphragms to connect the box girders. This is addressed in the next paragraph.

The timber and steel cross-sections have no space for a non-public footpath. An extension of the concrete slab can function as the load-bearing part of his path. This is illustrated in Figure 10.2. The loads are transferred to the timber and steel superstructure via the concrete slab.

Diaphragms

Connecting the two box girders with diaphragms will be beneficial for stability. Especially the dynamic response can be lowered by the damping potential this connection can have. However, the diaphragm structure must be designed to resist such dynamic forces. A steel frame lattice that functions as the maintenance and inspection path can be combined in the diaphragm design or be supported by it. The concept is shown in Figure 10.3, and the footpath location with a single diaphragm is also shown.

10.2.2. Cross-section aspects

Two practical aspects of the design are the cross-section's water protection and the alignment of the timber and steel section. Mainly regarding the double slotted-in steel plates in the timber at the connection.

Water protection

Timber elements are required to be protected from environmental influences. The cantilevered bottom flanges in the design risk water accumulation. This is an issue for both timber and steel. In Figure 10.2 the outstand bottom flanges are removed. Additionally, these flanges resulted in an outdated design look according to ZJA. Figure 9.1 looks similar to steel riveted bridges, thus outdated.

Alignment

The alignment of the steel plates of the connection with the steel cross-section can become an issue. The construction height of both sections is assumed to be equal, but this leads to bending moments in the endplate of the connection. In Figure 10.4 this issue is sketched. A better configuration is required, and two options are presented in the figure. The second option is a more standard approach to solving such issues. Double webs do not have to be problematic. These can even improve the buckling behaviour of webs and flanges. The steel section can have a variable construction height between the connection and the support to resist larger support forces.

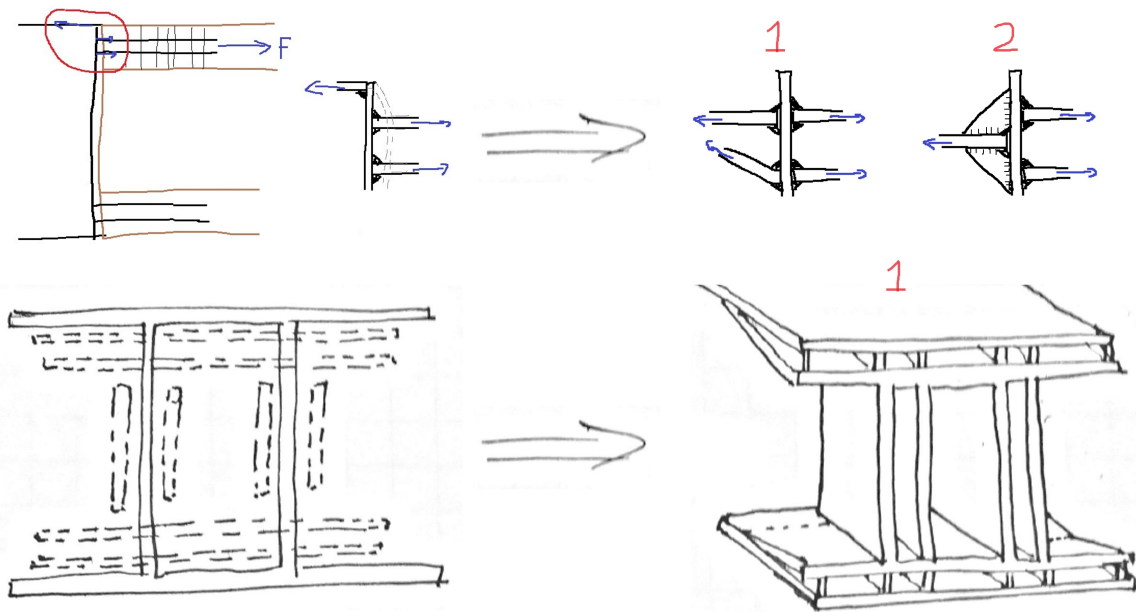


Figure 10.4: Detail of double slotted-in steel plates connection to steel section. A side and cross-section view of the current situation is shown on the left, including the sub-optimal force flow. The bending of the endplate can cause major issues, mainly regarding fatigue. To the right, two possible solutions are shown: 1) has inclined plates that gradually become a steel section with single flanges, as also shown in the 3D sketch, and 2) has the steel section flange positioned in the middle of the two slotted-in steel plates and is strengthened with vertical triangular welded pieces.

10.3. Architectural assessment

The architectural approach and the vision for this design are used to do the architectural assessment. It resulted in a specific concept for this railway bridge design, shown in Figure 10.5. The construction height has already become more desirable than in the previous study due to the single-track design. This creates a better proportion from a visual perspective and the architectural vision.

Continuity and rhythm must be visible in the design to have it fit in the surroundings it is situated in. Currently, it is disrupted by the abrupt change from the steel cross-section to the timber cross-section. More fluent conversions or constant parts are missing. The repetitive effect of timber-steel-timber is appealing but must be inferior to a continuous or constant part in the design.

The concrete slab track is present along the whole bridge. It is the constant line that is desired. A train also acts like a constant short line that moves across the bridge when looked upon from a distance. This line concept must be exaggerated by introducing more lines that are constant along the whole bridge. Ideally, these lines are both visually pleasing and structurally beneficial.

Timber is an important part of the structure. To emphasise this, a continuous top flange along the bridge can be installed right underneath the concrete slab track. This is not a structural improvement but also not a deficiency. It will also lead to less perpendicular to the grain area in which water can infiltrate and cause fungal growth or deterioration.

Steel web stiffeners are required against buckling. Placing these on the outside is an addition to the line concept. A sketch of this concept is shown in Figure 10.6. The slanted top side of the close stiffener can ensure no accumulation of water occurs. Closed stiffeners should be used to emphasise the lines by adding more depth. This alleviates the depth effect that is caused by the different thicknesses of the steel web and timber web.

Stiffeners are not required for the timber section, so the lines are not continuous. However, this can be solved by adding Venetian blinds on the timber for water protection. Venetian blinds to protect timber are commonly used to protect timber but are disliked by ZJA for the cluttered effect they can have on large structures. This effect is shown in Figure 10.7. However, if the lamellae of the Venetian blinds are produced with larger dimensions, the lines of the steel stiffeners can be continued.

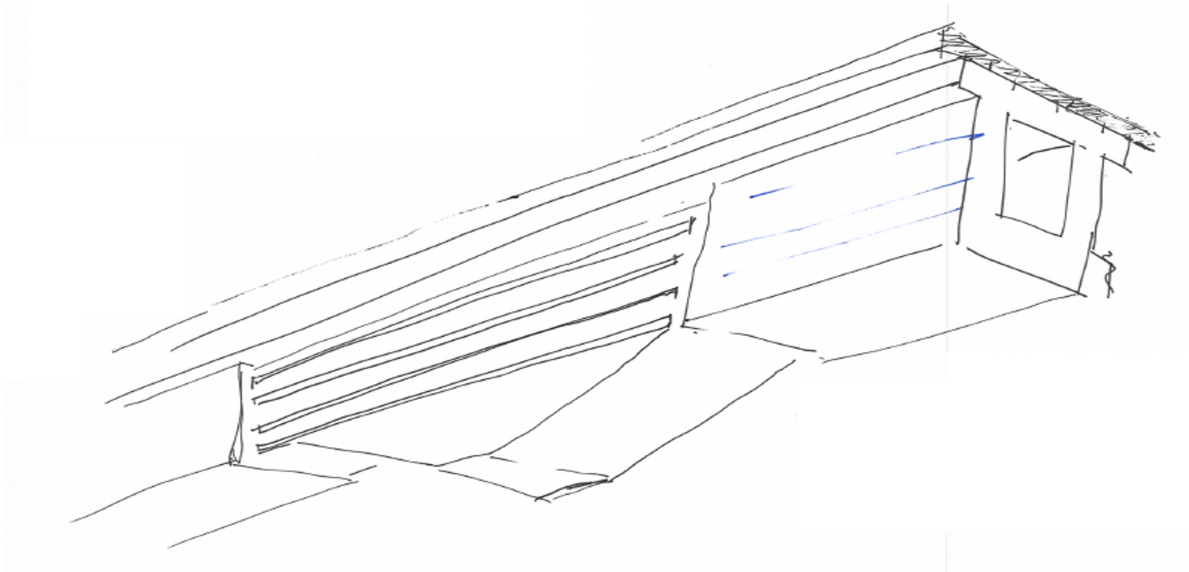
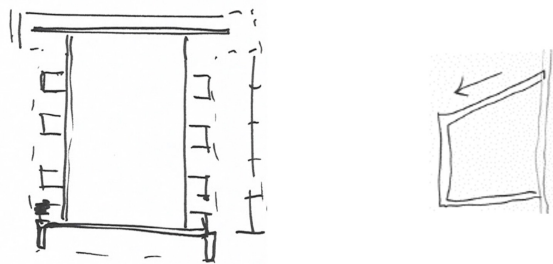


Figure 10.5: Sketch to visualise line play near the support of the timber en steel section.



(a) Stiffened steel box girder to visually 'enlarge' cross-section.

(b) Closed stiffeners with a downward slope to let water run away.

Figure 10.6: Sketches from architecture meeting with ZJA.

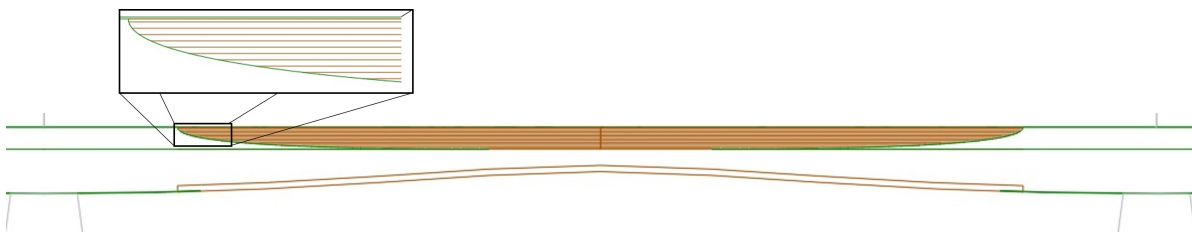


Figure 10.7: An impression of many small lamellae that leads to a cluttered effect.



Figure 10.8: Architecture drawing of the line concept design by ZJA.

Instead of external steel stiffeners, visual timber parts can be attached to the steel girder to satisfy continuity. A drawing from ZJA, Figure 10.8, shows the visual of this aspect. The steel stiffeners can be welded on the inside to safeguard the welds from environmental influences. Water protection can be installed by protective layers or coatings of the timber. These measures and changes to the design come in more detail in design phases further down the line.

10.4. Manufacturing and handling

Aside from the architectural assessment and the practicalities that followed from the cross-section design, manufacturing and handling are important factors in investigating a design. The availability and limitations of production techniques are vital for a project to be feasible.

A few glulam manufacturers have been contacted to answer the question if these sizes are hypothetically possible. The company Scantimber responded positively via their contacts at Hasslacher. Such a large cross-section is likely possible to construct, although many production steps are required to reach the desired shape. On another note, the transportation was pointed out to be very difficult. The cross-section size and length are too large for regular transport. However, exceptional transport via road or water can be used to tackle this. The bridge is such a large structure that special transporting solutions need to be part of the design project.

Derix only mentioned that their facilities could not handle the cross-section. The main downfall was the weight of the cross-section for the factory crane. Secondly, their production process would be disrupted by these sections.

It seems that the production of the section is possible. Transportation could be solved by using a factory, permanent or temporary, in a harbour to transport the beams via barge. A big unknown is the production process of the connection. Tolerances of large steel plates, the holes in which they are slotted, the alignment of dowel holes, and the welding of the steel endplate must be stringent. No response on the feasibility of the connection from a manufacturer was received. However, it should be noted that investigating this is only required when the connection is adequate for the design.

10.5. Environmental impact

This project originated from the urge of ZJA to use more sustainable materials. Material usage is the primary source of emissions that determine the environmental footprint of infrastructure projects, as discussed in the introduction (Huang et al., 2018). An elaborate study compares a concrete and timber-concrete box girder road bridge from an environmental perspective. It showed that the timber option was lighter and had a 20% lower environmental impact when only accounting for the materials (O'Born, 2018). A large part of the emissions came from the foundation. A large part of the lower environmental impact resulted from a lighter foundation required for a more lightweight superstructure.

The steel reduction for this design is approximately 75% if the connections are positioned at 5 m from the supports. This includes the steel plates and dowels that are used for the connection. However, the timber weighs 30% more per meter length than the steel class 4 section. This results in the need for larger foundations since the total weight is increased for a combined design versus a steel design. The secondary emissions resulting from the heavy superstructure will partly nullify the environmental profits by using timber instead of steel.

It should be noted that the superstructure in the research of a road bridge was a timber-concrete box girder (O'Born, 2018). Exploiting the concrete's strength, stiffness, and mass can help with the environmental footprint.

Definitive design

The design has been presented and discussed in Chapter 9, and it has been assessed from an architectural approach in the previous chapter. The following sections in this chapter present the definitive preliminary cross-section design. It presents the critical unity checks except for the shrinkage issue. This specific case is addressed elaborately with a potential conceptual solution.

Two alternative ways forward are discussed to avoid the complicated connection design. It conceptually discusses a road bridge instead of railway bridge and the use of only timber sections that are reinforced to resist the high loads at the bearing.

11.1. New cross-section

The new cross-section dimensions are based upon the governing unity checks and the changes proposed in the assessment, Chapter 10. The unity checks that were scattered throughout the report are presented in Table 11.1. It adds the unity checks of the new cross-section. The dimensions of this new cross-section are reported in a subsequent paragraph.

11.1.1. Unity checks

The unity checks above one are highlighted with the colour red. Ignoring the extreme unity check for timber shrinkage, as it will be discussed further on. Most governing are the creep deflection, the steel fatigue detail, and the timber net tension in shear at the connection. Deflection and fatigue can both be easily solved by increasing the height of the sections. A height increase is the most efficient second moment of area increase, which increases stiffness and reduces overall stresses. Specifically for the fatigue unity check, the steel section thicknesses can be slightly increased to lower the stresses and thus the stress ranges.

A height increase positively affects the shear area of the reduced cross-section. However, the smaller bottom flange will increase the load that the web has to resist. An increase in web thickness adds significant amounts of area, and a decrease in the number of dowels will lead to less cut-out timber. The latter is not achievable to the extent that will lower the unity check sufficiently as the required number of dowels is still large.

Under the assumption that a solution is found for the shrinkage problem, the new cross-section will have a height of 4.2 m, increased bottom flange and web thickness to 880 mm, and no bottom flange extensions. The steel section will have a height of 4 m at the support. The unity checks are calculated using the same calculations as for the initial cross-section. Only the values that matter are presented in Table 11.1, for some values will be obviously reduced and do not matter for this analysis. Deflection unity checks have reused the SCIA model implementing the new cross-sections.

The drop in unity checks is quite similar for the three limiting ones. Fatigue's unity check has dropped more but is significantly influenced by the specific steel cross-section. The differences between the class 2 and class 4 sections will affect fatigue unity checks more than deflection checks. For a more detailed fatigue analysis, an accurate FE model is required and the fatigue load models.

Unity checks	old	new
At midspan		
General deflection	0.57	
Passenger comfort deflection	0.75	
Creep deflection semi-rigid connection	1.13	1.00
Bending moment timber	0.50	0.44
At support		
Main bending moment class 4 section	0.38	
Fatigue of transverse plates	1.18	0.74
Connection at five metre		
Timber combined bending moment and normal force	0.35	0.31
Timber combined shear force and torsion moment	0.82	0.79
Timber block shear flange	0.41	
Timber net tension normal force flange	0.36	
Timber net tension normal force web	0.19	
Timber net tension shear force web	1.10	0.96
Timber shrinkage	8.32	-
Steel slotted-in plate in bearing	0.11	
Steel net tension governing ¹⁾	0.49	
Dowel shear stress	0.15	

1) Governing of normal and shear force in flange and web

Table 11.1: Several key unity checks of the combined girder design.

11.1.2. Connection shrinkage

The extreme unity check of shrinkage cannot be solved by adding more material. Moisture content changes will lead to restricted deformations from the rigid steel section. A potential solution is the use of modified timber. Multiple different treatments reduce the swelling and shrinkage of timber elements, called dimensional stability. Chemical and heat modification are two treatment groups that have received researchers' attention in the past century.

Specific chemical modification treatments are acetylation and furfurylation. Both increase dimensional stability outstandingly. The advantage of acetylation is an increase in compression strength and hardness while maintaining bending strength and stiffness (W. Homan & Tjeerdsma, 2000). Furfurylation reduces impact strength but has an increase in stiffness and excellent durability (W. J. Homan & Jorissen, 2004). The changes in strength properties for mass timber structures are limited, while the dimensional stability improves noteworthy. Larger cross-sections will experience difficulties due to the penetration depth of the chemicals and glue-line effect (Ayanleye et al., 2022).

Several different heat treatments exist. In essence, the timber is heated well over combustion temperature by steam. Removing oxygen from the air ensures the timber will not catch fire. Thermowood, Platowood, and the use of retifications and perdure are three different heat treatments. Each treatment either heats in a different manner, to a different temperature, or has an additional drying or curing step. The main advantage is the increase in durability class at the cost of its mechanical properties (W. J. Homan & Jorissen, 2004).

Experiments on timber elements with both treatments have significantly decreased swelling and shrinkage. Therefore, it would seem to be an appropriate solution for the connection of this design. However, this is only considering the strength aspect, not manufacturing or sustainability for example.



Figure 11.1: Schematised continuous cantilevered bridge.

11.2. Alternatives

As discussed before, the connection design is complicated. Using modified timber is suggested as solution. However, another solution would be to change the initial boundary conditions or design requirements. Two alternative approaches to use timber in bridge design are discussed.

11.2.1. Load reduction

As mentioned in the introduction, designing a railway bridge is challenging. The design has very strict requirements, and loading is very high. Having less strict requirements and lower loading is a road traffic bridge. This has a positive effect on the deflection limitation, fatigue limit, and cross-section size. A two-lane road would require a slightly wider cross-section, at least 5.4 m. Loading per length according to EN1991-2, including the safety factor, will be around 50 kN/m. This is a 65% decrease in live loads and will mean a significant decrease in construction height. The need for a large concrete slab has also disappeared.

It does lead to other complications for the cross-section. Cars will not drive perfectly on rails as trains do. Loading at different positions will lead to more notable torsional moments and transverse bending moments in the deck. Especially the transverse load transfer requires attention since timber is not strong perpendicular-to-grain. A deck of CLT becomes interesting to use. However, a shear connection between axially orientated glulam and CLT brings other complexities to the table.

In the case of steel, fatigue issues arise from transverse bending. These detail categories have been discussed and were assumed to be no problem for the perfect loading condition of trains. Cars that can be anywhere on the deck will influence the stresses in the connections between longitudinal stiffeners and transverse girders.

11.2.2. Total timber

The current connection design is required to be rigid or at least semi-rigid. A hinged connection leads to a mechanism that has little stability. Cantilevered continuous bridges, however, can be used. Every other span has two hinges or none, as the scheme in Figure 11.1 shows. The advantage is the use of a hinged connection without any concerns regarding deflection. It can be designed such that there is sufficient deformation capacity for shrinkage or swelling to occur.

However, the desire to have steel sections at the support would lead to a mostly steel bridge. Instead of steel sections, the bridge can be executed in only timber. Large slotted-in steel plates near the support can be installed to transfer the forces to a relatively small bearing, and strengthening measures can help to resist high local forces. Glued-in rods (Estévez et al., 2010; Serrano et al., 2017), shear strengthening (Dietsch et al., 2018), or FRP reinforcement (Brady & Harte, 2008; Gentile et al., 2002; Kliger et al., 2007) are all proven to increase strength and stiffness of timber elements.

A consequence of the total timber design is the requirement to create timber sections up to possibly 80 m. Transport and lifting will become limiting design factors. Using this design in combination with the choice for a road bridge does seem to have potential when the transportation and lifting challenge can be solved. Manufacturing sections at a factory next to a river is ideal.

Final remarks

This thesis has investigated a timber and steel railway bridge design in a preliminary phase. This chapter concludes the objective of this thesis; to investigate and design a timber bridge with steel cross-sections at the support and a proper connection between the cross-sections. Conclusions from the design investigations are presented, and recommendations are given for future research and potential ways forward with this design.

12.1. Conclusions

The main research question was the feasibility of a timber railway bridge with a steel cross-section at the support. The challenges for this thesis were the innovative hybrid timber and steel beam, the bridge size, and designing for a high-speed railway bridge. It should be stressed that the design was considered in a preliminary phase and collaboration with architect firm ZJA was important for the assessment.

Chapters 9 and 11 have described the design in more detail and a summary is given here. Figures 9.2, 9.3 and 10.2 show the cross-sections including dimensions and the conceptual definitive cross-section design. The design has box girder timber sections in glued laminated timber of 40 m length and is connected to steel box girder sections of 10 m length. The steel box girders are located at the bearings to transfer loads to the foundation. On top of this superstructure is a concrete slab to connect the track and protect the top surface of timber and steel. A dowel-type connection is chosen with double slotted-in steel plates in the flanges and webs of the timber box girder. Dowels are the steel fasteners used.

Ultimate and serviceability limit states were checked by formulae presented in numerous Eurocodes. Chapter 5 reports the limit states for the hybrid beam and Chapter 8 reports them for the connection. Cross-sectional forces were extracted from a finite element model using 1D beam elements and loading according to Eurocode. Governing limits were deflection after creep, shear strength of timber at the connection, and fatigue of the steel section. The use of a box girder cross-section was meant to save material but negatively affected both the deflection and shear strength. It appeared to have difficulty satisfying the strict limits and high loads of a railway bridge.

A separate significant issue is timber shrinkage that introduce perpendicular-to-grain stresses at the connection due to a rigid connection with steel. A rigid or semi-rigid connection must be used to have a globally stable structure. The designed connection will require a solution to limit the swelling and shrinkage of timber to become viable. The use of modified timber is a proposed potential solution.

The design of the timber railway bridge seems to have potential. A structure that meets the requirements has been designed, and there are possibilities to improve the timber performance. Introducing cooperation between the concrete slab track and timber reinforcement to resist bending and shear are suggested as strength and stiffness improvements.

From an architectural point of view, the construction height has become more desirable than in the previous study. Two single-track railway bridges suit the vision of ZJA. Continuity is achieved even though the change from timber to steel is very abrupt. A certain rhythm can be accomplished with additional timber parts, only with a visual impact, that continues along the steel section.

12.2. Recommendations

The preliminary nature of this innovative design concept leads to plenty of aspects that require further design iterations. A preliminary design is, per definition, not finished. There are two types of aspects that follow from this thesis. There are aspects of general nature, like timber design methods, and more specific aspects that address the timber and steel railway bridge design.

12.2.1. General aspects

Timber Eurocode methods and factors are based on small-scale tests. The most important assumption has been that these methods and factors can also be used for the huge timber cross-section in this thesis. It is recommended that the scaling of these factors is verified or to test such large cross-sections. The results of such large-scale tests would not only benefit this particular design but would also contribute to the future expansion of timber structures throughout society.

Linked to this scaling problem is the dimensional stability of such large sections. Shrinkage and swelling will occur, especially in infrastructure projects with structural elements outside. There are chemical and heat treatments that improve this property to a large extent. It is advised to further investigate this modified timber, specifically gaining knowledge on the effect and usage of modified timber in large structures. Railway bridge projects, or other large infrastructure projects, can benefit largely from more experience with this material.

Aside from the recommended scaling research and dimensional stability experiments, the properties of the timber material require more research. The selected grade of glued laminated timber for the box girder has its properties summarised in the Eurocodes. Stronger grades have an increased bending, tensile, and compression strength while also having improved stiffness values. However, the shear strength and stiffness do not change, regardless of strength grade. The design is governed by deflection and shear strength, of which deflection is strongly affected by shear stiffness. More studies that investigate a difference in shear stiffness based on its grade can yield positive results for the railway bridge design. Specific research on the shear strength of box girders can help even more.

Additionally, research on the resistance of combined stress states is recommended. The combination of torsion and shear, leading both to shear stresses, is not included in EC5. Larger structures often have combined stress states that are very complex and can lead to peak stresses in specific positions. Investigation into combined stress states will improve the general safety of timber engineering since it provides more checks.

From the perspective of the connection, it has been clear that extensive research has been done on dowelled connections. However, the size of this design is huge, and the slotted-in steel plates are mounted in vertical and horizontal directions. This dowelled connection configuration of this size is an interesting research direction. The size determines mainly the number of dowels, and increasing the number can prove to be insufficient due to the use of a reduction factor to account for the effective number of dowels. At some point, it could be that adding more fasteners does not improve the connection strength. Something more interesting to investigate is the particular configuration. Using slotted-in plates like it forms an I-profile can significantly improve the moment capacity of a timber section. For smaller sections, the dimensional stability problem does not occur and thus can be interesting for smaller structures.

12.2.2. Design specific

This project was partly initiated to investigate the environmental footprint improvement of using timber and steel versus only steel. Timber elements store CO₂, and production process emissions are much lower. The lightweight nature of timber is expected to reduce the total weight and thus reduce secondary emissions from transport and handling. Although the emissions due to timber are much lower than due to steel, the total weight of the structure is predicted to be larger than a complete steel railway bridge design. A study that proves that a timber bridge leads to less secondary emissions has considered a timber-concrete structure (O'Born, 2018). A future design investigation of a timber-concrete structure instead of the timber-steel structure could support this claim. It is recommended that more in-depth emission studies compare timber-steel and timber-concrete alternatives for their impact on the environment.

Specific to this project was the simultaneous combination of three challenges: (1) designing a timber-steel high-speed railway bridge by using a hybrid design, (2) with an innovative connection method, and (3) trying to expand the span limit for timber stringer bridges. It is recommended to break up these challenges and investigate them separately. A proper starting point is the innovative connection method on a slightly smaller scale. This scale can be achieved by considering a smaller span and lower loads.

Two alternative design approaches have already been suggested in Chapter 11. Using the design for a road bridge will lower the loads significantly, and it has less strict requirements regarding deflection and dynamics. Revisiting this design for a road bridge does not remove the shrinkage problem, but it might become easier to solve since the absolute displacement is less.

The other alternative is only to use timber and have two hinged connections in alternating spans. The hinged connection requires to only transfer of shear and normal forces, no bending moments. It will thus become a smaller design. Transportation of the longer timber beams will become more challenging. Investigation of such a total timber design can focus on the potentially improved environmental footprint.

At last, it should be noted that the objective had a specific origin. The argument was to have a steel section at the support and connect it to a timber section at some distance from the support. This design suggestion avoided the original issue of high local stresses in the timber section at the support. The current study has shown that new issues arose with the specific connection. Particularly this connection was identified as a critical element. Future designs are recommended to investigate and check timber connections at an early stage.

This design project has exposed many parts of designing a railway bridge in timber. Each step brings a solution closer towards the goal. Although the connection did not meet the strength requirements, all other aspects were found to be viable. With additional research on massive timber structures and other innovative design concepts, a timber railway bridge can become a reality.

Standards

All standards used in this thesis are listed below.

Abbreviation	Norm	Topic
EC0	NEN-EN 1990+A1+A1/C2:2019 nl NEN-EN 1990:2019/NB:2019 nl	Basis of Structural Design National Annex
EC1	NEN-EN 1991-1-1+C1+C11 nl NEN-EN 1991-1-3+C1+A1 nl NEN-EN 1991-1-4+A1+C2 nl NEN-EN 1991-1-5+C1:2011 nl NEN-EN 1991-2+C1:2015 nl EN 1991-2	Actions - General Actions - Snow Actions - Wind Actions - Temperature Actions - Traffic Loads on Bridges Actions - Traffic Loads on Bridges
EC3	NEN-EN 1993-1-1+C2+A1:2016 nl NEN-EN 1993-1-5+C1:2012 nl NEN-EN 1993-1-8+C2:2011 nl NEN-EN 1993-1-9+C2:2012 nl NEN-EN 1993-2+C1:2011 nl	Steel - General Steel - Plated structures Steel - Connections Steel - Fatigue Steel - Bridges
EC5	NEN-EN 1995-1-1+C1+A1:2011 nl NEN-EN 1995-2 nl	Timber - General Timber - Bridges
	NEN-EN 338 nl NEN-EN 14080 nl	Timber - Strength classes Timber - Glulam and glued solid timber

Bibliography

- Aasheim, E. (2019). Norwegian Timber Bridges: Current Trends and Future Direction.
- Aicher, S., & Stapf, G. (2014a). Block glued glulam - bridges, beams and arches. *World Conference on Timber Engineering*, (August). <https://doi.org/10.13140/2.1.3777.4720>
- Aicher, S., & Stapf, G. (2014b). Glulam from European White Oak: Finger Joint Influence on Bending Size Effect. *RILEM Bookseries*, 9, 641–656. https://doi.org/10.1007/978-94-007-7811-5_{ }58
- André, A., & Kliger, R. (2009). Strengthening of timber beams using FRP, with emphasis on compression strength: A state of the art review. *APFIS 2009 - Asia-Pacific Conference on FRP in Structures*, 193–202.
- Angst, V., Augustin, M., Bell, K., Hansen, A. S., Kuklík, P., Lokaj, A., Malo, K. A., Marynowicz, A., Materna, A., Premrov, M., & Tajnik, M. (2008). *Handbook 1 Timber Structures*. <https://doi.org/10.18356/c0abb969-en>
- Ayanleye, S., Udele, K., Nasir, V., Zhang, X., & Militz, H. (2022). Durability and protection of mass timber structures: A review. *Journal of Building Engineering*, 46(September 2021), 103731. <https://doi.org/10.1016/j.jobee.2021.103731>
- Ban, H., & Shi, G. (2018). A review of research on high-strength steel structures. *Proceedings of the Institution of Civil Engineers: Structures and Buildings*, 171(8), 625–641. <https://doi.org/10.1680/jstbu.16.00197>
- Bane Nor. (2019). The Dovre Line : Kleverud-Sørli-Åkersvika. *Tender Conference Presentation*. <https://www.banenor.no/contentassets/d01642b953ed4ace949803d2aebfa238/project-presentation-kleverud-sorli-akersvika.pdf%0A>
- Bjorhovde, R. (2004). Development and use of high performance steel. *Journal of Constructional Steel Research*, 60(3-5), 393–400. [https://doi.org/10.1016/S0143-974X\(03\)00118-4](https://doi.org/10.1016/S0143-974X(03)00118-4)
- Blass, H. J., & Sandhaas, C. (2017). *Timber Engineering Principles for design*.
- Bohannan, B. (1966). Effect of Size on Bending Strength of Wood Members. *Res. Pap. FPL-56*, 30. <http://trid.trb.org/view.aspx?id=709334>
- Brady, J. F., & Harte, A. M. (2008). Prestressed FRP flexural strengthening of softwood glue - Laminated timber beams. *10th World Conference on Timber Engineering 2008*, 2, 910–917.
- Brundtland, G. (1987). Report of the World Commission on Environment and Development: Our Common Future. https://doi.org/10.1007/978-1-4020-9160-5_{ }1126
- Buchanan, A. H. (1990). Bending Strength of Lumber. *Journal of Structural Engineering*, 116(5), 1213–1229. [https://doi.org/10.1061/\(asce\)0733-9445\(1990\)116:5\(1213\)](https://doi.org/10.1061/(asce)0733-9445(1990)116:5(1213))
- Cabrero, J. M., & Yurrita, M. (2018). Performance assessment of existing models to predict brittle failure modes of steel-to-timber connections loaded parallel-to-grain with dowel-type fasteners. *Engineering Structures*, 171(February), 895–910. <https://doi.org/10.1016/j.engstruct.2018.03.037>
- Cervero, C. S. (2017). *The influence of torsional resistance of the deck on the dynamic response of a high-speed railway bridge Case study : Ulla River Viaduct* (Doctoral dissertation). KTH Royal Institute of Technology.
- Chiniforush, A. A., Akbarnezhad, A., Valipour, H., & Malekmohammadi, S. (2019). Moisture and temperature induced swelling/shrinkage of softwood and hardwood glulam and LVL: An experimental study. *Construction and Building Materials*, 207, 70–83. <https://doi.org/10.1016/j.conbuildmat.2019.02.114>
- CLO. (2021). *Temperatuurextremen in Nederland, 1907-2019*. date accessed: 2021-11-17. <https://www.clo.nl/indicatoren/nl0589-temperatuur-extremen>
- Colla, C., Krause, M., Maierhofer, C., Höhberger, H. J., & Sommer, H. (2002). Combination of NDT techniques for site investigation of non-ballasted railway tracks. *NDT and E International*, 35(2), 95–105. [https://doi.org/10.1016/S0963-8695\(01\)00033-0](https://doi.org/10.1016/S0963-8695(01)00033-0)
- Dietsch, P., Kreuzinger, H., & Winter, S. (2018). Design of shear reinforcement for timber beams. *Working Commission W18 - Timber Structures*, 193–209.

- Estévez, J., Otero, D., Martín, E., & Vázquez, J. A. (2010). The use of adhesive bulbs in the inner end of drills in order to improve the axial strength of steel threaded bars glued in timber. *11th World Conference on Timber Engineering 2010, WCTE 2010*, 1, 27–34.
- Esveld, C. (2001). *Modern Railway Track - Selection of chapters and sections*.
- Esveld, C. (2005). Dictaat: Geometrisch en constructief ontwerp van wegen en spoorwegen; Deel D. Constructief ontwerp van spoorwegen.
- Esveld, C. (2003). Recent Developments in slab track. *European Railway Review*, 9(2), 81–85. http://www.esveld.com/Download/TUD/ERR_Slabtrack.pdf
- Gao, Q. F., Wang, Z. L., Liu, Y., & Guo, B. Q. (2012). Modified Formula of Estimating Fundamental Frequency of Girder Bridge with Uniform Cross-Section. *Advanced Engineering Forum*, 5(2), 177–182. <https://doi.org/10.4028/www.scientific.net/aef.5.177>
- Gao, Q., Wang, Z., Jia, H., Liu, C., Li, J., Guo, B., & Zhong, J. (2015). Dynamic Responses of Continuous Girder Bridges with Uniform Cross-Section under Moving Vehicular Loads. *Mathematical Problems in Engineering*, 2015. <https://doi.org/10.1155/2015/951502>
- García-Sánchez, D., Sañudo, R., Miranda, M., Tárrago, N., & Lenart, S. (2021). Rail expansion devices and maximum dilation length in railway bridges. An experimental study. *Engineering Structures*, 229(May 2020). <https://doi.org/10.1016/j.engstruct.2020.111605>
- Gavric, I., Fragiaco, M., & Ceccotti, A. (2015). Cyclic behaviour of typical metal connectors for cross-laminated (CLT) structures. *Materials and Structures/Materiaux et Constructions*, 48(6), 1841–1857. <https://doi.org/10.1617/s11527-014-0278-7>
- Gentile, C., Svecova, D., & Rizkalla, S. H. (2002). Timber Beams Strengthened with GFRP Bars: Development and Applications. *Journal of Composites for Construction*, 6(1), 11–20. [https://doi.org/10.1061/\(asce\)1090-0268\(2002\)6:1\(11\)](https://doi.org/10.1061/(asce)1090-0268(2002)6:1(11))
- Gilham, P. C. (2015). A New Look at Modern Timber Bridges. *westernwoodstructures - white paper*. <https://doi.org/10.1061/9780784479117.025>
- Global Railway Review. (2018). *Noway to invest NOK 120 billion in rail projects between 2018-2023*. date accessed: 2021-11-19. <https://www.globalrailwayreview.com/news/68626/norway-nok-120-billion-rail-projects/>
- Gocál, J., & Odrobiňák, J. (2019). Stiffness of steel-timber connection under cyclic loading. *Ce/Papers*, 3(3-4), 391–396. <https://doi.org/10.1002/cepa.1072>
- Guo, H., Hu, S., Liu, X., & Su, P. (2018). Displacement at girder end of long-span railway steel bridges and performance requirements for bridge expansion joint. *Proceedings of the 9th International Conference on Advances in Steel Structures, ICASS 2018*. <https://doi.org/10.18057/ICASS2018.P.035>
- Homan, W., & Tjeerdsma, B. (2000). Structural and other properties of modified wood. *Congress WCTE*, (August 2015), 1–1. <http://woodwestwood.com/Researches/3-5-1.pdf>
- Homan, W. J., & Jorissen, A. J. (2004). Wood modification developments. *Heron*, 49(4), 361–386.
- Huang, L., Krigsvoll, G., Johansen, F., Liu, Y., & Zhang, X. (2018). Carbon emission of global construction sector. *Renewable and Sustainable Energy Reviews*, 81, 1906–1916. <https://doi.org/10.1016/j.rser.2017.06.001>
- Iles, D., MacDonald, M., & Hayward, C. (2004). *SCI - Design Guide for Steel Railway Bridges - Publication P318*.
- Jeleč, M., Varevac, D., & Rajčić, V. (2018). Cross-laminated timber (CLT) - a state of the art report. *Gradjevinar*, 70(2), 75–95. <https://doi.org/10.14256/JCE.2071.2017>
- Johansen, K. W. (1949). Theory of Timber Connections. *IABSE: International Association of Bridge and Structural Engineering*, 9, 249–262. <https://doi.org/http://doi.org/10.5169/seals-9703>
- Jorissen, A. (1998). *Double shear timber connections with dowel type fasteners* (Doctoral dissertation). Technische Universiteit Delft.
- Jutila, A. (2003). Findings and points of interest of the Nordic Timber Bridge Projects. *Internationales Holzbau-Forum 2003*, 1–18.
- Kalstad, L. M. (2017). *Norske tog blant Europas tregeste*. date accessed: 2021-11-19. <https://www.nrk.no/rogaland/norske-tog-blant-europas-tregeste-1.13673286>
- Kliger, R., Al-emrani, M., Johansson, M., & Crocetti, R. (2007). Strengthening glulam beams with steel and composite plates. (January).
- Lefebvre, D., & Richard, G. (2014). Design and construction of a 160-Metre-Long Wood Bridge in Mistissini, Québec. *Internationales Holzbau-Forum 2014*, 1–15.

- Liuzzi, M. A., Fiore, A., & Greco, R. (2020). Some structural design issues on a timber bridge for pedestrians. *Procedia Manufacturing*, 44(2019), 583–590. <https://doi.org/10.1016/j.promfg.2020.02.252>
- Lokaj, A., & Klajmonová, K. (2015). Dowel Type Joints of Round Timber Exposed to Static and Cyclic Tension Forces. *Procedia Engineering*, 114, 240–247. <https://doi.org/10.1016/j.proeng.2015.08.064>
- Madhoushi, M., & Ansell, M. P. (2008a). Behaviour of timber connections using glued-in GFRP rods under fatigue loading. Part I: In-line beam to beam connections. *Composites Part B: Engineering*, 39(2), 243–248. <https://doi.org/10.1016/j.compositesb.2007.07.001>
- Madhoushi, M., & Ansell, M. P. (2008b). Behaviour of timber connections using glued-in GFRP rods under fatigue loading. Part II: Moment-resisting connections. *Composites Part B: Engineering*, 39(2), 249–257. <https://doi.org/10.1016/j.compositesb.2006.11.002>
- Madsen, B., & Buchanan, A. (1986). Size effects in timber explained by a modified weakest link theory. *Canadian journal of civil engineering*, 13(2), 218–232. <https://doi.org/10.1139/l86-030>
- Mallo, M. F. L., & Espinoza, O. (2014). Outlook for cross-laminated timber in the United States. *BioResources*, 9(4), 7427–7443. <https://doi.org/10.15376/biores.9.4.7427-7443>
- Malo, K. A. (2016). Timber bridges. *Innovative Bridge Design Handbook: Construction, Rehabilitation and Maintenance*, 273–297. <https://doi.org/10.1016/B978-0-12-800058-8.00011-6>
- Manalo, A., Aravinthan, T., Karunasena, W., & Ticoalu, A. (2010). A review of alternative materials for replacing existing timber sleepers. *Composite Structures*, 92(3), 603–611. <https://doi.org/10.1016/j.compstruct.2009.08.046>
- Maurer. (2015). Guided Cross-Tie Railway Expansion Joint.
- Miki, C., Homma, K., & Tominaga, T. (2002). High strength and high performances steels and their use in bridge structures. *Journal of Constructional Steel Research*, 58(1), 3–20. [https://doi.org/10.1016/S0143-974X\(01\)00028-1](https://doi.org/10.1016/S0143-974X(01)00028-1)
- Milne, D. R., Le Pen, L. M., Thompson, D. J., & Powrie, W. (2017). Properties of train load frequencies and their applications. *Journal of Sound and Vibration*, 397(April), 123–140. <https://doi.org/10.1016/j.jsv.2017.03.006>
- Misconel, A., Ballerini, M., & Van De Kuilen, J. W. (2016). Steel-to-timber joints of beech-LVL with very high strength steel dowels. *WCTE 2016 - World Conference on Timber Engineering*.
- Morin-Bernard, A., Blanchet, P., Dagenais, C., & Achim, A. (2021). Glued-laminated timber from northern hardwoods: Effect of finger-joint profile on lamellae tensile strength. *Construction and Building Materials*, 271. <https://doi.org/10.1016/j.conbuildmat.2020.121591>
- Norwegian ministry of transport. (2021). (white paper) National Transport Plan 2022-2033 English Summary. <https://www.regjeringen.no/nb/dokumenter/stmeld-nr-024-2003-2004-/id197953/?docId=STM200320040024000DDDEPIS&ch=1&q=>
- O’Born, R. (2018). Life cycle assessment of large scale timber bridges: A case study from the world’s longest timber bridge design in Norway. *Transportation Research Part D: Transport and Environment*, 59(February), 301–312. <https://doi.org/10.1016/j.trd.2018.01.018>
- Ou, F. L., & Weller, C. (1986). Overview of Timber Bridges. *Transportation Research Record*, 1–12.
- Pedersen, M. (2002). *Dowel Type Timber Connections Strength modelling* (Doctoral dissertation). Technical University of Denmark.
- Pierer, H. (2014). *Wennerbrücke*. date accessed: 2022-02-14. <https://pierer.photoshelter.com/gallery/Wennerbruecke/G0000K62qEcGxb8s/C00000OYxCCmUu7w>
- Pousette, A., Malo, K. A., Thelandersson, S., Fortino, S., Salokangas, L., & Wachter, J. (2017). Durable Timber Bridges: Final Report and Guidelines.
- Rail One. (2011). RHEDA 2000 © BALLASTLESS TRACK SYSTEM.
- Ranta-Maunus, A., & Kevarinmäki, A. (2003). Reliability of timber structures theory and dowel-type connection failures. *CIB-W18 timber structures, Colorado, USA, Paper 36–7–11*.
- Reynolds, T., Harris, R., & Chang, W. S. (2014). Stiffness of dowel-type timber connections under pre-yield oscillating loads. *Engineering Structures*, 65(April 2018), 21–29. <https://doi.org/10.1016/j.engstruct.2014.01.024>
- Reynolds, T. P., Miranda, W., Trabucco, D., Toumpanaki, E., Foster, R. M., & Ramage, M. H. (2018). Stiffness and slip in multi-dowel fitch-plate timber connections. *WCTE 2018 - World Conference on Timber Engineering*.
- Ritter, M. a. (1990). *Timber bridges: design, construction, inspection and maintenance*.

- Rogelj, J., Den Elzen, M., Höhne, N., Fransen, T., Fekete, H., Winkler, H., Schaeffer, R., Sha, F., Riahi, K., & Meinshausen, M. (2016). Paris Agreement climate proposals need a boost to keep warming well below 2 °C. *Nature*, 534(7609), 631–639. <https://doi.org/10.1038/nature18307>
- Sandhaas, C. (2012). *Mechanical Behaviour of Timber Joints With Slotted-in Steel Plates* (Doctoral dissertation). Technische Universiteit Delft.
- Sawata, K., Sasaki, T., & Kanetaka, S. (2006). Estimation of shear strength of dowel-type timber connections with multiple slotted-in steel plates by European yield theory. *Journal of Wood Science*, 52(6), 496–502. <https://doi.org/10.1007/s10086-006-0800-9>
- Schweigler, M. (2013). *A numerical model for slip curves of dowel connections and its application to timber structures* (Doctoral dissertation). Technische Universität Wien.
- Senaratne, S., Mirza, O., Dekruif, T., & Camille, C. (2020). Life cycle cost analysis of alternative railway track support material: A case study of the Sydney harbour bridge. *Journal of Cleaner Production*, 276, 124258. <https://doi.org/10.1016/j.jclepro.2020.124258>
- Serrano, E., Steiger, R., & Lavisici, P. (2017). 5 Glued-in rods.
- Shi, Y. (2012). Recent developments on high performance steel for buildings. *Advances in Structural Engineering*, 15(9), 1617–1622. <https://doi.org/10.1260/1369-4332.15.9.1617>
- Silva, É. A., Pokropski, D., You, R., & Kaewunruen, S. (2017). Comparison of structural design methods for railway composites and plastic sleepers and bearers. *Australian Journal of Structural Engineering*, 18(3), 160–177. <https://doi.org/10.1080/13287982.2017.1382045>
- Simon, A., & Koch, J. (2016). The new generation of timber bridges - Durable by protection. *WCTE 2016 - World Conference on Timber Engineering*, (August).
- Smith, I., Landis, E., & Gong, M. (2003). *Fracture and Fatigue in Wood*. Wiley.
- Svedholm, C. (2017). *Efficient Modelling Techniques for Vibration Analyses of Railway Bridges* (Doctoral dissertation). KTH Royal Institute of Technology.
- Tran, V. D., Oudjene, M., & Méausoone, P. J. (2016). Experimental investigation on full-scale glued oak solid timber beams for structural bearing capacity. *Construction and Building Materials*, 123, 365–371. <https://doi.org/10.1016/j.conbuildmat.2016.07.002>
- Tschumi, M. (2012). EU-Russia Regulatory Dialogue: Construction Sector Subgroup EU-Russia Regulatory Dialogue: Construction Sector Subgroup Seminar ' Bridge Design with Eurocodes' JRC-Ispra, 1-2 October 2012 Organized and supported by Russian Federation Europea.
- UNFCCC. (2015). Adoption of the Paris Agreement. <https://doi.org/10.1007/BF02327128>
- UNFCCC. (2021). COP26 The Glasgow Climate Pact. <https://ukcop26.org/wp-content/uploads/2021/11/COP26-Presidency-Outcomes-The-Climax-Pact.pdf>
- United States Department of Agriculture, Forest Service, & Forest Products Laboratory. (2010). *Wood Handbook: Wood as an Engineering Material* (Centennial). USDA.
- Vican, J., Gocal, J., Odrobotin, J., Moravcik, M., & Kotes, P. (2015). Determination of railway bridges loading capacity. *Procedia Engineering*, 111. <https://doi.org/10.1016/j.proeng.2015.07.155>
- Wacker, J. P., Dias, A., & Hosteng. (2017). Investigation of Early Timber-Concrete Composite Bridges in the United States. *ICTB 2017, 3rd international conference on timber bridges*, 11.
- Weatherbase. (2021). Lillehammer, Norway. date accessed: 2021-11-17. <https://www.weatherbase.com/weather/weather-summary.php?s=87310&cityname=Lillehammer,+Norway>
- Weibull, W. (1939). A statistical theory of the strength of materials. *Ingeniörsvetenskapsakademiens handlingar*, 151(15).
- Windfinder. (n.d.). *Jaarlijkse wind- en weerstatistieken voor Lillehammer*. date accessed: 2022-03-30. windfinder.com/windstatistics/lillehammer-saetherengen
- Worldbank.org. (2021a). *Country Netherlands*. date accessed: 2021-11-17. <https://climateknowledgeportal.worldbank.org/country/netherlands/climate-data-historical>
- Worldbank.org. (2021b). *Country Norway*. date accessed: 2021-11-17. <https://climateknowledgeportal.worldbank.org/country/norway/climate-data-historical>
- WorldData.info. (2021). *The climate in Norway*. date accessed: 2021-11-16. <https://www.worlddata.info/europe/norway/climate.php>
- Xia, H., Zhang, N., & Guo, W. W. (2006). Analysis of resonance mechanism and conditions of train-bridge system. *Journal of Sound and Vibration*, 297(3-5), 810–822. <https://doi.org/10.1016/j.jsv.2006.04.022>
- Yau, J. D. (2001). Resonance of continuous bridges due to high speed trains. *Journal of Marine Science and Technology*, 9(1), 14–20. <https://doi.org/10.51400/2709-6998.2430>

- Yurrita, M., & Cabrero, J. M. (2021). On the need of distinguishing ductile and brittle failure modes in timber connections with dowel-type fasteners. *Engineering Structures*, 242, 112496. <https://doi.org/10.1016/j.engstruct.2021.112496>
- Yurrita, M., Cabrero, J. M., & Quenneville, P. (2019). Brittle failure in the parallel-to-grain direction of multiple shear softwood timber connections with slotted-in steel plates and dowel-type fasteners. *Construction and Building Materials*, 216, 296–313. <https://doi.org/10.1016/j.conbuildmat.2019.04.100>
- Zhang, J., Liu, Z. F., Xu, Y., Zhang, M. L., & Mo, L. C. (2021). Cyclic Behavior and Modeling of Bolted Glulam Joint with Cracks Loaded Parallel to Grain. *Advances in Civil Engineering*, 2021. <https://doi.org/10.1155/2021/6612886>
- ZJA. (2019). ZJA schetsontwerpen presentatie.
- Zweistra, S. (2020). *Technische grenzen van een houten kokerligger* (tech. rep.). Hogeschool Rotterdam.

Part V

Appendices



Span length

This appendix presents the background of the choice on the span and outer span length.

A.1. Temperature length effect

Timber and steel have different temperature coefficients α . Timber has different coefficients in axial, tangential, and radial direction. Axial direction is only required and is $\alpha_{timber//} = 0.5 \times 10^{-5} \text{ }^\circ\text{C}^{-1}$. For steel $\alpha_{steel} = 1.2 \times 10^{-5} \text{ }^\circ\text{C}^{-1}$. Axial deformation due to expansion and contraction can be calculated using A.1.

$$\Delta L = \alpha \Delta T L \quad (\text{A.1})$$

Part of the bridge is timber and a smaller part is steel. Assume that a fifth part of the total length is steel, which is 5 m on either side of each span.

$$L_{timber} = \frac{4}{5} * 1040 \text{ m} = 832 \text{ m} \quad L_{steel} = \frac{1}{5} * 1040 \text{ m} = 208 \text{ m}$$

Simply add both parts together and determine the axial deformation with the respective thermal coefficients. A temperature difference of 40 °C is assumed.

$$\Delta L = (\alpha_{steel} L_{steel} + \alpha_{timber} L_{timber}) \Delta T \\ \approx 266 \text{ mm}$$

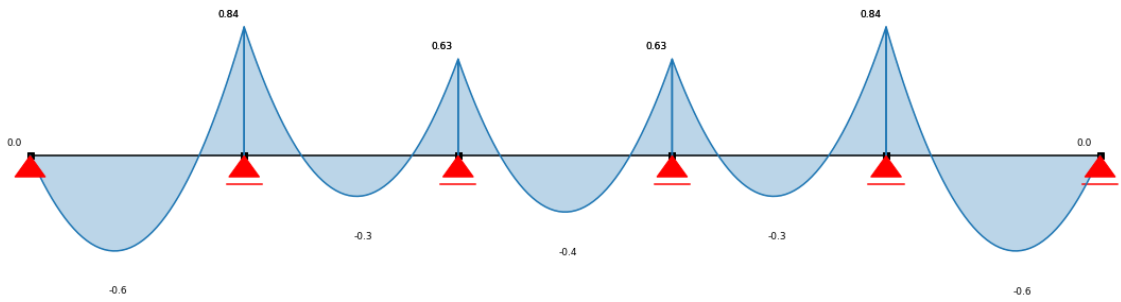
A.2. Outer spans

The outer spans of a continuous beam influence the load distribution, as shown in Figure A.1. This section determines the optimal length for the outer spans to have hogging moments that are similar at each intermediate support, and sagging moments at each midspan.

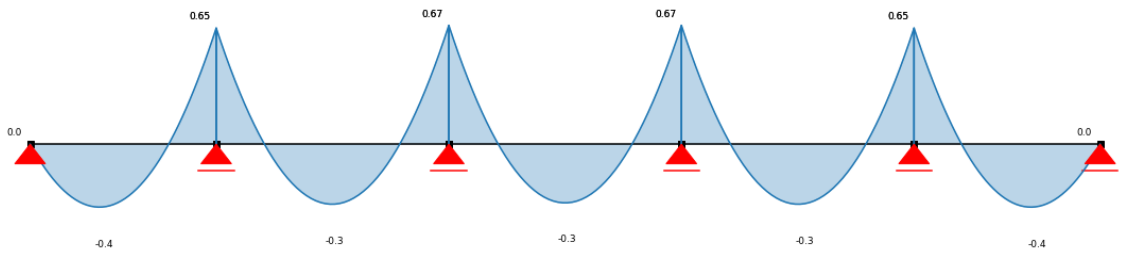
An arbitrary continuous beam with n number of spans is considered, as shown in Figure A.2. To solve the indeterminate system the force method is used. The continuous beam is divided at each intermediate support by introducing a hinge and unknown bending moment. The outer spans have a length equal to αL , while the main spans have length L . Compatibility conditions are additional equations to solve the introduced unknowns. The rotation ϕ is equal above intermediate supports.

$$\phi_i^{left} = \phi_i^{right} \quad (\text{A.2})$$

The use of forget-me-nots, see Figure A.3 based on Euler-Bernoulli beam theory results in a solvable system of equations. The case of four spans, and three unknown moments, as shown in Figure A.2 is presented below.



(a) Moment distribution of five span continuous beam with equal spans.



(b) Moment distribution of five span continuous beam with 0.8L outer spans.

Figure A.1: Moment distribution for constant stiffness and distributed load in terms of $qL^2/8$.

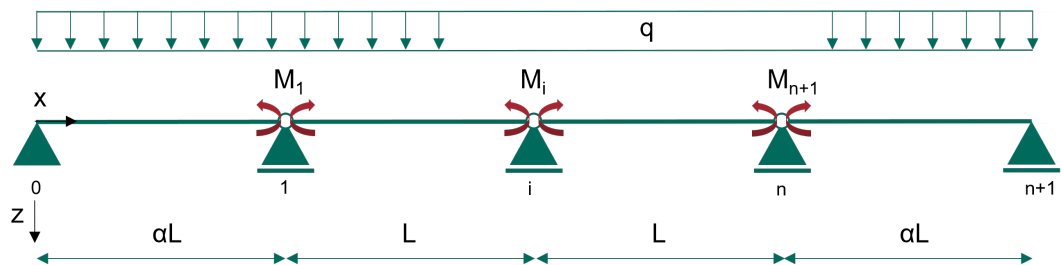


Figure A.2: Continuous beam with introduced hinges and unknown moments.

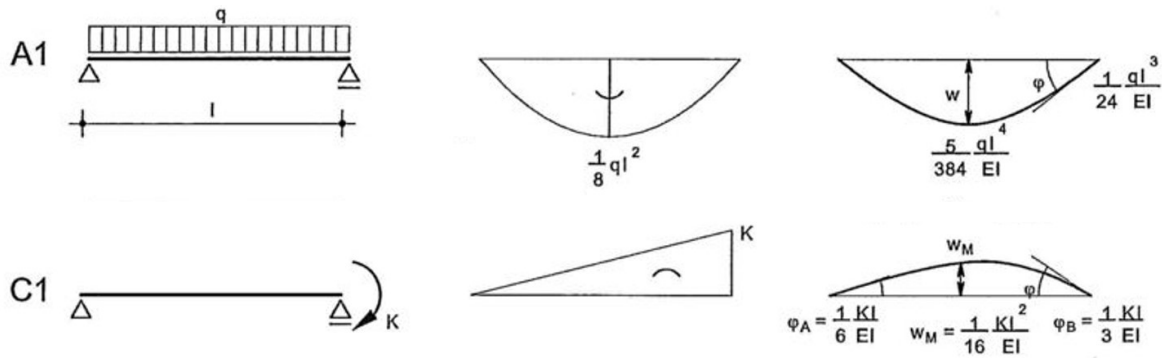


Figure A.3: Mechanic schematics for simply supported structures with a constant distributed load and a bending moment at a support.

$$\phi_{1-0} = \phi_{1-2} \tag{A.3}$$

$$\frac{q(\alpha L)^3}{24EI} + \frac{M_1 \alpha L}{3EI} = \frac{-qL^3}{24EI} - \frac{M_1 L}{3EI} - \frac{M_2 L}{6EI} \tag{A.4}$$

$$\phi_{2-1} = \phi_{2-3} \tag{A.5}$$

$$\frac{qL^3}{24EI} + \frac{M_1 L}{6EI} + \frac{M_2 L}{3EI} = \frac{-qL^3}{24EI} - \frac{M_2 L}{3EI} - \frac{M_3 L}{6EI} \tag{A.6}$$

$$\phi_{3-2} = \phi_{3-4} \tag{A.7}$$

$$\frac{qL^3}{24EI} + \frac{M_2 L}{6EI} + \frac{M_3 L}{3EI} = \frac{-q(\alpha L)^3}{24EI} - \frac{M_3 \alpha L}{3EI} \tag{A.8}$$

This system of equations can be expressed in tensor notation. The unknown bending moments are stored in vector **m** and the force vector is **f**. The matrix **A** hold the bending stiffness values.

$$\mathbf{A}\mathbf{m} + \mathbf{f} = \mathbf{0} \tag{A.9}$$

In expanded form it will become

$$\begin{bmatrix} \frac{(\alpha+1)L}{3EI} & \frac{L}{6EI} & 0 \\ \frac{L}{6EI} & \frac{(1+1)L}{3EI} & \frac{L}{6EI} \\ 0 & \frac{L}{6EI} & \frac{(1+\alpha)L}{3EI} \end{bmatrix} \begin{bmatrix} M_b \\ M_c \\ M_d \end{bmatrix} + \begin{bmatrix} \frac{(\alpha^3+1)L^3}{24EI} \\ \frac{(1+1)L^3}{24EI} \\ \frac{(1+\alpha^3)L^3}{24EI} \end{bmatrix} q = \begin{bmatrix} 0 \\ 0 \\ 0 \end{bmatrix} \tag{A.10}$$

Substituting values for α , L , EI , and q will solve for the unknown bending moments. For different number of spans the matrix grows in size. The hogging bending moments are solved for a suitable range for α and divided by the minimum moment. The only variable to effect the solution is the number of spans. This is shown in Figure A.4. The optimal value is 0.81 which is achieved with very small steps for α .

The optimisation for α is only based on the values for the hogging bending moment. The sagging bending moments for this optimal outer span length are expected to not deviate much between different spans. To check this a 2D FEM package written in Python, called AnaStruct, is used to check this. The continuous beam is programmed, values are substituted and results are extracted. In Figure A.5 both the sagging and hogging bending moments are normalised to its minimal value. The value of 0.81 is visible in the graph for hogging bending moment. The sagging bending moment optimal value is a little under 0.8.

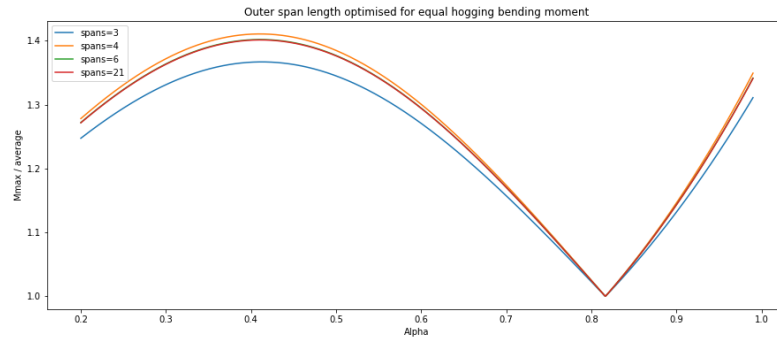


Figure A.4: Optimisation of α with respect to a minimal hogging moment difference, in which the red line 'spans=21' covers the green line 'spans=6'.

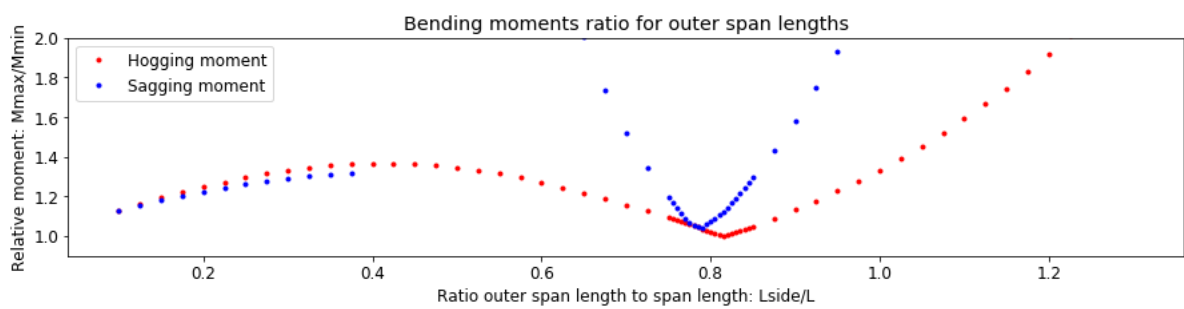


Figure A.5: Bending moment ratio with different outer span ratios.

B

Loads

This appendix shows the determination of the different load values. It includes an elaborate determination of temperature values and wind speed distribution.

B.1. Permanent loads

Two permanent loads are present for railway bridges. The track structure and its self-weight. The self-weight is estimated after a few iterations of cross-section design and is estimated at 40 kN/m. As track system the RHEDA2000 is chosen. Its width is assumed to be 3.2 m and the height of the concrete slab 0.5 m. With the reinforced weight of concrete being 25 kN/m³ the dead load per track becomes 40 kN/m. Including the rail beam weight and other structures related to a railway it is assumed that the total weight of the track structure becomes 45 kN/m. The total permanent load thus becomes 85 kN/m.

This value is used as an estimate. The self-weight of any element in SCIA is calculated automatically from the model. It can be ignored in load combinations.

B.2. Train loads

There are different train load models. EN1991-2 has combined real train loads into a few loading models. Either these imaginary train load models are used, or real trains if these are given by the client. The lack of project information resulted in using the standard load models. These are LM71, SW/0, and SW/2. The first is the standard train load model, the second is used for continuous beams, and the third represents heavy train traffic.

As a simplification of the train load models a continuous distributed load per track of 133 kN/m can be used, which is conservative. Modelling the bridge with FE software the actual load models are used as input.

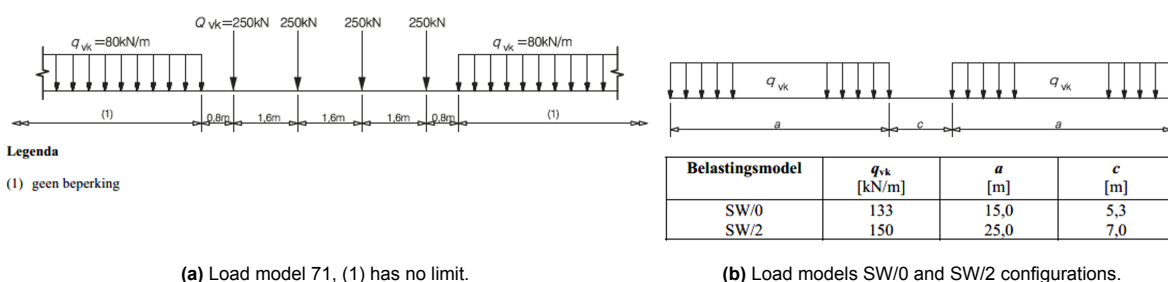


Figure B.1: Vertical train load models from EN1991-2.

There are two sets of horizontal actions. A transverse nosing force with a value of 100 kN. This force acts perpendicular at the rail track. The second set are traction and braking forces. The characteristic values are dependent on the load model and presented in EN1991-2.

Traction force $Q_{lak} = 33 \text{ kN/m} L_{a,b} \leq 1000 \text{ kN}$
for Load Models 71, SW/0, SW/2 and HSLM

Braking force $Q_{lbk} = 20 \text{ kN/m} L_{a,b} \leq 6000 \text{ kN}$
for Load Models 71, SW/0 and Load model HSLM

$Q_{lbk} = 35 \text{ kN/m} L_{a,b}$
for Load model SW/2

Vertical loads can have an eccentricity. In Figure B.2 this eccentricity is defined. It has a limit of 80 mm.

$$e \leq \frac{r}{18} \approx 80 \text{ mm}$$

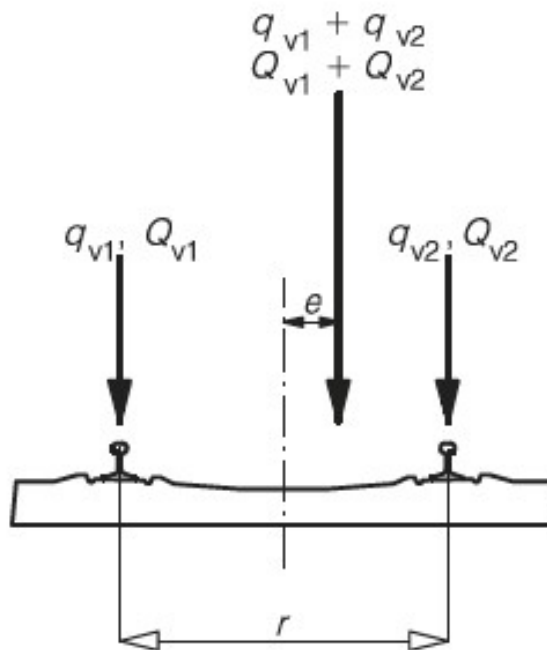


Figure B.2: Eccentricity of vertical train loads, figure 6.3 in EN1991-2.

B.3. Temperature

The national annex of Norway was not available, thus the design temperature values are determined by the author. With help of the Dutch national annex, other sources on average and extreme temperatures, and location information the values were determined to cover a range of 25 °C to -30 °C, see Table B.1. The average building temperature is assumed to be 5 °C. These value are used to determine the contraction and expansion component according to EN1991-1-5 section 6. The type is assumed to be 1, which is the most conservative.

$$T_{e,max} = T_{max} + 16$$

$$T_{e,min} = T_{min} - 3$$

$$\Delta T_{N,exp} = T_{e,max} - T_0 = 36 \text{ °C}$$

$$\Delta T_{N,con} = T_0 - T_{e,min} = 38 \text{ °C}$$

The uniform bridge temperature component, dT_N , is the difference between $T_{e,max}$ and $T_{e,min}$. This component is not used. A continuous beam requires to consider the temperature difference component,

	The Netherlands Norway, Mjøsa Temperature °C		
National Annex EN1991-1-5	30 to -25	25 to -30 ¹⁾	
Latitude	52	60	
Klöppen climate classification	Cfb	Dfb	
Klöppen temperature	22 to -3	22 to -3	
World Bank Group (Worldbank.org, 2021a, 2021b)	24 to 0	18 to -8	average
CLO (CLO, 2021)	35 to -7		extreme
Lillehamer (Weatherbase, 2021)		16 to -7	average
		31 to -31	extreme

1) these are determined by the author

Table B.1: Temperature values to use for design. The gathered values for the Netherlands and Norway were used to estimate the design temperature values for Norway.

ΔT_N , which is chosen to be 15 °C. Article 6.1.4.4 in EN1991-1-5 states this value is advised for large concrete box girders, which can have similar thicknesses to the timber box girder. And article 6.1.6 states that generally 15 °C is used for differences between structural elements. Thus:

$$\begin{aligned}\Delta T_{N,exp} &= 36 \text{ °C} \\ \Delta T_{N,con} &= 38 \text{ °C} \\ \Delta T_N &= 15 \text{ °C}\end{aligned}$$

The effect on the bending moment of the temperature difference component was performed with SCIA and checked with mechanics taught in construction mechanics 3 at the TU Delft.

B.4. Wind

The horizontal wind loads are determined using simplified method presented in section 8.3.2 in EN1991-1-4. Equation (B.1) is used to calculate the wind load of the structure.

$$F_W = \frac{1}{2} \cdot \rho \cdot v_b^2 \cdot C \cdot A_{ref,x} \quad (\text{B.1})$$

- ρ is the air density, advised to be 1.25 kg m⁻³ in 4.5(1) Note 2
- v_b is the wind speed, when dealing with trains it is 25 m s⁻¹ according to article 8.1(5)
- C is the wind factor from table 8.2 in EN1991-1-4. For a double track box girder the value would be 6 and for a single track box girder it would be 7
- $A_{ref,x}$ is the reference area, which is the sum of the box girder height and the train height. The latter is defined as 4 m according to 8.3.1(5)b). The double track height used 3 m and the single track height 4 m.

Wind loading per area can be acquired by setting $A_{ref,x}$ to 1 and conservatively assuming C to be 7, which results in the following horizontal wind load per area:

$$F_{W,y} = 2.7 \text{ kN/m}^2$$

Vertical wind loads are assumed to be calculated with the same procedure as for the horizontal wind loads, but with a different C factor. It is assumed that only $c_{f,x}$ changes to $c_{f,z}$, which is part of C . $c_{f,x}$ and $c_{f,z}$ are 1.3 and 0.9 respectively, according to 8.3.1 and 8.3.3 in EN1991-1-4. Leading to the following C factor and wind force.

Monthly wind speed statistics and directions for Lillehammer

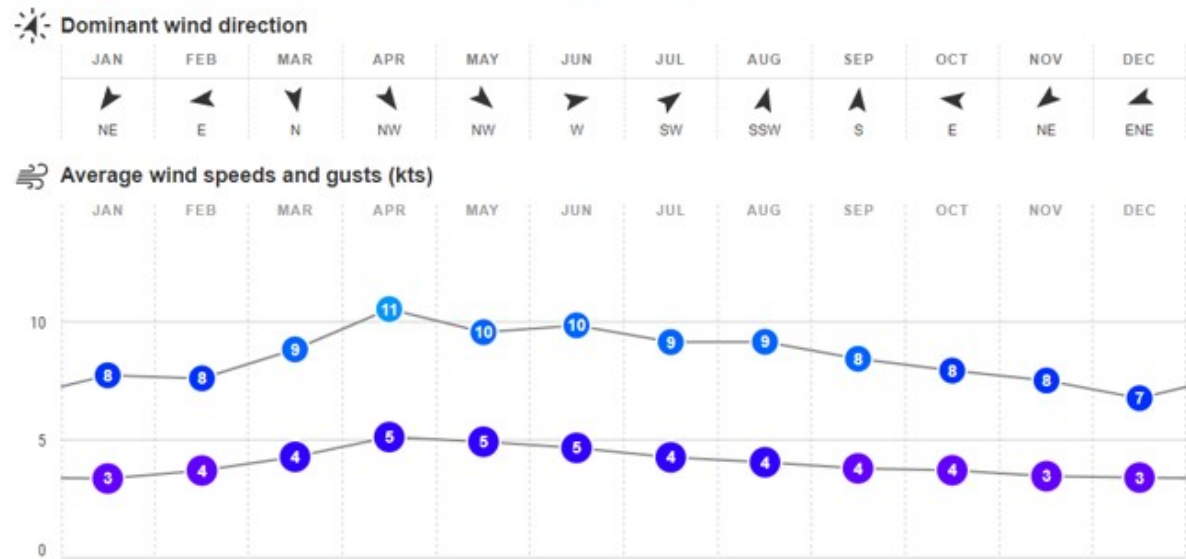


Figure B.3: Monthly average wind speeds in Lillehamer (Windfinder, n.d.).

$$C_z = \frac{c_{f,z}}{c_{f,x}} C_x = \frac{0.9}{1.3} \cdot 7 = 4.85$$

$$F_{W,z} = 1.9 \text{ kN/m}^2$$

B.4.1. Wind distribution

To estimate a wind speed distribution Windfinder (n.d.) is used. This distribution is then used to assume a load distribution for fatigue loading. A value estimate of the distribution in Figure B.4 is assumed to be on the high end of the range.

wind speed	
kts	m/s
1	0.5
5	2.6
10	5.1
15	7.7
20	10.2

Table B.2: Speed transfer table knots to meter per second.

Monthly wind direction and strength distribution

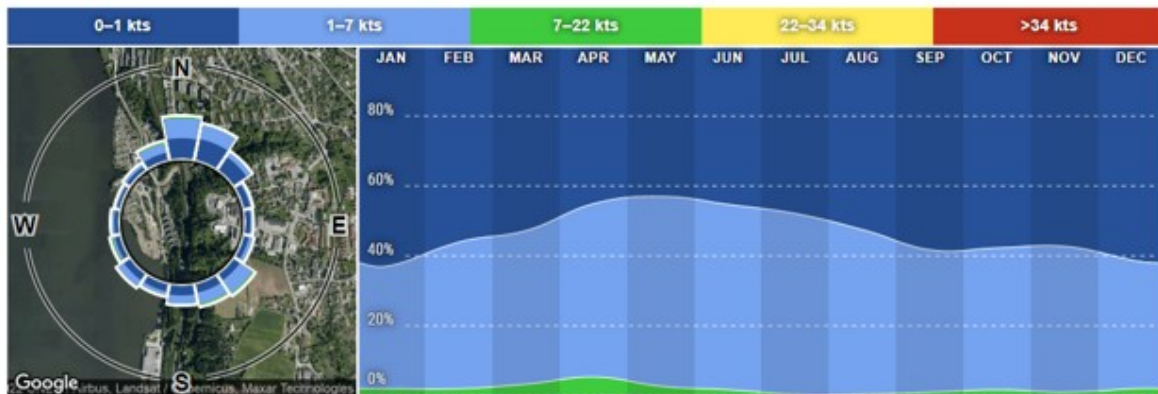
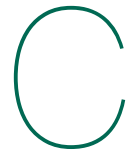


Figure B.4: Monthly average wind speed distribution in Lillehamer (Windfinder, n.d.).



Steel cross-sections

This appendix presents the calculations for both steel sections more in detail.

C.1. Steel class 2 design

The cross-section drawing is shown in Figure C.1.

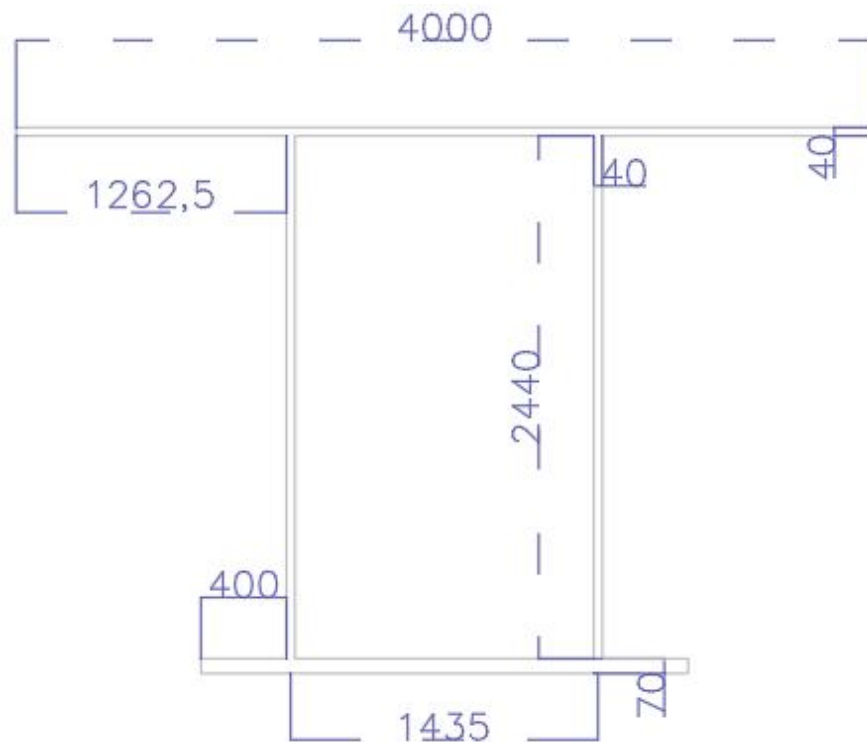


Figure C.1: Steel cross-section with thick plates such that it is class 2.

C.1.1. Classification

The classification of the plates is based on the bending moment around the major axis located above a support. Such that the bottom flange is in compression and the web is in bending. The limit values are shown in Table C.2 and the actual class is presented in Table C.1.

C.1.2. Shear lag

Since there is no class 4 plate only shear lag reduction is required. Shear lag occurs both in tension and compression. The procedure in EN1993-1-5 chapter 3 is used, table 3.1 for the formula. Only a support moment occurs with a value for κ within certain limits.

Classification	b/t	
web	61	class 2
inner bottom flange	20.5	class 1
outer bottom flange	6	class 1

Table C.1: Classification plates in (partial) compression.

$t \leq 40 \text{ mm}$ $\epsilon = 0.81$								
Inner plate bending			Inner plate compression			Outer plate compression		
class 1	72 ϵ	58.32	class 1	33 ϵ	26.73	class 1	9 ϵ	7.29
class 2	83 ϵ	67.23	class 2	38 ϵ	30.78	class 2	10 ϵ	8.1
class 3	124 ϵ	100.44	class 3	42 ϵ	34.02	class 3	14 ϵ	11.34

$t > 40 \text{ mm}$ $\epsilon = 0.84$								
Inner plate bending			Inner plate compression			Outer plate compression		
class 1	72 ϵ	60.48	class 1	33 ϵ	27.72	class 1	9 ϵ	7.56
class 2	83 ϵ	69.72	class 2	38 ϵ	31.92	class 2	10 ϵ	8.4
class 3	124 ϵ	104.16	class 3	42 ϵ	35.28	class 3	14 ϵ	11.76

Table C.2: Classification for S355 grade for full compression and symmetric bending from table 5.1 and 5.2 in EN1993-1-1.

$$\beta = \beta_2 \frac{1}{1 + 6 \left(\kappa - \frac{1}{2500\kappa} \right) + 1.6\kappa^2} \quad (\text{C.1})$$

with:

$$\kappa = \frac{\alpha_0 b_0}{L_e} \quad \alpha_0 = \sqrt{1 + \frac{A_{st}}{b_0 t}}$$

where:

b_0 = considered plate width

L_e = effective length

A_{st} = total area of stiffeners, in this case 0

t = thickness of the plate

The effective length is dependent on the span lengths of both sides of the support location that is checked. The worst case is the support that has a 50 m and 40 m span.

$$L_e = 0.25 * (L_1 + L_2) = 22.5 \quad (\text{C.2})$$

	Outstand top flange	Inner top flange	Inner bottom flange	Outstand bottom flange
b_0	1.2625	0.6975	0.6975	0.400
κ	0.056	0.031	0.031	0.018
β_2	0.770	0.901	0.901	1.000
β_2^κ	0.985	0.997	0.977	1.000

Table C.3: Shear lag reduction factors for the flanges.

C.1.3. Reduced cross-section properties

These reductions are used to reduce the widths of the flanges as per Figure C.2. With reduced widths a neutral axis can be calculated to the bottom. The values show that the bottom flange is reduced more for ULS than SLS, this is expected since the bottom flange is in compression.

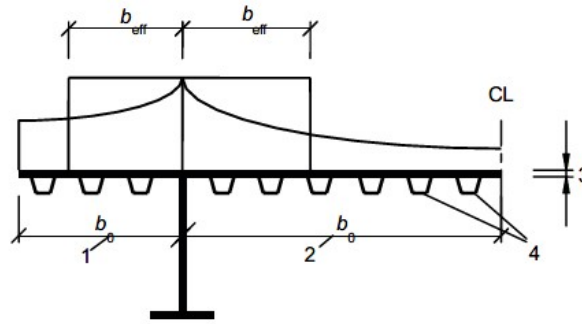


Figure C.2: Shear lag reduction to b_{eff} according to EN1993-1-5.

$$z_{na} = \frac{\sum A_i z_i}{\sum A_i} \tag{C.3}$$

$$z_{na,uls} = 1.29 \text{ m}$$

$$z_{na,sls} = 1.24 \text{ m}$$

With the neutral axis known the cross-sectional properties can be calculated for ULS and SLS.

Steel ULS		Steel SLS	
A_{eff}	0.406 m ²	A_{eff}	0.370 m ²
$A_{z,eff}^{1)}$	0.195 m ²	$A_{z,eff}^{1)}$	0.195 m ²
$A_{y,eff}^{2)}$	0.308 m ²	$A_{y,eff}^{2)}$	0.272 m ²
$I_{y,eff}$	0.529 m ⁴	$I_{y,eff}$	0.427 m ⁴
$W_{y,eff}$	0.419 m ³	$W_{y,eff}$	0.380 m ³
$I_{z,eff}$	0.306 m ⁴	$I_{z,eff}$	0.210 m ⁴
$W_{z,eff}$	0.243 m ³	$W_{z,eff}$	0.169 m ³
A_m	3.501 m ²		
1) only webs		1) only webs	
2) only effective flanges		2) only effective flanges	

Table C.4: Effective cross-section properties due to shear lag.

C.1.4. Resistance

These are used to determine the cross-sectional resistances and the unity checks. The bending and shear resistance are straightforward to calculate by multiplying it cross-sectional property with the yield strength. For the torsional resistance the inner box is assumed to only resist torsion and use thin-walled theory. The web plate is governing since that is the thinnest and it coincides with the largest shear force.

$$M_{i,Rd} = W_{i,eff} * f_y \tag{C.4}$$

$$V_{i,Rd} = A_{i,eff} * f_y \tag{C.5}$$

$$T_{Rd} = 2 * A_m * t * f_y \tag{C.6}$$

C.2. Steel class 4 design

The cross-section drawing with dimensions is shown in Figure C.3. The stiffener size and location are based upon general advised values in table C.1 in EN1993-2, which gives specific dimensions for open stiffeners for railway bridges. The cross girder distance is set at 2.5 m.

The distance between stiffeners and the webs are set to be all equal for ease of manufacturing and calculation. This results in a bottom flange that is just short of 4 m width. The stiffener geometry and properties are presented in Table C.5.

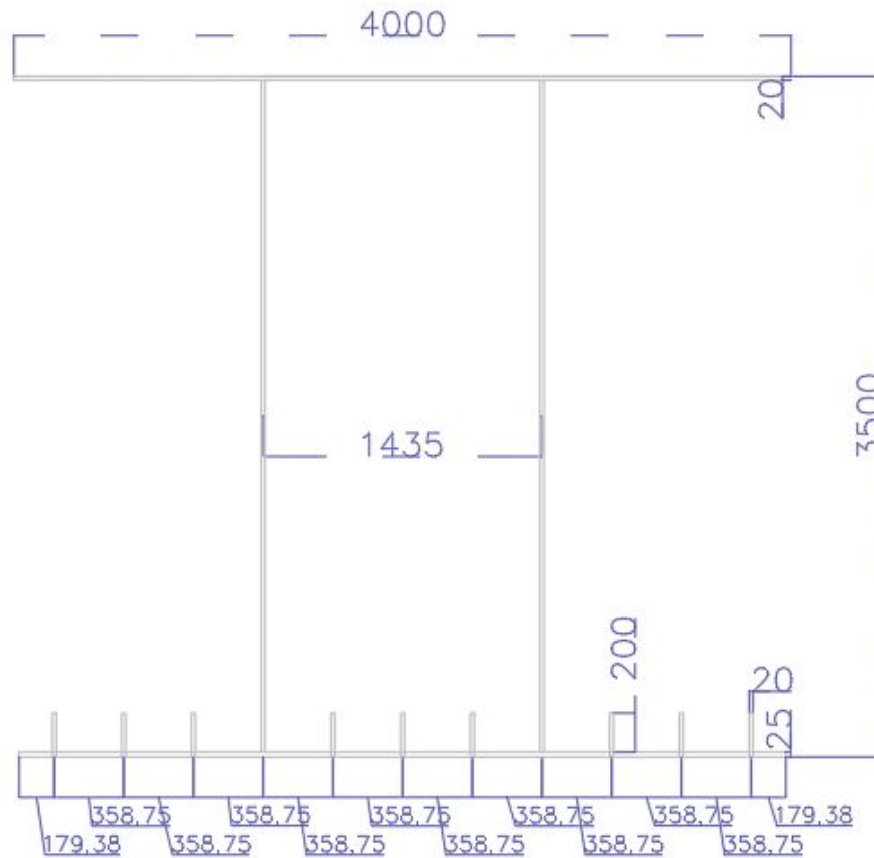


Figure C.3: Steel cross-section for slender design with only stiffeners at the bottom flange.

Stiffener			
h_{sl}	200 mm	A_{sl}	4000 mm^2
t_{sl}	20 mm	I_{sl}	$1.33 \times 10^7 \text{ mm}^4$
e_{sl}	358.75 mm		
$e_{crossbeam}$	2.5 m		

Table C.5: Stiffener dimensions and properties.

C.2.1. Classification

The classification of the flanges and webs, excluding the stiffeners, leads to only class 4 plates when comparing the b/t values with Table C.2. So it is valid to use stiffeners to increase the effective properties.

Classification	b	t	b/t	
web	3455 mm	20 mm	172.75	class 4
inner bottom flange	1435 mm	25 mm	57.40	class 4
outer bottom flange	1256 mm	25 mm	50.23	class 4

Table C.6: Classification plates in (partial) compression.

The local plate dimensions, mainly the stiffener thickness and length, are chosen such that every local

plate is at least class 3. This ensures no reduction due to local buckling is required and such uses its material efficient.

Classification	b	t	b/t	
stiffener	200 mm	20 mm	10	class 3
inner local plate	358.750 mm	25 mm	14.35	class 1
outstand local plate	179.375 mm	25 mm	7.18	class 1

Table C.7: Classification local plates in full compression.

C.2.2. Shear lag

Shear lag reductions are calculated for the top and bottom flange again. The same procedure is used as previously used with Equation (C.1). This instance does have a stiffener area. The effective length is still the same.

	Inner bottom flange	Outer bottom flange	Inner top flange	Outstand top flange
$A_{sl,tot}$	6000 mm ²	12 000 mm ²	0 mm ²	0 mm ²
b_0	717.5 mm	1255.625 mm	717.5 mm	1282.5 mm
α_0	1.155	1.176	1	1
κ	0.037	0.066	0.032	0.057
β_2	0.864	0.733	0.895	0.766
β_2^R	0.995	0.980	0.996	0.985

Table C.8: Shear lag reduction factors for the flanges of slender steel section.

To determine the effective properties for SLS no reduction due to plate buckling is required. The reduction from shear lag is more severe. Equation (C.3) is used to determine the neutral axis based on reduced widths of the top and bottom flange from shear lag. Factor β_2 in Table C.8 is used to determine the reduced area. With the procedure described in Section 3.4 a new effective width is calculated, presented in Table C.9. Note that outstand bottom and top flange only represent values to account for one side. There are two outstand bottom and top flange parts.

	Inner bottom flange	Outstand bottom flange	Inner top flange	Outstand top flange
A_{eff}	41 341 mm ²	31 812 mm ²	28 686 mm ²	27 488 mm ²
b_{eff}	667 mm	952 mm	1147 mm	550 mm

Table C.9: Effective width reduced for shear lag for SLS checks.

C.2.3. Bottom plate buckling

Stiffened plate buckling consists of orthotropic plate buckling and column buckling. A combined reduction factor can be calculated and its reduction may be a uniform cross-section reduction according to clause 4.5.1 (7) EN1993-1-5.

Orthotropic plate buckling

The orthotropic plate buckling reduction uses an equivalent plate to determine its critical stress to calculate its slenderness. The critical plate stress can be calculated with Annex A from EN1993-1-5.

$$\sigma_{cr,p} = k_{\sigma,p} \sigma_E \quad (\text{C.7})$$

With σ_E as the Euler plate stress of only the bottom flange.

$$\sigma_E = \frac{\pi^2 E t^2}{12(1 - \nu^2) b^2} = 190000 \frac{t^2}{b^2} \quad (\text{C.8})$$

where:

t = considered orthotropic plate thickness

b = considered orthotropic plate width

And $k_{\sigma,p}$ is the plate factor that accounts for the stiffeners.

$$k_{\sigma,p} = \frac{2((1 + \alpha^2)^2 + \gamma - 1)}{\alpha^2(\psi + 1)(1 + \delta)} \quad \alpha \leq \sqrt[4]{\gamma}$$

$$k_{\sigma,p} = \frac{4(1 + \sqrt{\gamma})}{(\psi + 1)(1 + \delta)} \quad \alpha > \sqrt[4]{\gamma}$$

with:

$\alpha = \frac{a}{b} \geq 0.5$ = aspect ratio of plate

$\gamma = \frac{I_{sl}}{I_p}$ = relative bending stiffness of a stiffener including plate part to plate

$\delta = \frac{A_{sl}}{A_p}$ = relative axial stiffness of a stiffeners to plate

$\psi = \frac{\sigma_2}{\sigma_1} \geq 0.5$ = stress distribution, 1 in case of full compression

where:

a = plate dimension longitudinal axis, equal to crossbeam distance of 2.5 m

b = plate dimension transverse axis, equal to plate width

I_{sl} = gross inertia of all stiffeners and plate

$I_p = \frac{bt^3}{12(1-\nu^2)}$ = plate inertia for plate bending

A_{sl} = gross area stiffeners

A_p = gross area plate

The slenderness $\bar{\lambda}_p$ also uses the relative effective area $\beta_{A,c}$, which is one since no local plates are class 4 and thus require no reduction.

$$\bar{\lambda}_p = \sqrt{\frac{\beta_{A,c} f_y}{\sigma_{cr,p}}} \quad (\text{C.9})$$

The reduction factor ρ can now be determined dependent on the plate and its slenderness.

Inner, compression element

$$\rho = 1 \quad \text{for } \bar{\lambda}_p \leq 0,5 + \sqrt{0,085 - 0,055\psi}$$

$$\rho = \frac{\bar{\lambda}_p - 0,055(3 + \psi)}{\frac{-2}{\bar{\lambda}_p}} \leq 1 \quad \text{for } \bar{\lambda}_p > 0,5 + \sqrt{0,085 - 0,055\psi} \quad (\text{C.10})$$

Outstand, compression element

$$\rho = 1 \quad \text{for } \bar{\lambda}_p \leq 0.748$$

$$\rho = \frac{\bar{\lambda}_p - 0,188}{-2} \leq 1 \quad \text{for } \bar{\lambda}_p > 0.748 \quad (\text{C.11})$$

In Table C.10 the values are presented used to calculate the reduction factor. The inner orthotropic plate requires no reduction, but the outstand does. The equivalent plate theory can only be used for plates connected on all sides. It is assumed that an outstand plate can be doubled and mirrored and the

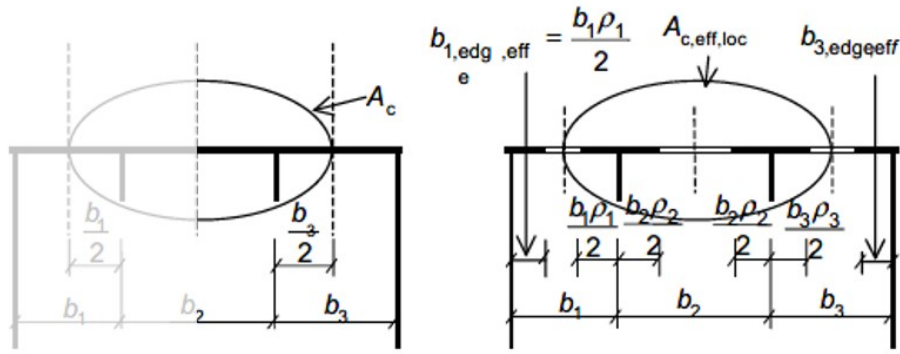


Figure C.4: Orthotropic stiffened plate with representation of local effective area and a visualisation of the mirrored outstand plate.

reduction could be calculated for this fictitious plate. In Figure C.4 a supporting figure from EN1993-1-5 is shown.

Inner flange		Outstand flange	
α	1.74	α	1.74
I_{sl}	$1.31 \times 10^8 \text{ mm}^4$	I_{sl}	$2.57 \times 10^8 \text{ mm}^4$
I_p	$2.05 \times 10^5 \text{ m}^4$	I_p	$3.59 \times 10^6 \text{ m}^4$
A_{sl}	12 000 m ²	A_{sl}	24 000 m ²
A_p	35 875 m ²	A_p	62 781 m ²
γ	64.19	γ	71.79
δ	0.33	δ	0.38
$\kappa_{\sigma,p}$	17.87	$\kappa_{\sigma,p}$	19.00
σ_E	57.67 MPa	σ_E	18.83 MPa
$\sigma_{cr,p}$	1030.76 MPa	$\sigma_{cr,p}$	357.74 MPa
$\bar{\lambda}_p$	0.587	$\bar{\lambda}_p$	0.996
ρ	1	ρ	0.782

Table C.10: Orthotropic plate buckling reduction for the inner bottom flange and the outstand bottom flange that uses numbers as if it was an inner plate of double the outstand size.

Column buckling

Column buckling considers the buckling of a stiffener and its accompanying plate as if it was a column. In general this is more conservative than the orthotropic plate buckling.

It considers straightforward column buckling described in EN1993-1-1. The critical stress to calculate the slenderness are Euler buckling as if the stiffener and plate part is a pinned-pinned column with buckling length equal to the crossbeam distance.

$$\sigma_{cr,c} = \sigma_{cr,sl} = \frac{\pi^2 EI_{sl,1}}{A_{sl,1} a^2} \tag{C.12}$$

where:

E = E-modulus of steel

$I_{sl,1}$ = gross inertia of column

$A_{sl,1}$ = gross area of stiffener and plate part

a = crossbeam distance, which is 2.5 m

The slenderness is calculated using Equation (C.9) with the relative effective area β_{Ac} again being 1.

The reduction factor χ_c uses a buckling factor α specific for open stiffeners.

$$\chi_c = \frac{1}{\Phi + \sqrt{\Phi^2 - \bar{\lambda}^2}} \quad (\text{C.13})$$

with:

$$\Phi = 0.5 (1 + \alpha_e (\bar{\lambda} - 0.2) + \bar{\lambda}^2) \quad (\text{C.14})$$

where:

$\bar{\lambda}$ = plate slenderness

$\alpha_e = \alpha + \frac{0.09}{i/e}$ = buckling curve reduced for stiffened plates

α = buckling curve c for open stiffeners, value of 0.49

$i = \sqrt{I_{sl,1} A_{sl,1}}$ = radius of gyration

$e = \max(e_1, e_2)$ = largest distance to centroid column

e_1 = centroid stiffener to centroid column

e_2 = centroid plate to centroid column

Since the geometry of the stiffeners is equal for all, only a single column buckling value is calculated. The reduction factor and intermediate values are presented in Table C.11.

Stiffener	
$I_{sl,1}$	$4.15 \times 10^7 \text{ mm}^4$
$A_{sl,1}$	$1.30 \times 10^4 \text{ mm}^2$
i	56.5 mm
e_1	69.2 mm
e_2	30.8 mm
e	69.2 mm
α_e	0.45
λ	0.58
Φ	0.753
χ_C	0.810

Table C.11: Column buckling of a single stiffener with its parent plate.

Combined buckling

The combination of the orthotropic plate buckling factor is calculated with Equation (C.15).

$$\rho_c = (\rho - \chi_C) \zeta (2 - \zeta) + \chi_C = \mathbf{0.810} \quad (\text{C.15})$$

with:

$$\zeta = \frac{\sigma_{cr,p}}{\sigma_{cr,c}} - 1 \text{ but } 0 \leq \zeta \leq 1 \quad (\text{C.16})$$

C.2.4. Bottom flange reduction

The bottom plate should be reduced both for buckling and shear lag. To account for both EN1993-1-5 presents a formula based on figure Figure C.4.

$$A_{eff} = A_{c,eff} \beta^{\kappa} = \left(\rho_c A_{c,eff,loc} + \sum b_{edge,eff} t \right) \quad (\text{C.17})$$

where:

β^κ = the shear lag reduction for ULS

ρ_c = the combined reduction factor for buckling

$A_{c,eff,loc}$ = the local effective area of the stiffened plate, which is now the gross area

$b_{edge,eff}$ = the plate parts next to the webs, excluded in $A_{c,eff,loc}$

t = the bot flange thickness

As stated in Section 3.4 an effective width is calculated based on this effective area. These values are shown in Table C.12. It should be noted again, that the outstand bottom and top flange occur twice, and the values in the table are for a single side.

	Inner bottom flange	Outstand bottom flange	Inner top flange	Outstand top flange
A_{eff}	40 282 mm ²	35 290 mm ²	25 264 mm ²	28 598 mm ²
b_{eff}	645 mm	1076 mm	1263 mm	715 mm

Table C.12: Effective width reduced for shear lag and plate buckling.

C.2.5. Web buckling

The web is class 4, and thus must be reduced appropriately. With the reduced top and bottom flange the neutral axis is shifted and a new stress distribution in the web occurs. With Equation (C.3) the new neutral axis is calculated.

$$z_{na} = 1.537 \text{ mm}$$

The stress distribution is now, instead of -1:

$$\psi = -1.263$$

The shift in neutral axis has not lead to a different classification, but with it the effective width of the web can be calculated. For this unstiffened plate the slenderness is calculated differently.

$$\bar{\lambda}_p = \frac{\bar{b}t}{28.4\epsilon\sqrt{k_\sigma}} \quad (\text{C.18})$$

where:

\bar{b} = plate width

t = plate thickness

$$\epsilon = \sqrt{\frac{235}{f_y}}$$

k_σ = plate buckling factor dependent on the stress distribution ψ

The plate buckling factor is taken from Figure C.5.

$$k_\sigma = 5.98(1 - \psi)^2 \quad (\text{C.19})$$

With the slenderness known and the dimensions of the web the reduction factor ρ can be calculated using Equation (C.10). The effective widths follow from Figure C.5. This reduction leads to a new neutral axis, and after a few iterations a convergence can be found.

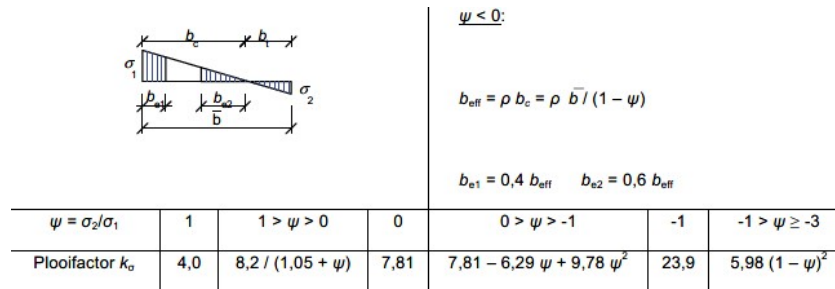


Figure C.5: Stress distribution inner element in bending with the plate buckling factor for different ψ , snapshot of table 4.1 in EN1993-1-5.

$$\rho = 0.706$$

C.2.6. Reduced cross-section

For ULS this new neutral axis is used to calculate the effective first moment of area. It includes reductions for plate buckling of the bottom flange, web plate buckling due to a bending moment, and shear lag. For SLS only shear lag is considered.

$$\begin{aligned} z_{na,uls} &= 1492 \text{ mm} & z_{na,sls} &= 1484 \text{ mm} \\ I_{y,eff,uls} &= 0.581 \times 10^{12} \text{ mm}^4 & I_{y,eff,sls} &= 0.498 \times 10^{12} \text{ mm}^4 \\ W_{y,eff,uls} &= 0.389 \times 10^9 \text{ mm}^3 & & \end{aligned}$$

The second moment of area is calculated including the parallel axis theorem.

$$I = \sum_{i=1}^n \frac{1}{12} b_i h_i^3 + b_i h_i |z_i - z_{na}|^2 \quad (\text{C.20})$$

The first moment of area is calculated by dividing the second moment of area by the maximal fibre distance from the neutral axis.

$$W = \frac{I}{\max(H - z_{na}; z_{na})} \quad (\text{C.21})$$

C.2.7. Resistance

The bending moment resistance becomes

$$M_{y,Rd} = W_{y,eff} * f_y \quad (\text{C.22})$$

C.2.8. Deflection

The deflection is calculated using Equations (3.4) and (3.6), shown here again. The quasi-permanent deflection is used for creep, and steel has no creep, so it is not used. Substituting the appropriate values results in the deflection values in Table 3.14.

$$w_{sls} = \left(\frac{2L^4}{384EI} + \frac{L^2}{8GA} \right) q_{sls,live} + 0 \quad (\text{Equation (3.4)})$$

$$w_{passcomf} = \left(\frac{2L^4}{384EI} + \frac{L^2}{8GA} \right) q_{sls,LM71} + 0 \quad (\text{Equation (3.6)})$$

C.2.9. Mass

The assumption is that the area ratio between webs and flanges is equal for the class 2 and class 4 section. First the ratio is calculated for the class 2 section.

	Area m ²	Ratio -
Top flange	0.140	0.88
Web	0.171 7	1.08
Bottom flange	0.159	1

Table C.13: Class 2 area ratios with respect to bottom flange area

The ratios are assumed to be equal for the class 4 section. Only the area of the stiffened bottom flange is known. In the second column the desired area is calculated. The difference between the desired area and the actual area, in first column, is calculated in the last column. This area is assumed to be added via stiffeners. The top flange would require around nine stiffeners and the web around two. A stiffener area is 0.004 m².

	Area m ²	Desired area m ²	Ratio -	Added area m ²
Top flange	0.080	0.119	0.88	0.039
Web	0.138	0.145	1.08	0.007
Bottom flange	0.135	0.135	1	-

Table C.14: Class 4 area ratios with respect to stiffened bottom flange area

From this desired area the mass can be calculated in a straightforward manner.

$$m_{s,cl4}^* = A_{tot} \cdot \rho_s = (0.119 + 0.145 + 0.135) * 7850 = 3132 \text{ kg/m}$$



Connection calculations

This appendix shows the calculation and actual values for the determination of the number of dowels per flange and web. There are two sections that represent the two lists in Section 8.2

D.1. Local criteria - fastener

The two procedures in Section 8.2 are worked out in two different parts.

D.1.1. Required number of dowels

The steps to determine the required number of steel fasteners are repeated.

1. Calculate the characteristic resistance of each failure mode for a given timber thickness, steel fastener diameter, and embedment direction;
2. Determine the mode with the lowest resistance;
3. Distribute the cross-sectional forces as in Figure 8.3;
4. Calculate the resultant force and its angle to the grain;
5. Calculate the design resistance per fastener by multiplying the characteristic resistance of the fastener by the number of shear planes and dividing it with a partial safety factor for dowel connections, $\gamma_M = 1.3$;
6. Divide the resultant force with the design resistance per fastener to get the required number of fasteners, shown in Equation (8.1).

Only the calculation for a double slotted-in steel plate is presented. The single slotted-in steel plate is not chosen for the design but uses the same procedure. The main difference is the use of the Eurocode failure modes instead of Pedersen failure modes. The latter failure modes are given here again.

$$F_y = \min \left\{ \begin{array}{ll} \frac{1}{4} (2t_1 + t_2) df_h & \text{Mode I} \\ \left(-\frac{1}{2}t_1 + \frac{t_2}{4} + \sqrt{\frac{1}{2}t_1^2 + \frac{M_y}{df_h}} \right) df_h & \text{Mode IIa} \\ \sqrt{4M_y df_h} & \text{Mode IIb} \\ \left(\frac{1}{2}t_1 + \frac{1}{2} \sqrt{t_1^2 + \frac{2M_y}{df_h}} \right) df_h & \text{Mode IIIa} \\ \left(\sqrt{\frac{M_y}{df_h}} + \frac{1}{2}t_1 \right) df_h & \text{Mode IIIb} \\ \left(\sqrt{\frac{M_y}{df_h}} + \frac{1}{4}t_2 \right) df_h & \text{Mode IIIc} \\ \left(-\frac{1}{2}t_1 + \sqrt{\frac{1}{2}t_1^2 + \frac{M_y}{df_h}} + \sqrt{\frac{M_y}{df_h}} \right) df_h & \text{Mode IIId} \end{array} \right. \quad (\text{Equation (7.3)})$$

where:

- t_1 = thickness of outer timber element
- t_2 = thickness of inner timber element
- d = fastener diameter

f_h = timber embedment strength, similar to $f_{h,k}$ in Equation (7.2)

M_y = Yield moment of fastener, similar to $M_{y,Rk}$ in Equation (7.2)

Several timber properties are required to use these failure modes. The thickness is chosen such that t_2 is double the value of t_1 . This limits the amount of failure modes, specifically IIIb and IIIc in Figure 7.2 have equal values. The thickness of the flange is 560 mm and for the web is 840 mm. The slotted-in steel plate is 20 mm thick.

$$t_{1,flange} = (560 - 2 * 20)/4 = 130mm$$

$$t_{2,flange} = (560 - 2 * 20)/2 = 260mm$$

$$t_{1,web} = (560 - 2 * 20)/4 = 200mm$$

$$t_{2,web} = (560 - 2 * 20)/2 = 400mm$$

The timber embedment strength can be found in EC5. It is an empirical formula that uses the fastener diameter and the timber density.

$$f_{h,k} = 0.082(1 - 0.01 * d)\rho_k = 24.682 \text{ N/mm}^2$$

The characteristic embedment strength is dependent on the angle to the grain. A specific k_{90} factor must be used for glulam. The correct embedment strengths are shown in Table D.1.

$$f_{h,\alpha,k} = \frac{f_{h,k}}{k_{90} \cdot (\text{SIN}(\alpha)^2 + \text{COS}(\alpha)^2)}$$

$$k_{90} = 1.35 + 0.015d = 1.8$$

The steel fastener yield moment is also an empirical formula in EC5 and is dependent on the ultimate steel strength and the fastener diameter.

$$M_{y,Rk} = 0.3f_u d^{2.6} = 1018198 \text{ Nmm}$$

With all formulae and values known the different failure modes are calculated. Only a few angles are considered. The ones that are used are based on the force direction. The angles have been rounded towards their next multiple of three. Mode IIb and IIIc are very close and the governing values. These modes activate the plastic capacity of the dowel. The weakest is used in future calculations.

α	$f_{h,\alpha,k}$	Governing	Mode						
			I	IIa	IIb	IIIa	IIIb	IIIc	IIId
Flange									
0	24,68	53	96	73	55	100	76	76	53
3	24,63	53	96	73	55	100	75	75	53
6	24,47	52	95	73	55	99	75	75	52
Web									
27	21,19	51	127	93	51	130	89	89	55
30	20,57	50	123	91	50	126	87	87	54
33	19,95	49	120	88	49	122	85	85	53

Table D.1: Failure mode values for three angles to the grain for flange and web

Cross-sectional forces distribution The cross-sectional forces that are present at the connection location are shown in Table D.2. The distribution among the flanges and webs follows Figure 8.3. Important are the dimensions of the connection plates. The flange has slotted-in plates of 3.8 m wide, and the webs have steel plates of 2.2 m wide slotted-in.

The internal lever arm is needed to distribute bending moments. In the transverse direction this is 1.435 m and in vertical direction it is 2.94 m. Basically centre-to-centre line of the flanges. For the torsional moment the value can be calculated by assuming there is only a single unknown. The ratio between the web torsion shear and the flange torsion shear is dependent on the geometry

	5 m
M_y	-29.3 MNm
M_z	6.3 MNm
M_x	1.3 MNm
V_z	6.2 MN
V_y	0.65 MN
N	11 MN

Table D.2: Cross-sectional forces at the connection at five meter.

This leads to the following normal and shear forces in the flange web.

$$\begin{aligned}
 N_{N,flange} &= \frac{N * 3.8}{2 * (3.8 + 2.2)} &&= 3.48MN \\
 N_{M_y,flange} &= \frac{M_y}{2.94} &&= 9.97MN \\
 V_{M_x,flange} &= \frac{M_x * 1.435}{1.435^2 + 2.2^2} &&= 0.27MN \\
 V_{V_y,flange} &= \frac{V_y}{2} &&= 0.33MN \\
 \\
 N_{N,web} &= \frac{N * 2.2}{2 * (3.8 + 2.2)} &&= 2.02MN \\
 N_{M_z,web} &= \frac{M_z}{1.435} &&= 4.39MN \\
 V_{M_x,web} &= \frac{M_x * 2.2}{1.435^2 + 2.2^2} &&= 0.41MN \\
 V_{V_z,web} &= \frac{V_z}{2} &&= 3.1MN
 \end{aligned}$$

Resultant force The resultant force can be calculated by summing the normal and shear forces separately and using the Pythagorean theorem. The angle to the grain of the resultant force is also calculated by this theorem.

	Flange	Web
N	13.50 MN	6.40 MN
V	0.60 MN	3.50 MN
α	2.54	28.67
$F_{res,tot}$	13.51 MN	7.29 MN

Table D.3: Calculation of resultant force at 5m connection for flange and web

Required number of dowels This is calculated by Equation (8.1). The resultant force is known, the force per fastener per shear plane is known from Table D.1, and the safety factor is known, $\gamma_M = 1.35$. The amount of shear planes in a double-slotted connection is the amount of plates times two, which is the number of shear planes for a slotted-in steel plate.

$$n_{req} = \frac{F_{res}}{F_v(\alpha)/\gamma_M} \quad (\text{Equation (8.1)})$$

$$n_{req,flange} = \frac{13.51 \text{ MN}}{53 \text{ kN} * 4/1.3} = 85$$

$$n_{req,web} = \frac{7.29 \text{ MN}}{53 \text{ kN} * 4/1.3} = 48$$

D.1.2. Effective number of dowels

Let the steps first be repeated.

1. Choose the size of the slotted-in steel plate;
2. Choose the edge and internal distance, complying to spacing limitations;
3. Calculate the maximum amount of possible fasteners in a column;
4. Choose the number of fasteners per row and column;
5. Calculate the number of effective fasteners in a row;
6. Multiply number of columns by effective number of rows to get effective number of fasteners.

The size of the slotted-in steel plate has been chosen to be 3.8 m and 2.2 m wide and high respectively. The length of both plates will be dependent on the required number of dowels and the chosen spacing. The spacing to the edges is $7d = 210 \text{ mm}$ and the internal distances are $9d = 270 \text{ mm}$ for both the flange and web dowels. Using the same spacing for both will reduce the possibility of errors.

Maximal number of fasteners in column The width or height of the plate and the spacing determine the maximal amount of dowels that can fit in the connection. It is beneficial to separate the fasteners over the full width or height. Spacing distances are defined in Figure 7.4 and Table 7.1. a_1 is the internal distance in longitudinal direction, which is equal to a_2 , the internal transverse direction. a_4 is the transverse edge distance and a_3 the longitudinal edge distance.

$$n_{col,flange} = \text{ROUNDDOWN} \left(\frac{2.2 \text{ m} - 2 * a_4}{a_2} + 1 \right) = 13$$

$$n_{col,web} = \quad \quad \quad = 7$$

It should be rounded up so all internal are satisfied. The left-over range is added to the edge distance. The edge distance for the flange has become 280 mm and for the webs 290 mm.

Effective fasteners in a row The maximal number of dowels in a column is chosen as the geometrically maximal possible number. So 13 and 7 for the flange and web respectively. The number of dowels in a single row follows from the required number of fasteners calculated before. Dowels in a row are not activated 100%, only the effective number of dowels can be used in calculations. This is calculated using Equation (7.4). For multiple numbers of fasteners in a row the effective number and percentage are given in Table D.4.

$$n_{ef} = \min \left\{ \begin{array}{l} n \\ n^{0.9} \sqrt[4]{\frac{a_1}{13d}} \end{array} \right. \quad (\text{Equation (7.4)})$$

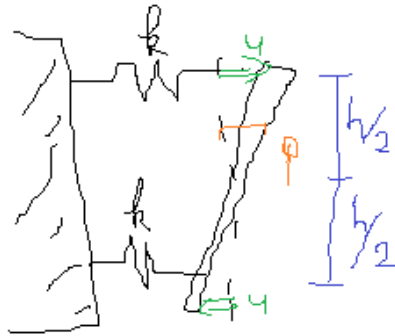


Figure D.1: Sketch of rotational stiffness principle based on Figure 8.5

n	5	6	7	8	9	10	11	12
n_{ef}	3.88	4.58	5.26	5.93	6.59	7.25	7.89	8.54
percentage active	78%	76%	75%	74%	73%	73%	72%	71%

Table D.4: Multiple effective number of dowels in a row. With a diameter of 30 mm and spacing $a_1 = 270$ mm

The chosen number of dowels in a row can be for both flange and web be ten, with 73% effective.

D.1.3. Stiffness

The slip modulus per slip plane per fastener is calculated with Equation (7.5).

$$K_{ser} = 2 \cdot \rho_m^{1.5} \frac{d}{23} = 2 * 480^{1.5} * 30/23 = 27\,433 \text{ N/mm}^2$$

The connection has four slip planes for each fastener and thus the total stiffness is the multiplication of the number of fasteners times the number of slip planes times the single slip plane stiffness value.

$$K_{ser,tot,flange,eff} = 94.25 * 4 * 27433 = 10\,343 \text{ MN/m}$$

$$K_{ser,tot,web,eff} = 50.72 * 4 * 27433 = 5569 \text{ MN/m}$$

To determine the rotational capacity of the connection the slotted-in plates with steel fasteners are modelled as springs. These springs will have a rotational capacity. The following equations are the derivation of K_r in spring stiffness and lever arm.

$$\phi = \frac{u}{\frac{h}{2}} = \frac{2u}{h}$$

$$F = ku$$

$$M = K_r \phi$$

$$M = \sum Fr_i = ku \cdot \frac{h}{2} + ku \cdot \frac{h}{2} = kuh \cdot \frac{h}{2} = \frac{2u}{h} \cdot \frac{1}{2} kh^2$$

$$K_r = \frac{M}{\phi} = \frac{1}{2} kh^2$$

The k is the spring stiffness, which is in the case of the connection either $K_{ser,tot,flange,eff}$ for the flange or $K_{ser,tot,web,eff}$ for the web. Subsequently the rotational spring stiffness for the effective number of fasteners becomes the following.

$$K_{r,fl} = 11175 \text{ MNm}$$

$$K_{r,w} = 1433 \text{ MNm}$$

D.2. Global criteria

Multiple different global criteria need to be checked. There are two different main elements: the timber section and the steel section. The steel fastener itself should also be checked on shear strength.

$$F_{v,Rd} = \frac{0.6f_u\pi d^2}{4\gamma_{M2}} = 166 \text{ kN} \quad (\text{D.1})$$

For long connections a reduction is applied according to section 3.8 in EN1993-1-8.

$$\beta_{L_f} = 1 - \frac{L_j - 15d}{200d} \text{ for } 0.75 \leq \beta_{L_f} \leq 1.0 \quad (\text{D.2})$$

where:

L_j = distance between outer fasteners

d = diameter steel fastener

$$\beta_{L_f,fl} = 0.75$$

$$\beta_{L_f,web} = 0.76$$

D.2.1. Timber section

The timber section has two standard global criteria, net tension and block shear. The shrinkage resistance is explained and calculated in Chapter 8, not in this appendix.

Net section At the connection the net section of timber should be checked. The area is reduced by the drilled holes but requires to still resist the cross-sectional forces.

The area of the flange and web are calculated as follows.

$$A_{net,fl} = (t_{fl} - n_s \cdot t_s) \cdot (B - d_0 n_{col,fl}) = 1.877 \text{ m}^2$$

$$A_{net,w} = (t_w - n_s \cdot t_s) \cdot (h_w - d_0 n_{col,w}) = 1.736 \text{ m}^2$$

where:

t_{fl} = flange thickness

t_w = web thickness

t_s = steel plate thickness

n_s = number of steel plates

n_{col} = number of fasteners in column

B = width of flange

h_w = height of web

The stresses are calculated with the following formulae. Assuming the maximal shear stress occurs. The results are found in Chapter 8.

$$\sigma_N = \frac{N}{A}$$

$$\tau_V = \frac{3}{2} \frac{V}{A}$$

Block shear This is a specific failure mode based on stress in certain areas. The areas used in the calculation are calculated in the following manner.

$$\begin{aligned}
 A_{net,t,fl} &= (n_{col,fl} - 1)(a_2 - d)(t_{fl} - n_s t_s) \\
 &= (13 - 1)(270 - 30)(560 - 2 * 20) = 1.498 \text{ m}^2 \\
 A_{net,v,fl} &= 2 \cdot (a_3 + (n_{row,fl} - 1) \cdot a_2)(t_{fl} - n_s t_s) \\
 &= 2(210 + (10 - 1) * 270)(560 - 2 * 20) = 2.746 \text{ m}^2 \\
 A_{net,t,w} &= (n_{col,w} - 1)(a_2 - d)(t_w - n_s t_s) \\
 &= (7 - 1)(270 - 30)(800 - 2 * 20) = 1.152 \text{ m}^2 \\
 A_{net,v,w} &= 2 \cdot (a_3 + (n_{row,w} - 1) \cdot a_2)(t_w - n_s t_s) \\
 &= 2(210 + (10 - 1) * 270)(800 - 2 * 20) = 4.224 \text{ m}^2
 \end{aligned}$$

where:

$$n_{row} = \text{number of fasteners in row}$$

These areas can be used to determine the design block shear strength.

$$\begin{aligned}
 F_{b,Rd} &= A_{net,t} \cdot f_{t,0,g,d} + A_{net,v} \cdot f_{v,g,d} \\
 &= 1.498 * 17.28 + 2.746 * 2.52 = 32.8 \text{ MN} \\
 &= 1.152 * 17.28 + 4.224 * 2.52 = 30.6 \text{ MN}
 \end{aligned}$$

D.2.2. Steel section

The steel plate can fail in bearing, net tension, and block shear. As stated before, block shear is not checked. Only bearing and net tension calculations are presented here.

Bearing Bearing capacity is dependent on the bearing formula from EC5. Below the precise formulation is given with the k_1 and α_b factor that follow from geometry of the dowel configuration.

$$F_{b,Rd} = \frac{k_1 \alpha_b f_u d t}{\gamma_{M2}} \quad (\text{Equation (8.2)})$$

There are four different steel fastener locations that can have a different factor for k_1 and α_b .

	Flange	Web	
p_1	270	270	mm
e_1	210	210	mm
p_2	270	270	mm
e_2	280	290	mm

Table D.5: Steel geometry edge and internal distances of steel plate

$$\alpha_b = \min(\alpha_d ; \frac{f_{ub}}{f_u} ; 1.0)$$

$$\alpha_d = \frac{e_1}{3d_0} \quad \text{for end bolts}$$

$$\alpha_d = \frac{p_1}{3d_0} - \frac{1}{4} \quad \text{for inner bolts}$$

$$1 = \min\left(2.8 \frac{e_2}{d_0} - 1.7 \quad ; \quad 1.4 \frac{p_2}{d_0} - 1.7 \quad ; \quad 2.5\right) \quad \text{for end bolts}$$

$$1 = \min\left(1.4 \frac{p_2}{d_0} - 1.7 \quad ; \quad 2.5\right) \quad \text{for inner bolts}$$

Calculation of these values for the different edge distances result in k_1 of 2.5 and α_{b} of 1.0. These are the maximal values and thus is the bearing resistance of each bolt in each direction the same.

$$F_{b,Rd} = 588 \text{ kN}$$

Multiplying the effective number of dowels with the individual bearing resistance is the total bearing resistance of the plate.

Net section The net area of the steel plate must be checked on tension and shear. The resultant force is divided into its components and checked with the area. The area is calculated in a similar manner as the timber net section.

$$\begin{aligned} A_{net,fl} &= t_s * (3.8 - n_{col,fl} * d_0) \\ &= 20 * (3800 - 13 * 33) = 0.067 \text{ m}^2 \\ A_{net,w} &= t_s * (2.2 - n_{col,w} * d_0) \\ &= 20 * (2200 - 7 * 33) = 0.039 \text{ m}^2 \end{aligned}$$

The hole diameter is 3 mm larger than the dowel diameter, as per EC3 is required for large holes. The normal and shear stresses are calculated in the same manner as for the timber section. Now the steel strength is used, grade S355.